



Chair of Drilling and Completion Engineering

Master's Thesis



Hybrid Model for Detecting Abnormal
Drilling Behaviors

Andreas Lindner, BSc

November 2020

I dedicate my Thesis to my father Wolfgang Lindner († Nov 29th, 2005).

“Science can amuse and fascinate us all, but it is engineering that changes the world.”

- Isaac Asimov



EIDESSTÄTTLICHE ERKLÄRUNG

Ich erkläre an Eides statt, dass ich diese Arbeit selbständig verfasst, andere als die angegebenen Quellen und Hilfsmittel nicht benutzt, und mich auch sonst keiner unerlaubten Hilfsmittel bedient habe.

Ich erkläre, dass ich die Richtlinien des Senats der Montanuniversität Leoben zu "Gute wissenschaftliche Praxis" gelesen, verstanden und befolgt habe.

Weiters erkläre ich, dass die elektronische und gedruckte Version der eingereichten wissenschaftlichen Abschlussarbeit formal und inhaltlich identisch sind.

Datum 06.11.2020

Unterschrift Verfasser/in
Andreas, Lindner

Abstract

Unplanned and unexpected events during drilling a well do not only lead to a massive loss of resources by increasing the amount of non-productive time, but also cause the necessity of plugging a well and starting a contingency side-track, which will add environmentally and economically risks to the originally planned project. Therefore, detecting the undesirable downhole drilling trouble at the earlier stages may help avoid the matters above.

Several surface drilling parameters can be used to predict the downhole drilling problems in real-time. Nevertheless, torque and standpipe pressure are considered to be the most critical and useful parameters. Therefore, several methods utilizing the two indicated surface parameters for detecting the downhole drilling problems were published in the last decade. However, these methods have flaws, mainly related to delays in receiving the necessary information, uncertainties associated with involved data, human error by potential incomplete data sets (due to sensor misreading), as well as human error interpretation of the data. Thus, linking sequential pattern recognition for possible drilling event determination is impacted. Consequently, recognizing drilling parameter anomalies in real-time using one single approach, such as data-driven or model-driven, can lead to an excessive increase in the nonproductive time due to the generation of undue false alarms. Thus, integrating a stochastic model with a data-driven model will reduce the associated uncertainties and make the predictive model more effective. From this perspective, the ultimate goal of this thesis is to develop a hybrid model that provides better accuracy in detecting abnormal behavior of measured drilling parameters such as standpipe pressure and torque.

A standalone application based on a hybrid model was developed during the thesis work by the implementation of statistical calculations based on actual and predicted data channels. As a result, uncertainty windows are created and compared to the actual data points in order to detect abnormal drilling behavior and triggering alerts to provide warnings to the user. In order to evaluate and determine the shortcomings of the developed workflow, the developed hybrid model, a case study was conducted. The final results of the case study reveal that the workflow is reliable and easy to use.

Zusammenfassung

Ungeplante und unerwartete Ereignisse während des Bohrens eines Bohrlochs führen nicht nur zu einem massiven Ressourcenverlust, indem die Menge an unproduktiver Zeit erhöht wird, sondern verursachen auch die Notwendigkeit, ein Bohrloch zu verschließen und eine Nebenbohrung aufgrund unvorhergesehener Ereignisse zu starten, die neben ökologischen Auswirkungen die wirtschaftliche Risiken für das ursprünglich geplante Projekt erhöht. Daher kann das Erkennen der unerwünschten Bohrprobleme im Bohrloch in den früheren Stadien dazu beitragen, die oben genannten Probleme zu vermeiden.

Verschiedene Oberflächenbohrparameter können verwendet werden, um die Bohrlochprobleme in Echtzeit vorherzusagen. Trotzdem werden Drehmoment und Standrohrdruck als die kritischsten und nützlichsten Parameter angesehen. Daher wurden im letzten Jahrzehnt mehrere Methoden veröffentlicht, bei denen die beiden angegebenen Oberflächenparameter zur Erkennung der Bohrprobleme im Bohrloch verwendet wurden. Diese Verfahren weisen jedoch Mängel auf, die hauptsächlich auf Verzögerungen bei der Übertragung der erforderlichen Informationen, auf Ungenauigkeiten im Zusammenhang mit den verwendeten Daten, auf menschliches Versagen durch möglicherweise unvollständige Datensätze (aufgrund von Sensorfehlern) sowie auf menschliches Versagen bei der Interpretation der Daten zurückzuführen sind. Somit wird die Verknüpfung der sequentiellen Mustererkennung für eine mögliche Bestimmung des Bohreignisses beeinflusst. Folglich kann das Erkennen von Anomalien von Bohrparametern in Echtzeit aufgrund eines einzigen Ansatzes, z. B. datengesteuert oder modellgesteuert, zu einer übermäßigen Erhöhung der unproduktiven Zeit führen, wenn Fehlalarme generiert werden. Die Integration eines stochastischen Modells in ein datengesteuertes Modell verringert somit die damit verbundenen Ungenauigkeiten und macht das Vorhersagemodell effektiver. Aus dieser Perspektive besteht das ultimative Ziel dieser Arbeit darin, ein Hybridmodell zu entwickeln, das eine erhöhte Genauigkeit bei der Erkennung abnormalen Verhaltens gemessener Bohrparameter wie Standrohrdruck und Drehmoment bietet.

Eine eigenständige Anwendung basierend auf einem Hybridmodell wurde während der Arbeit durch die Implementierung statistischer Berechnungen basierend auf tatsächlichen und vorhergesagten Datenkanälen entwickelt. Infolgedessen werden Unsicherheitsfenster erstellt und mit den tatsächlichen Datenpunkten verglichen, um abnormales Bohrverhalten zu erkennen und Alarme auszulösen, um den Benutzer zu warnen. Um die Mängel des entwickelten Workflows, des entwickelten Hybridmodells, zu bewerten und zu analysieren, wurde eine Fallstudie durchgeführt. Die endgültigen Ergebnisse der Fallstudie zeigen, dass der Workflow zuverlässig und einfach zu verwenden ist.

Acknowledgements

- DI Asad Elmgerbi, University of Leoben (MUL) for the outstanding support throughout the thesis.
- Prof. Dipl.-Ing. Dr.-Eng. Andreas Nascimento (UFES) who invited me to UFES Univerity in Brasil for testing the developed software (cancelled due to COVID-19).
- TDE Thonhauser Data Engineering GmbH Heads for supporting me throughout my study period and providing necessary resources for my studies and thesis.
- Equinor for providing opensource data (Volve).
- All colleagues from proNova Operations Department.
- Special thanks to the following colleagues: Miodrag Ivanovic, Dimitar Todorov, Prasad Zende and Uros Cendak who provided the base and technical support to this topic and its outcome.
- Stefanie Lindner (Mother) for her patience, Markus Lindner (Brother), Daniela Lindner (Sister) and Apollo (Dog).
- Wolfgang Lindner Senior and Elfriede Lindner (Grandparents) who inspired me to become an international engineer.

Contents

Chapter 1 Introduction.....	5
1.1 Overview.....	5
1.2 Motivation.....	6
1.3 Objective.....	6
1.4 Thesis Structure.....	7
Chapter 2 Abnormal Drilling Behaviors Verification Methods.....	8
2.1 Overview.....	8
2.2 Drilling Problems.....	9
2.2.1. Pipe Sticking.....	9
2.2.2. Differential Sticking	9
2.2.3. Mechanical Sticking	10
2.2.4. Tight Hole.....	12
2.2.5. Bit Balling	13
2.2.6. Matrix Losses	13
2.2.7. Kicks	14
2.2.8. Equipment Related Downhole Issues.....	15
2.3 Methods and Approaches used to Detect Downhole Problems	18
2.3.1 Torque and Drag as Index for Detecting Downhole Problems.....	18
2.3.1.1 The Principal of “Torque and Drag”	18
2.3.1.2 Torque and Drag Modeling	20
I. Soft-string Model.....	20
II. Stiff-string Models.....	23
2.3.1.3 Torque and Drag Simulation.....	24
2.3.1.4 Torque and Drag Real-time Monitoring	24
2.3.2 Standpipe Pressure as Index for Detecting Downhole Problems.....	26
2.3.2.1 Standpipe Pressure Modeling	26
2.3.2.2 Standpipe Pressure Simulation	29
2.3.2.3 Standpipe Pressure Real-Time Monitoring	30
2.3.3 Delta Flow for Detecting Kicks and Fluid (Matrix) Losses.....	32
2.3.4 Analysis of historical data (offset wells)	32
2.3.5 Machine Learning Approach.....	33
2.3.5.1 Overview	33
2.3.5.2 Machine Learning Approaches Applied for Drilling Parameters.....	33
2.3.5.2.1 Statistical Learning Models.....	33
2.3.5.2.2 Deep Learning for Torque Predictions.....	37
2.3.5.2.3 Lost Circulation Prediction Via Deep Learning.....	39
2.3.5.2.4 Drilling Hydraulic Optimization Via Deep Learning.....	41
2.3.5.3 Limitations of Machine Learning for Predicting Torque and Standpipe Pressure	44

Chapter 3 Developed Methodology to Detect Anomalies in Drilling Behaviors	45
3.1 Background	45
3.2 Data Processing	46
3.2.1 Data Acquisition	46
3.2.2 Data Selectivity.....	47
3.2.3 Data Handling.....	47
3.2.3.1 Outliers, Data Gaps, and Conversions	47
3.2.3.2 Raw versus Filtered Data	48
3.3 Building Predictive Model.....	48
3.3.1 ANN for Actual Time Prediction	49
3.3.2 ANN for Future Prediction	50
3.3.3 ANN for Future Trend Prediction.....	50
3.4 Construction of Uncertainty Windows	51
3.4.1 Overview.....	51
3.4.2 Extraction of Actual and Predicted Data.....	53
3.4.3 Compute Mean Squared Error (MSER).....	53
3.4.4 Obtain Standard Deviation.....	53
3.4.5 Create Windows.....	54
3.4.6 Compare Actual Data with Predictive Windows.....	54
3.5 Alert Level Definition and Activation.....	54
3.6 Standalone Application.....	54
3.6.1 Data Import and Filter	57
3.6.2 Train Torque Network.....	57
3.6.2.1 ANN for Actual TQA.....	58
3.6.2.2 ANN for future TQA prediction	58
3.6.2.3 ANN for Future Trend Prediction	58
3.6.3 Train SPPA Network.....	59
3.6.3.1 ANN for actual SPPA	59
3.6.3.2 ANN for Future SPPA Prediction	60
3.6.4 Calculate Torque Window	60
3.6.5 Calculate SPPA Window	61
3.6.6 TxD Plot Results.....	62
3.6.7 Advantages and Limitations of The Standalone Application	64
Chapter 4 Case Studies	65
4.1 Model Definition	65
4.2 Performed Scenarios	66
4.2.1 Excessive Torque.....	66
4.2.2 Decreased Torque	67
4.2.3 Excessive Standpipe Pressure	68
4.2.4 Decreased Standpipe Pressure.....	70
4.3 Case Study Conclusion.....	71

Chapter 5 Conclusions and Future Work.....	73
5.1 Conclusions.....	73
5.2 Future work.....	74

Chapter 1 Introduction

1.1 Overview

Drilling operations are always encountered with the risk of equipment, procedure, and downhole environmental related issues, which can influence drilling performance negatively and, in a worst-case scenario, lead to loss of the well being drilled. Common problems that are encountered during drilling formation can be classified into two categories, minor issues related to hole cleaning or bit balling, and major issues such as twist offs, stuck pipe, fluid losses, kicks, and critical hole conditions like a tight hole, washouts through to the collapse of the hole. It is important to understand that drilling problems appear at each well being drilled and can be mitigated to an acceptable level by keeping control over the drill string and downhole conditions. There are several routine options and state of the art procedures to detect or recognize potential risk and issues during drilling. However, most of them required human interference; hence, there is the potential of such risks being missed or might be recognized too late, and it will be no enough time to take the proper actions to reduce the impacts.

Continuously monitoring the surface torque and standpipe pressure data provides a good indication of the possible issues mentioned above; hence most of the existing methods that deal with identifying the downhole problems rely on these two parameters. In the state-of-the-art drilling industry, surface sensor data is used to apply simulation models and algorithms and to evaluate the actual data that is acquired, e.g., via WITSML real-time data streams.

- Torque and drag simulation vs. real-time monitoring
- Deterministic approach for pressure loss calculation
- Standpipe pressure simulation vs. real-time monitoring
- Analysis of historical data (offset wells)
- Machine learning approach

Torque and drag simulation and monitoring as a down-hole problem detection method were introduced decades ago. Different simulations are performed upfront to the good operations according to varying equipment and conditions that are being expected. Once drilling is performed, torque and hook load data are being recorded in real-time, and a data plot based on the actual data will be generated on the fly. The actual “torque and drag plot” can be compared to the simulated data, and deviations from the expected range and potential upcoming drilling issues respectively can be identified.

Major disadvantages of the torque and drag analysis are the required pre-work simulation on the one hand and that the required analysis parameters on the other. For example, once a component of the drill string is being changed, the simulated curve will not apply realistically anymore, leading to additional re-simulation work. Another disadvantage is that the actual torque and hook load data could potentially be misinterpreted due to invalid sensor data and human factors. If the simulation was done based on offset data, this applies another factor of uncertainty.

A common method to estimate the pressure loss of the system is a deterministic approach. It is a complex method with consideration of drilling mud rheology,

downhole conditions, and time-related effects on the mud properties and equipment related input. On the market, a wide range of hydraulic simulation software tools is available. Real-time applications use the streaming mud logging sensor data, that is, e.g., transmitted via WITSML or WITSO, as an input for the simulator and recalculate the pressure regimes.

1.2 Motivation

As it was clarified in the previous section, all of the mentioned methods have flaws; the points below summarize the most obvious ones:

- Manual input of some specific parameters that need to be identified in the laboratory and can often not be provided frequently to update the models.
- Lack of a systematic approach for filling up the missing data. As a result, relevant input data is reduced, or the filling is done by the human, which could lead to uncertainties due to invalidity and human factors.
- Use of the off-set well data as the main source for building the models. In most cases, such data never match the exact environmental conditions of another wellbore; hence its scope of application is limited to operational performance related analysis and planning, but not to downhole conditions related simulations in terms of health safety and environmental (HSE) aspects.
- For machine learning methods, usually, they used to fill data gaps in case of missing timestamps of a specific sensor data channel without considering possible deviations related to the uncertainty of the provided data. This gave the basic idea for extending sensor data-driven neural networks by calculating an operational window after comparing predicted and actual data to make the predictive model more effective.

1.3 Objective

The prime objective of this thesis is to develop a hybrid model that provides better accuracy in detecting abnormal behaviors of measured drilling parameters such as hook load, standpipe pressure, torque, flow-out, and validate the model by using made-up cases of manipulated data. It was decided to focus on torque and standpipe pressure data since these are significant for detecting and predicting the following drilling problems:

- Stuck pipe
- Losses
- Kick
- Tight hole
- Washout
- Hole collapse
- Hole cleaning
- Twist off
- Bit balling

In order to accomplish the prime goal of the thesis a set of sequential objectives were defined;

1. Data Collection: Get in touch with the supporting company with data enough for performing what is aimed. It should relate to at least sequential 03 (three) hours of drilling, or sequential drilling data of a drilled joint, as a minimum necessity. The more data is provided, the better it is.
2. Data filtering and processing: All data received may be susceptible to gaps, unreliable data-points, and outliers, needing filtering and processing in order to be able to be used for the purpose of the thesis. This is intended to be done with a developed script, allowing fast processing in a more automated manner.
3. Development of predictive model: The predictive model to be programmed using to be used is part of this step. Once data is collected and processed, several predictive models will be generated based on the number of drilling parameters to be studied.
4. Development of alert window sub-function and signs shown: Based on step 3 and as an enhancement of the coding, determination of window for triggering different alerts and also different levels is to be defined and implemented.
5. Stand-alone application: A user interface will be generated to provide a quick evaluation of real-time data.
6. Model Validation: At this stage, with all developed, the test is to be run, results analyzed, corrective measures applied. Tests will be performed based on historical datasets from Equinor's "Volve" open source.

1.4 Thesis Structure

The research was undertaken, which is covered in Chapter 2, prior to the development work for the creation of a standalone application. Starting with the most common issues arising in the daily business of a drilling rig, state of the art procedures for detecting those issues are explained in detail, as well as up-to-date developments in the field of machine learning approaches are introduced.

Chapter 3 gives insights into the methodology behind the developed standalone application. Data processing, building the predictive models, and statistical calculations are explained in detail. Considerations for triggering alerts and building the standalone application are illustrated further.

Finally, Chapter 4 compiles the results of a performed case study, where manipulated data was used to test the capabilities of the standalone application. Different scenarios have been created by manipulating original data sets without abnormal drilling behavior to evidently abnormal trends in the data channels is to be investigated.

Chapter 2 Abnormal Drilling Behaviors Verification Methods

2.1 Overview

This chapter provides an overview of common drilling problems, their prediction, detection, and mitigation methods of today's drilling industry. There are many problems that can occur whilst drilling is performed. Figure 1 illustrates an example for the distribution of root causes for average non-productive time (percentage compared to drilling days) compiled from 263 wellbores drilled over six years and below 600 feet water depth (waiting on environmental conditions excluded). It can be noticed that the majority of the problems are related to equipment failures and downhole issues, for instance, stuck pipe, stuck pipe, kicks, or loss of circulation.

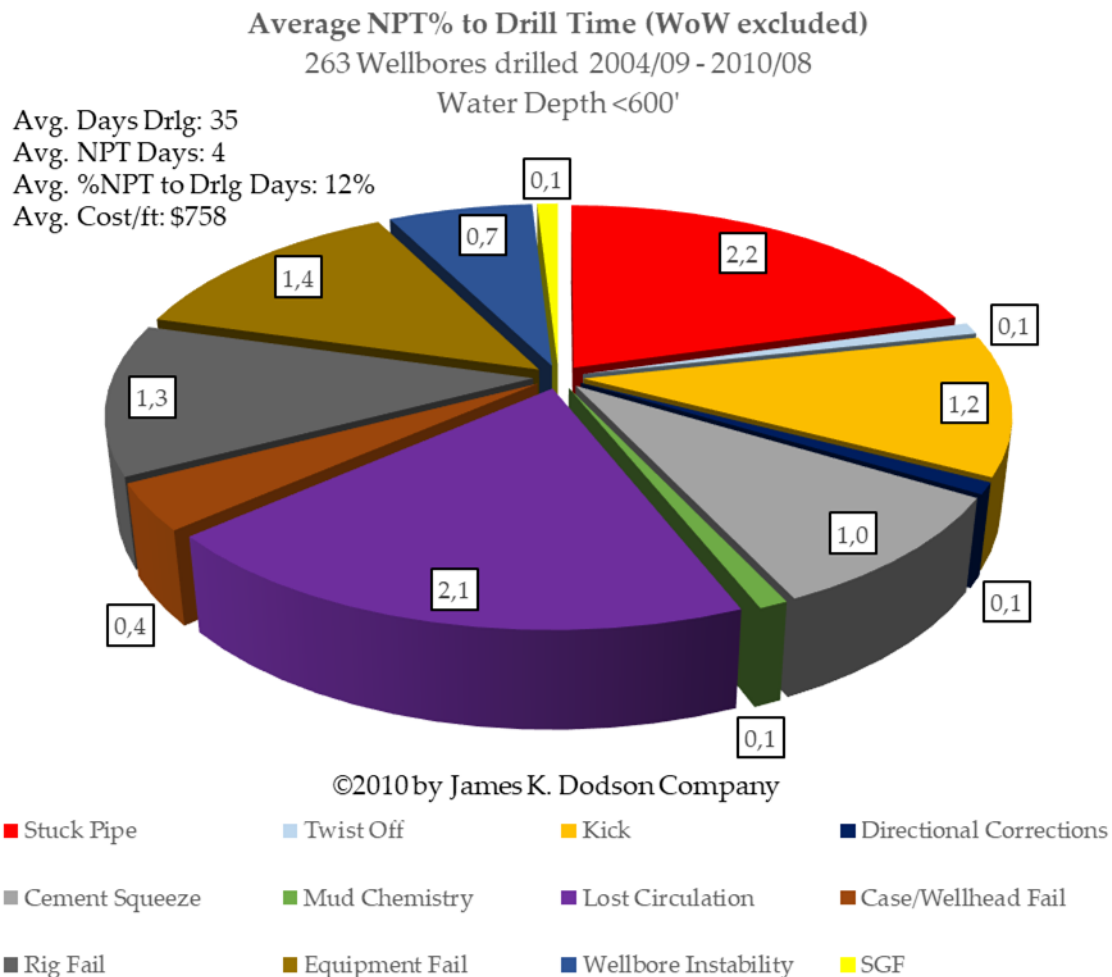


Figure 1: Example non-productive time (NPT) distribution (modified from Pritchard et al. 2012)

The main focus of the following subchapters lies in the explanation of the major issues that could be avoided by considering methods for verifying abnormal drilling behavior and techniques of monitoring torque and standpipe pressure trends.

2.2 Drilling Problems

2.2.1. Pipe Sticking

Pipe sticking is the major reason for causing the drill string to get stuck (stuck pipe). A differentiation between differential sticking that is induced by differential forces in the borehole and mechanical sticking, which the origin may be subsurface material (formation) or equipment related.

2.2.2. Differential Sticking

Differential sticking can occur when the drill string gets in contact with the filter cake. While normal drilling is carried out with slight overbalance (higher than the pore pressure of the formation and equal to the filter cake's differential pressure), once the drill string is partly embedded in the filter cake, the pressure will be different in the fluid surrounding the area of the string and therefore forcing it to get stuck with time.

Figure 2 illustrates the conditions that lead to differential sticking.

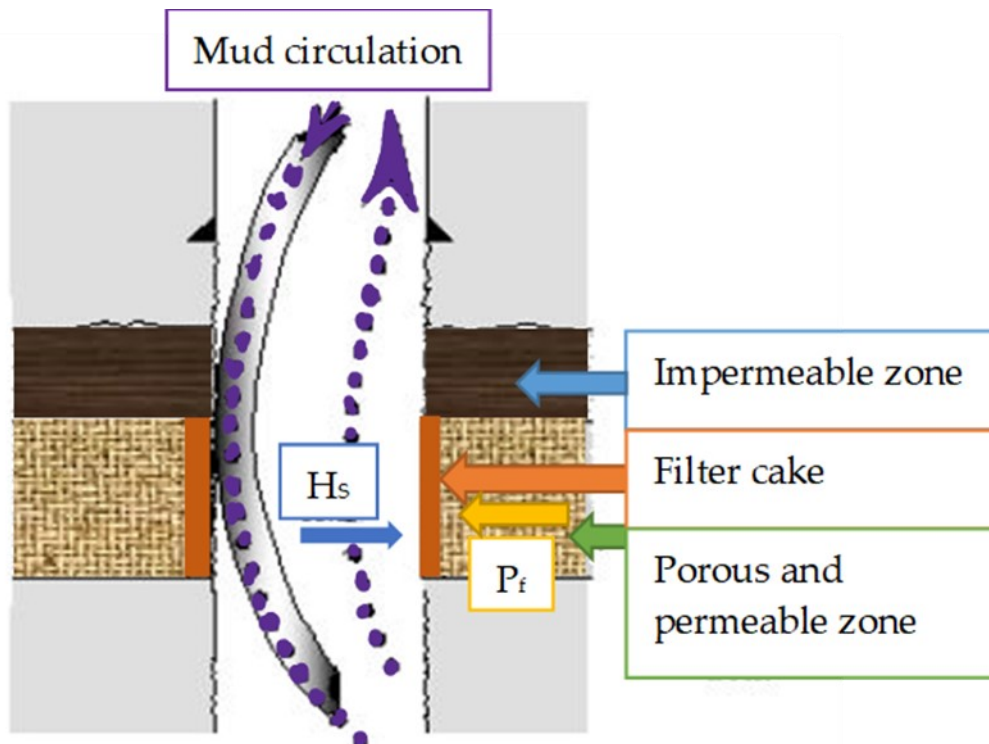


Figure 2: Differential sticking (Hussain Rabia, 2015)

It is important to mention that any differential force will add to the forces that are already present in the drill string related to the path and geometry of the well. The magnitude of overbalance and friction is critical to the magnitude of the differential sticking force (overpull). The friction factor is prone to increase over time. The following formula (1) considers pressure conditions and friction factor to calculate the differential sticking force.

$$DSF = (H_s - P_f) \times A_c \times ff \quad (1)$$

where DSF is the differential sticking force in lb., H_s the hydrostatic pressure of the mud, P_f the formation pressure in psi, A_c the effective contact area in in^2 (2) and ff represents the friction factor.

$$A_c = 2h \times \sqrt{\left\{ \left(\frac{H_s}{2} - t_{mc} \right)^2 - \left[\frac{H_s}{2} - t_{mc} \left(\frac{H_s - t_{mc}}{H_s - OD_p} \right) \right]^2 \right\}} \quad (2)$$

Where h is the thickness of the permeable zone, t_{mc} the thickness of the filter cake in inches and OD_p the outer diameter (OD) of the drill pipe or collars in inches.

Figure 3 shows an example of the magnitude of overpull at a contact perimeter of 1200 in^2 resulting in 1200000 lb.

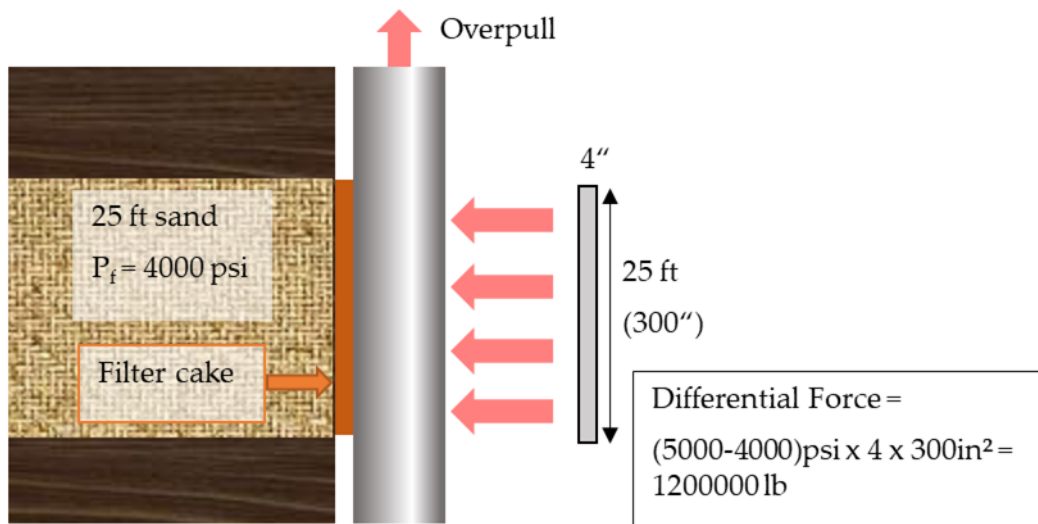


Figure 3: Magnitude of differential sticking force (Hussain Rabia, 2015)

The difficulty in early detection of differential sticking is that circulation will not be influenced (no change of surface parameters). The major indicator is an abrupt increase of surface torque values (torque and drag), in which the alerting period may be too short to prevent it completely from getting stuck. After differential sticking is being noticed, mud weight can be reduced while circulating to mitigate the symptoms; however, this method will increase the danger of an unrecognized kick. Other methods are displacing the choke with seawater (offshore well) and the U tube method (Hussain Rabia, 2015).

2.2.3. Mechanical Sticking

The leading cause of mechanical sticking is related to pack off or formation and bottom hole assembly (BHA). Partly collapsed hole material, as a result of insufficient hole cleaning or formation instability, is “bridging” around the drill string, where the pipe diameter changes downwards, or it is “packing off” between the borehole wall and the pipe shortly above the drill bit and prevents the ability to pull back-wards while rotating the string is still possible (overpull). Besides decreasing drilling performance, torque will increase before getting stuck. Hence torque and drag simulation and monitoring are commonly done, and the developed torque window could ease early detection of it. The following figure illustrates packing off and bridging behavior while drilling.

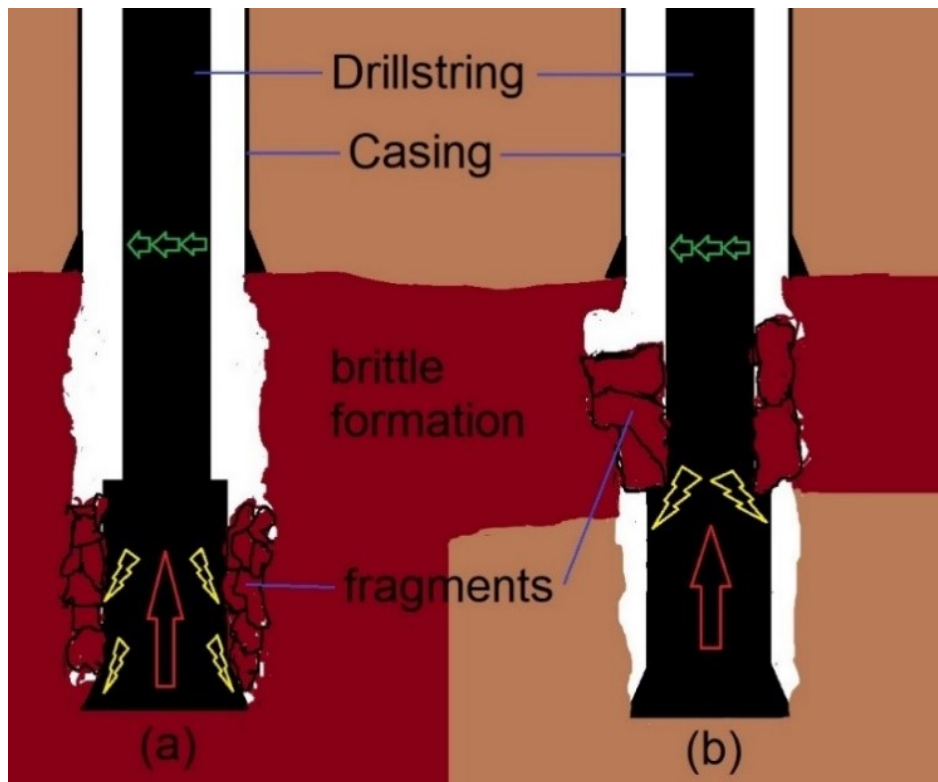


Figure 4: Sketch of "pack off" (a) and "bridging" (b) (Hussain Rabia, 2015)

Especially highly inclined wells tend to form cutting beds on the low side of the well while drilling, and removing them can be impossible. Once the string is being pulled, the cuttings bed will accumulate around the drill string and stuck the pipe mechanically (Hussain Rabia, 2015). Figure 5 shows how hole cleaning conditions change with the well paths deviation. While fast cleaning is appearing at lower inclinations ($<30^\circ$), the speed of cleaning may be reduced with increasing deviation. At the inclined section $>65^\circ$, a cuttings bed tends to be developed. Hence proper hole cleaning should be carried out according to the degrees of inclination and after guidelines for effective hole cleaning (Abdelaziz Gabr, 2017).



Figure 5: Guidelines for effective hole cleaning (Abdelaziz Gabr, 2017)

Referring to the conditions illustrated in Figure 5, well inclination and cuttings bed behavior can be categorized into three types (Type 1-3) (Asad Elmgerbi, 2019).

Type one (I) is valid for wellbore inclinations below 30° and can form pack-offs or bridging, as illustrated in Figure 4. Type two (II) is valid for an inclination of 30° - 65° . In such cases, the particles tend to move downwards again after a velocity decrease during uplift and due to gravity. The particles will be held in a state of local circulation between the drill string and the borehole wall and may lead to stuck pipe conditions due to accumulation. The particles will form accumulations, and the so-called phenomenon of avalanche effect can appear, whereas an abrupt downward movement of the accumulated cuttings is induced and will cause the drill string to be stuck.

Type three (III) is valid for highly inclined wells of more than 65° . The particles will form accumulations at the low side of the well. Pipe rotation is a critical parameter to avoid formation damage and viscous coupling of particles onto the drill string (maintain optimum RPM).

Reaming and circulating the hole clean needs to be performed carefully to avoid the cuttings bed to slide down (avalanching). A common procedure is to perform frequent short trips. Sufficient hole cleaning is highly related to the mud parameters, flow rate, the cuttings size, and their annular velocity and can be influenced by changing the mud system (fluid properties, rheology, additives, solvents, etc.), the setup of the bottom hole assembly (can cause dog legs, etc.) or hydraulics (pump rate, pump volume, etc.), hence proper prediction of the pressure losses of the complete system is obligatory.

In general, turbulent flow is desired for optimum hole cleaning behavior. However, for laminar flow regimes, the flow rate needs to be increased accordingly, although the optimum flow rate is hard to determine under realistic conditions (unconsolidated formations, cutting size, etc.) [Hussain Rabia, 2015].

The predicted standpipe pressure window could therefore improve procedures of adjusting the flow parameters at an early stage of developing hole cleaning problems, as the pressure losses are reflecting changes in the flow as well.

2.2.4. Tight Hole

Tight holes are usually developing in reactive formations (e.g., shales) and lead to restricted rotary or vertical movement of the drill string and may end up in stuck-pipe. The effect can be intensified by the particular sticking mechanism. The symptom can be detected by increasing, and erratic rotary torque and drag (overpull to lift the pipe or increased weight when lowering the pipe), as well as via monitoring the standpipe pressure (or pump pressure) since an increasing trend is a clear indicator of tight hole formation.

The swelling of shale appears when the filtrate from the drilling fluid is being absorbed and will lead to tight hole conditions. Hence it is critical to select the proper mud to mitigate chemical effects with the formation. Mud inhibitors and oil-based muds are used to lower the effect of swelling.

Over pressured formations, in other words, formations with a higher pore pressure than normal for the depth of their occurrence, are the result of incomplete compaction and de-watering during the burial process. These formations apply another source of tight hole condition and may be indicated by:

- increased pressure and reduction in hole size
- shale cavings are falling into the hole, which might accumulate on the bottom of the hole.

Tight hole conditions can lead to extended operational timings and a number of scheduled runs due to the necessity of additional reaming and hole cleaning operations (wiper trips or additional conditioning runs before drilling ahead), logging operations, and additional casings to be set as severe hole stability problems may occur.

2.2.5. Bit Balling

The symptoms of bit balling are close to that of forming a tight hole, whereas in such case, the BHA will be adhered to by the reactive formation material, and the bit nozzles may be plugged with time. Formations of low permeability are characteristic for bit balling conditions, shales for instance, which is strongly influenced and increased by its (sticking) clay mineral content (A. Hayatdavoudi, 2011).

The theory behind bit balling can be explained by the plasticity of the clays, which lead to a longer state of the plasticity of the shale before being hydrated to a liquid (less sticky state). "This extended plasticity state is believed to contribute towards cuttings becoming molded onto the steel parts of the bottom hole drilling assembly (BHA) and being plastered onto the walls of the wellbore." (G. De Stefano, S. Young, 2009).

Amongst other factors, the liquid and plastic limit depends on the type of the clay mineral (e.g., kaolinite or montmorillonite), clay fraction, and type of cations present and its radius. While Na^+ has the smallest impact on the PL/LL ratio, Al^{3+} has the largest on it. Mechanical force is reducing accretion and delaying it significantly with reduced magnitude.

The "stickiness" of the shale surface may be enhanced by additives that absorb surface water rapidly. The cuttings size is significantly influencing the accretion, whereas the accretion will be reduced over time with increasing cuttings size. However, at smaller cuttings size, the resulting greater surface area can lead to support plasticity and accretion to lower timings.

While on the one hand, water-based fluid systems and additives have improved wellbore stability whilst drilling; on the other hand, majority of non-productive time is related to bit balling. The standpipe pressure will rise due to the plugged nozzles and the resulting smaller annular diameter. Torque and drag will increase whilst pulling the string (overpull), and a higher weight needs to be applied on the bit. The drilling performance will be reduced dramatically (ROP); hence actions will be required (change mud properties, additives), including necessary extra trips to clean the bit.

Alternatively, to water-based drilling fluids, oil-based or synthetic muds can be used and will lower the risk of operational problems due to bit balling, agglomeration, and accretion of drilled cuttings. The use of oil-based and synthetic muds is often associated with higher costs for cuttings treatment, waste stream processing, compliance testing, and higher costs for the material in general (G. De Stefano, S. Young, 2009).

2.2.6. Matrix Losses

Loss of circulation describes the fluid being lost to the formation whilst drilling. Lost material is a major issue in terms of economics and health safety and environment (HSE).

There are various reasons for induced fluid losses. The loss can be due to the natural composition and geometry of the formation (porosity, permeability, brittleness, etc.), caused by the wrong drilling procedure or underestimation of the annular conditions (cuttings volume, pressure, etc.) respectively. Further, a tight mud window can lead to exceeding the (formation) fracture pressure. Fractures will be formed, and fluid will be lost. Besides mud rheology and pressure control, the volume of the cuttings in the annulus needs to be considered and can be determined by the following formula (3), which describes the ratio of the total mass to the total volume of the mud and cuttings (Hussain Rabia, 2015).

$$\rho_{eff} = \frac{\rho_m \times Q + 141.4296 \times 10^{-4} \text{ROP} \times d_b^2}{Q + 6.7995 \times 10^{-4} \text{ROP} \times d_b^2} \quad (3)$$

where ρ_{eff} is the effective mud density in the hole, ppg

ρ_m is the density of the mud at the surface, ppg

Q is the mud flow rate, gpm

ROP is the rate of penetration, ft/hr

and d_b is the bit size, in

The equivalent circulating density is given by summing up (4).

$$ECD = \text{static mud density} + \text{drillcuttings contribution} + \text{annular pressure loss contribution} \quad (4)$$

To reduce the loss severity while tripping, tripping speeds should be restricted whilst running into the hole (surge pressure), which can be monitored in real-time. The magnitude of the loss can be determined by the circulating pressure difference before and after the losses appear compared to the mud weight. Therefore, a predictive window for monitoring the pressure could advance the detection of losses.

In a case of fluid loss, the symptoms can be mitigated by reduction of the mud weight or using loss circulation material (LCM). An abrupt change in the monitored pressure loss (standpipe pressure) will clearly indicate abnormal circulation behaviors (losses) and may avoid kick situations. The methods of evaluating the pressure losses will be described at a later point in the thesis.

2.2.7. Kicks

Kicks are no big issue if control can be maintained, and the “unwanted influx from the formation” can be circulated out through the well control system after following the specific procedures accordingly. It is important to mention that when drilling with a bottom hole pressure (BHP) close to the pore pressure of the formation, so-called “mini Kicks” can appear at gas wells, which can lead to a misleading interpretation of the pressure readings. In case of a gas influx into the annulus, the standpipe pressure will decrease gradually (Anton Lettner, 2019). It is preferred to stay rather close to the pore pressure than to the formation fracture pressure since a kick may be easier to control than a fractured casing shoe (severe loss of the well operation) (Anton Lettner, 2019).

However, the main purpose is to avoid kicks completely, if possible. Hence the pressures need to be monitored at all times, and critical pressure changes should be recognized initially. If the fluid flow becomes uncontrollable, a “blowout” is induced either;

- on the surface (fluids flowing at the surface) or
- underground where fluids are flowing between subsurface formations.

Causes of kicks can be related to:

- the formation pressure
- insufficient hold fill while tripping
- swabbing while tripping (frictional pressure caused by mud movement whilst pulling the string leads to a reduction of mud hydrostatic).
- insufficient mud weight
- lost circulation
- excessive ROP through gaseous sands

The major reason for kicks is insufficient mud weight. The friction between the drill string and the borehole wall may also lead to a reduction (swab, whilst pulling out of a hole) or increase (surge, whilst running in a hole) of the BHP.

Amongst others (return flow, pit volume), kicks can be indicated by loss of circulation and an increase in torque and drag. This once more clearly shows the importance of monitoring pressure changes, torque, and drag. The most common signs of the kick are:

- increased ROP or drilling breaks
- falling pump pressure
- increase in mud flow from the annulus
- increase in pit levels
- gas cut, water cut, and salinity (reduction in the mud weight)

In general, once a kick was noticed (e.g., the flow was observed during a flow check), the mud weight needs to be increased after safely shutting in the well and circulating out the kick. There are standardized “killing” procedures for kick situations by the International Association of Drilling Contractors (IADC) and the International Well Control Forum (IWCF).

2.2.8. Equipment Related Downhole Issues

While issues related to the bottom hole assembly (BHA), such as bit damages (nozzles) or twist-offs, can be indicated by an abrupt decrease of the standpipe pressure, developing washouts are indicated by a gradual decrease. Washouts can lead to severe additional stresses under compression and result in drill pipe failure.

Key seats or doglegs may be formed by the couplings (joints) of the drill string, touching the borehole wall whilst pulling out of the hole. The location of potential doglegs is usually known upfront and can be monitored via torque and drag to prevent the stuck pipe during tripping operations (increase in drag). Figure 6 illustrates the formation of a key seat whilst pulling out of the hole by the smaller diameter of the pipe rotating

against the borehole wall. The string can be caused to get stuck when, e.g., a stabilizer is reaching the spot, and a sudden overpull will be experienced. Another indication may be either constant or increase in standpipe pressure will be experienced due to unrestricted circulation (Colin Bowes, Ray Procter, 1997)

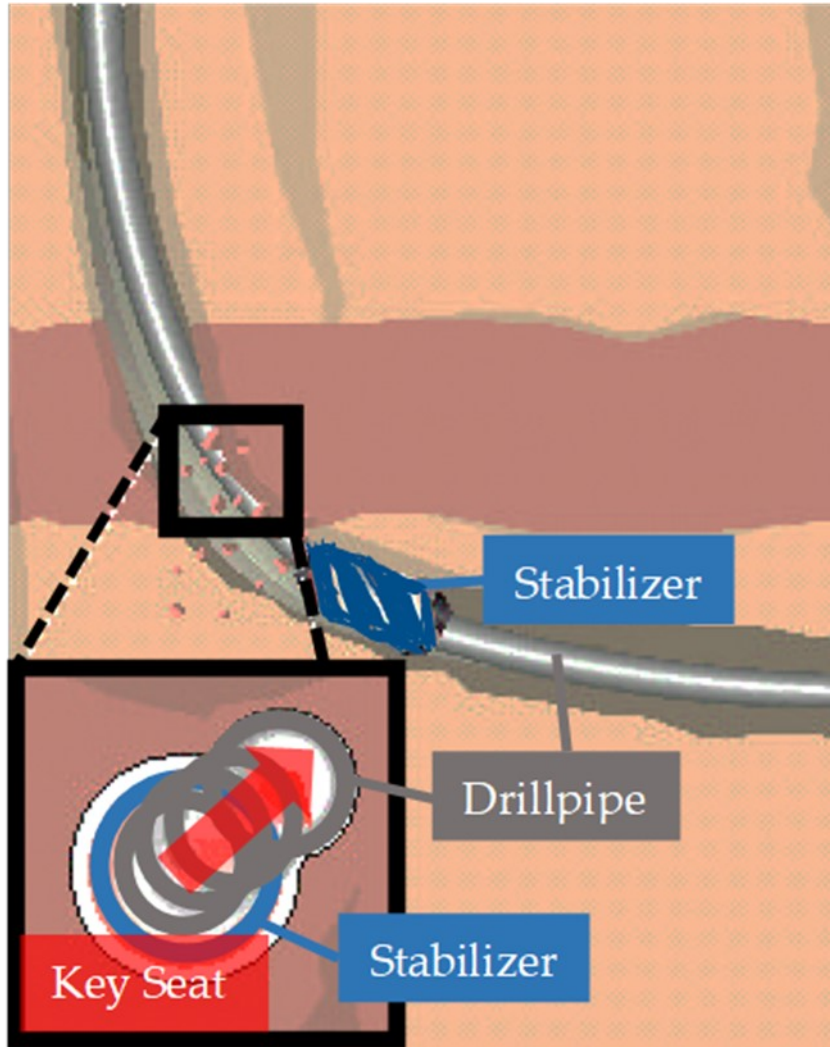


Figure 6: Formation of a key seat (Sedco Forex, 1997)

Doglegs (Figure 7) tend to form in varying formation layers (e.g., soft and hard formation beds) that force the drill string to change the direction (accidentally) and are often related to unsuitable setups of the BHA, too frequent change of BHA or too frequent or abrupt changes in the direction of the rotary steerable system (RSS).

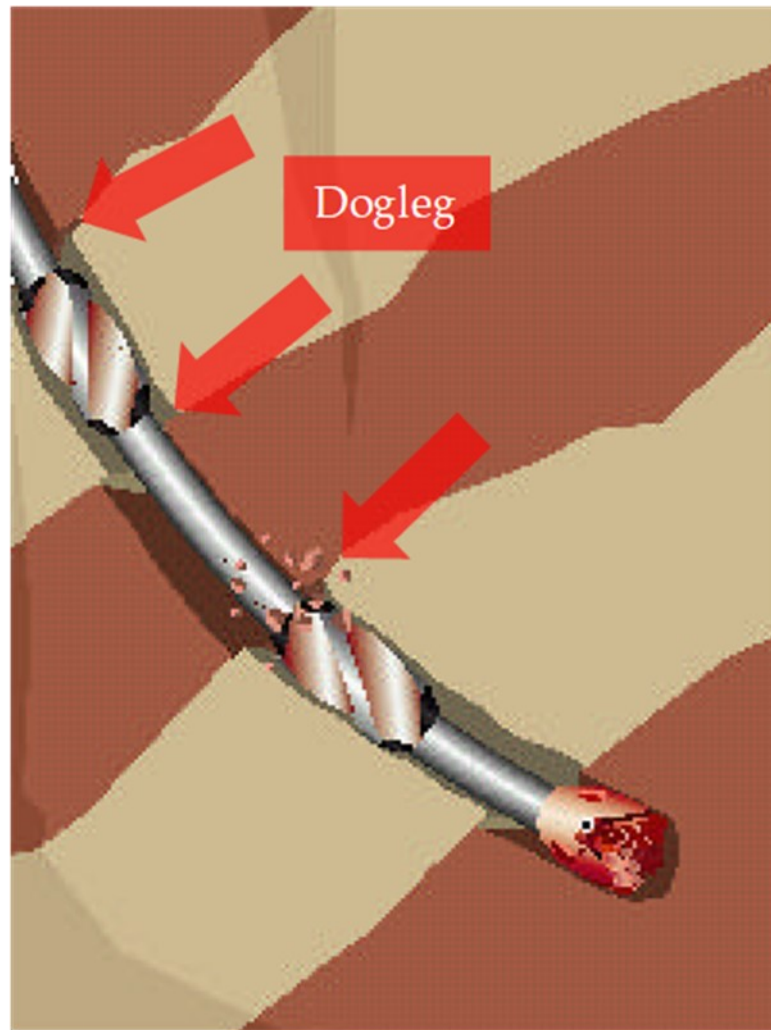


Figure 7: Formation of a dogleg (Sedco Forex, 1997)

Dogleg severity is calculated during the planning stage of a wellbore (drill string design), considering the maximum allowable bending in the drill pipes and couplings.

While key seats and doglegs can only form whilst pulling out of the hole, change of the bit (e.g., PDC after roller cone) can cause under gauge hole conditions. Bit wear or coring bottom hole assembly (BHA) can result in under gauged hole diameters, and the post-run BHA can jam into it, causing severe equipment failures. Reaming should be performed after coring and in danger of under gauging conditions. Stabilizers and protected equipment should be used. Frequent logging runs should be carried out at varying formation conditions to evaluate the well path for restrictions or obstacles.

Indications are under gauged parts of the BHA, sudden decrease of the string weight up to experienced stuck pipe while the circulation shows rather unrestricted (Colin Bowes, Ray Procter, 1997). A critical issue related to human factors is dropped objects in the wellbore, which can lead to a significant amount of non-productive time due to additional operational runs (fishing runs). An incident of a so-called “junk” is caused by non-compliance with the health, safety, environmental, and quality (HSEQ) regulations on the rig floor. Hence such incidents (and near incidents) should be tracked and evaluated properly.

2.3 Methods and Approaches used to Detect Downhole Problems

2.3.1 Torque and Drag as Index for Detecting Downhole Problems

2.3.1.1 The Principal of “Torque and Drag”

Torque and drag planning, monitoring, and analysis are essential for safe drilling operations. The principals and applications in the drilling industry are explained in the following subchapters. The principle of torque and drag is well known and is already applied in the drilling industry for decades; it is related to kinematics. The base calculations can be traced back to the free body diagram in Figure 8 that illustrates the forces acting on a body on an inclined plane. Since the body of a drill string will be in motion, friction forces need to be considered. Friction acts in the opposite direction of the motion, hence whilst running in the hole, it acts upwards (Figure 8) and downwards whilst pulling out of the hole.

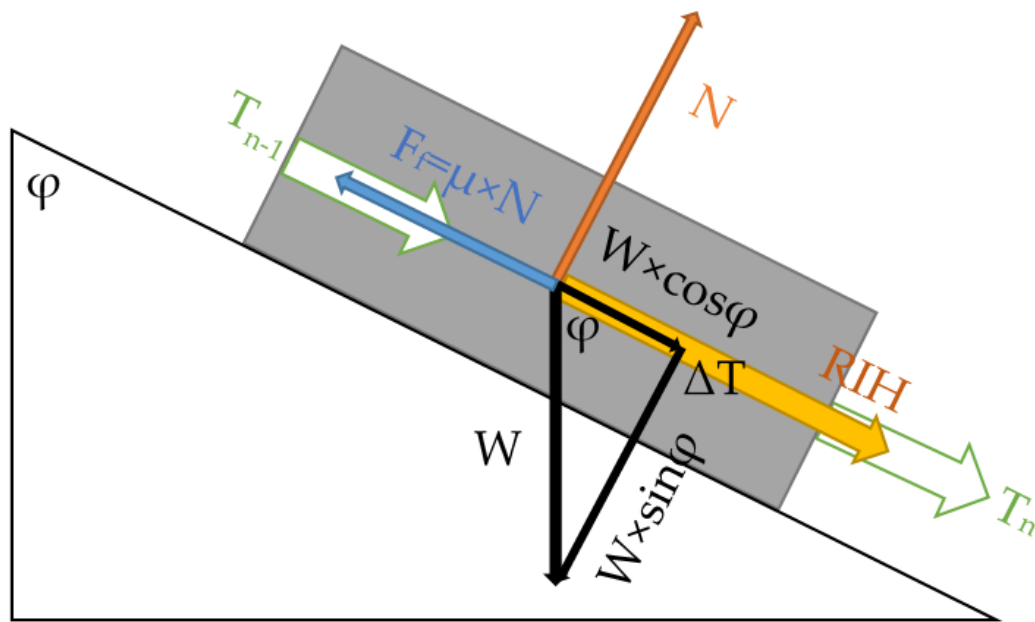


Figure 8: Free body diagram of a moving body on an inclined plane ($\mu = \mu_k$).

The resulting force for running or pulling is given according to the sketch.

$$F = \Delta T \pm F_f \quad (5)$$

Where F is the force required to move the pipe in the specific direction, F_f the friction force, N the normal force, W reflects the buoyed weight, and therefore the axial tension ΔT is given, and the formula can be solved as followed.

$$F = W \times \cos\phi \pm \mu \times W \times \sin\phi \quad (6)$$

The following table shows the default values for the (kinematic) friction coefficient μ . The friction factors can vary significantly under realistic conditions and should be obtained as accurately as possible from field measurements.

Mud Type	Cased hole (CH)	Open hole (OH)
Water based mud (WBM)	0.24	0.29
Oil based mud (OBM)	0.17	0.21
Brine	0.30	0.30

Table 1: Default friction factors based on historical well data (M.L. Payne & F. Abbassian 1996)

Drag is an axial-force generated due to friction between the drill string and the borehole wall. To calculate the drag of a specific drill string element, starting from the bottom where the drag force will be equal to weight on bit (WOB), the resulting formula can be generated from the free body diagram (Figure 8).

$$T_{n-1} = T_n + \Delta T - F_f = -WOB + \Delta T - F_f \quad (7)$$

Especially at extended reach wells, drilling drag is very critical due to the excessive compressional forces (axial) in the drill string during running into the hole or whilst sliding drilling. When reaching critical loads (increasing WOB), buckling will be induced to drill string and lead to additional stresses that may result in drill pipe failure and fatigue, respectively.

Figure 9 shows different scenarios of buckling, depending on the magnitude of WOB.

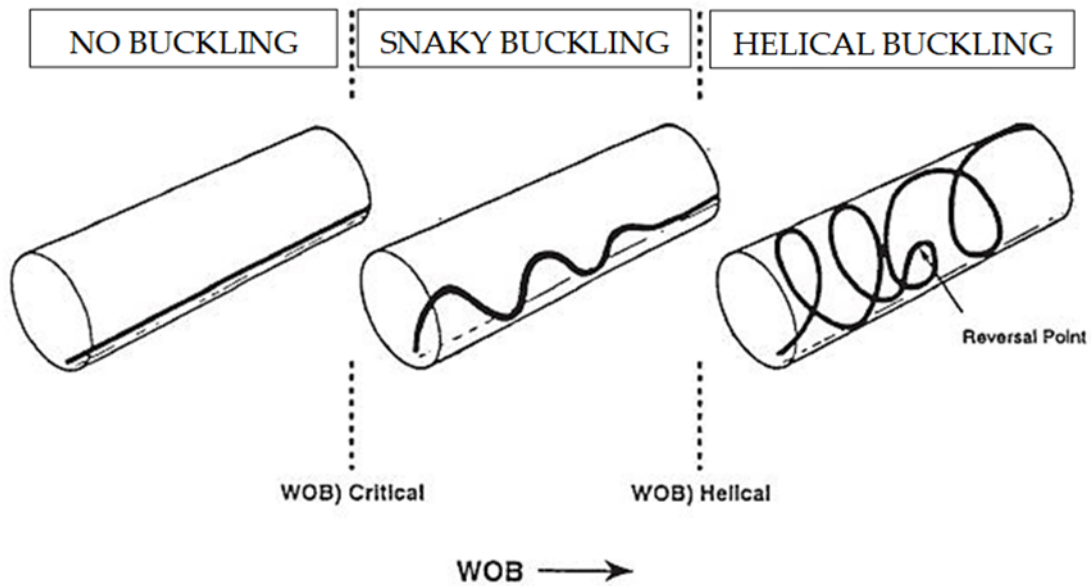


Figure 9: Drill string buckling behavior under increasing compressive load. (M. L. Payne, Fereidun Abbassian, 1997)

Torque measurements provide a lot of information about the downhole conditions whilst ongoing drilling operations. Torque is created by the friction when the rotating drill string gets in contact with the borehole wall. The sketch in Figure 10 illustrates the forces and torque on a rotating drill pipe.

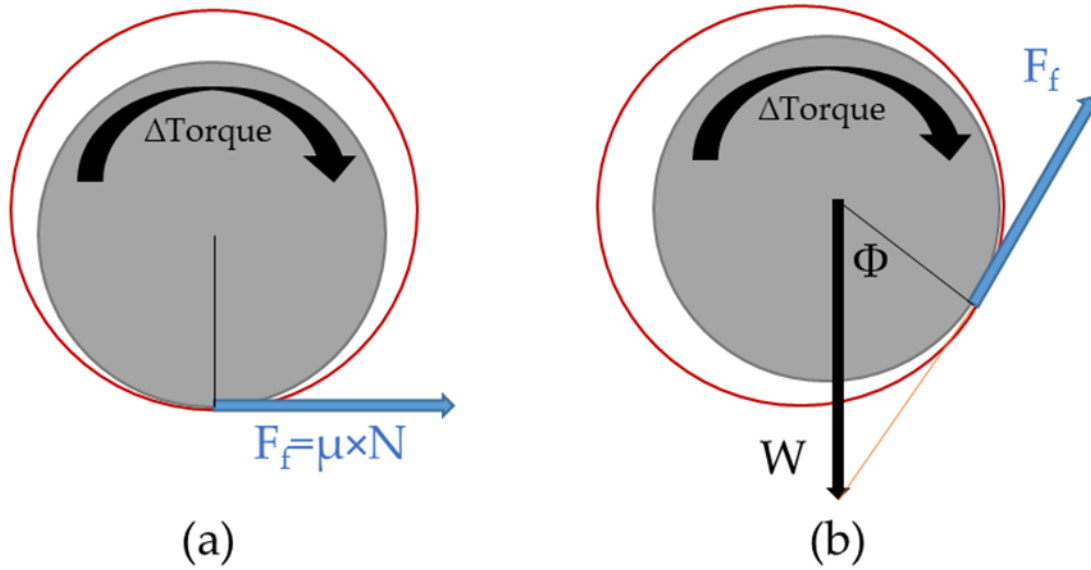


Figure 10: Torque on a rotating drill pipe at a low well inclination (a) and high well inclination (b) section ($\mu=\mu_k$).

$$\Delta Torque = F_f * DP_{OD} = \mu \times N \times DP_{OD} \quad (8)$$

where

DP_{OD} is the outer diameter of the drill string element.

Considering an uplift of the drill string to the high side of the well the torque can be calculated as followed.

$$\Delta Torque = W \times \left(\frac{DP_{OD}}{2}\right) \times \sin\Phi \quad (9)$$

where

$$\Phi = \text{atan } \mu \quad (10)$$

2.3.1.2 Torque and Drag Modeling

Torque and drag modeling are the pre-calculation of a drilling scenario in terms of equipment and operations related limits in order to provide a safe drill string design that considers tension and compression whilst running in the hole (RIH), pulling out of hole (POOH) and drilling compared to buckling limits (vibrations) that were evaluated by calculation of appearing torque and forces.

There are two major models for calculating torque and drag:

- Soft-string model
- Stiff-string model

I. Soft-string Model

The soft string model considers a simplified picture of the drill string as a uniform weighted steel chain without joints or clearance. It further neglects any deformation of the drill string (no stiffness, no bending). Besides the critical considerations, which can lead to underestimation of buckling prediction, the model can be applied below a build of $1.5^\circ/100\text{m}$. Figure 11 illustrates the forces on the drill string during pick up and the

prediction of buckling can be calculated by the previous explanations and additional formulas given below. The method is applied by starting from the bottom of the string and calculating torque and drag for each element (drill collars, heavy-weight drill pipes, drill collars, etc.) until the top and summation of the results afterward.

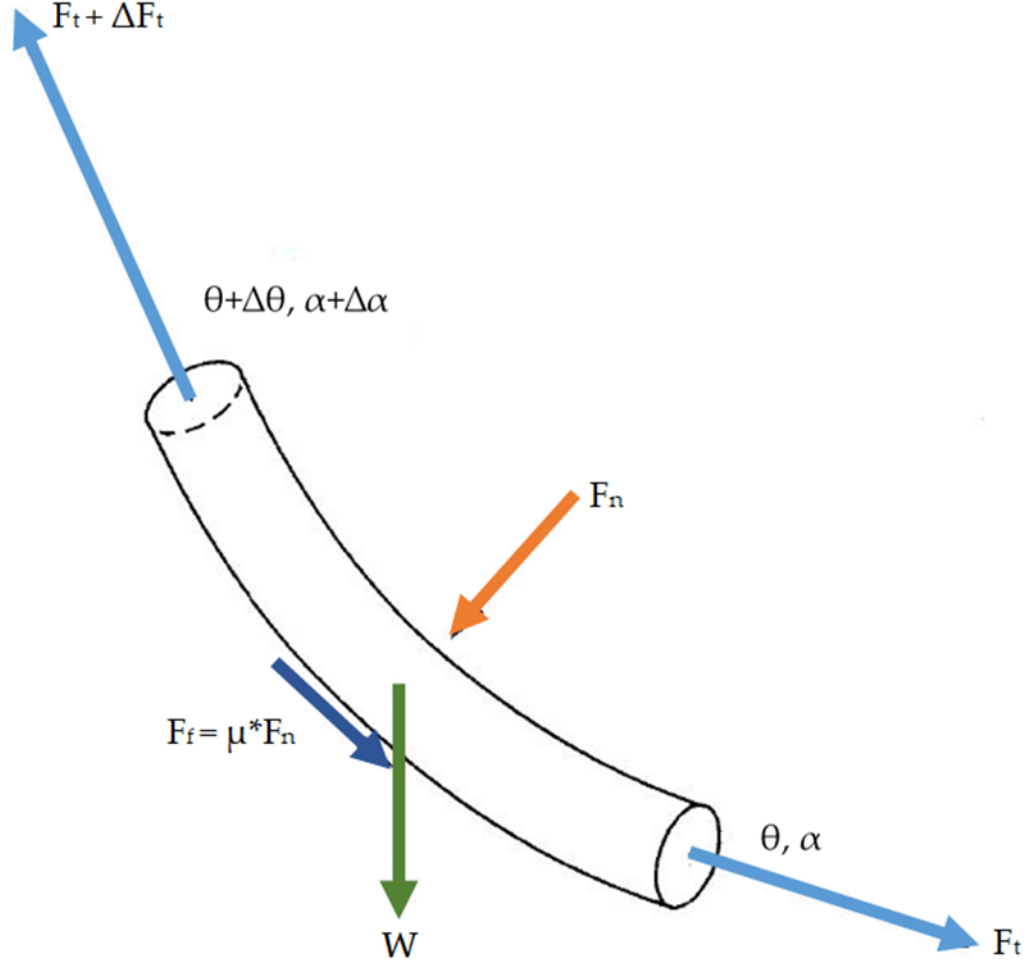


Figure 11: Forces acting on drill string element during pickup. (C.A. Johancsik, D.B. Friesen, Rapier Dawson, 1984)

Buckling Limits (by Dawson-Pasley):

$$OH: r = \frac{1}{2} \times (BH_D - DP_{OD}) \quad (11)$$

$$CH: r = \frac{1}{2} \times (CSG_{ID} - DP_{OD}) \quad (12)$$

$$I = \frac{\pi}{64} \times (DP_{Pipe}^4 - ID_{Pipe}^4) \quad (13)$$

$$F_{crit,sin} = -2 \times \frac{\sqrt{E \times I \times W_e \times \sin \theta}}{r} \quad (14)$$

$$F_{crit,hel} = (2\sqrt{2} - 1) \times F_{crit,sin} \quad (15)$$

where BH_D is the borehole diameter, CSG_{ID} the inner diameter of the casing, E the E-modulus for steel = $2,06843 \times 10^{11}$ Pa, I the moment of inertia, W_e the unit weight [N/m], F the critical forces where sinusoidal and helical buckling may occur.

The following information is required as input for each element of the drill string to the model:

- MD
- Trajectory
- Inclination
- CH or OH
- Friction coefficient
- Torque at bit
- WOB
- Young's Modulus
- Mud and steel density
- Buoyancy factor
- Casing and well diameter
- Pipe specification

After the required data was obtained, the calculation starts from the bottom up:

- Weight per element in the mud
- Normal force
- Tensional force
- Friction force
- RIH force
- POOH force
- Torque

The next step is to calculate the load profile by the cumulation of:

- RIH force (RIH profile)
- POOH force (POOH profile)
- Drill with WOB profile (formula (7), start with WOB and torque at bit)
- Torque (Torque profile)

Finally, the critical buckling limits can be calculated and can be compared in a tension and compression plot (Figure 12). The curves for RIH (dark blue), POOH (red), and drilling (light blue) must not exceed the curve for helical buckling (purple). Sinusoidal buckling (green) allows tolerances but may be avoided if possible. It can be noticed that the profile changes from tensional conditions (positive area) to compressional conditions (negative area) at approximately 2200 meters. This point is called the neutral point and appeared exactly at the kickoff point (KOP, end of vertical section), where the first contact of the drill string with the borehole wall is considered within the soft-string model.

In case a curve exceeds the limits, the setting of the drill string can be changed by varying available pipe specifications and repeated until the model shows a safe profile. The planning needs to be done realistically (e.g., avoiding HWDP in horizontal sections), and the number of different used pipe gradings may be kept small.

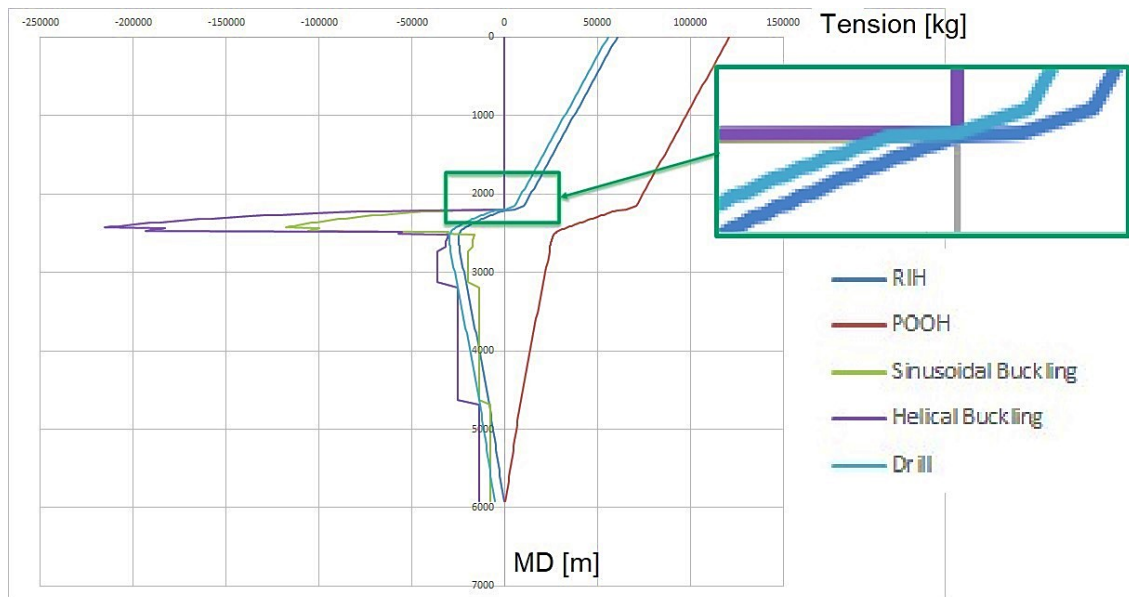


Figure 12: Example of a tension and compression plot for a planned drill string (soft-string model)

II. Stiff-string Models

Stiff-string models consider bending stiffness of the drill string elements, clearance, contact, and mechanical integrity for calculating the tension and compression curves. A stiffness-factor can be added to the soft-string model. The soft-string model tends to become inaccurate with increasing compressional conditions, and the difference between stiff and soft-string can be significant.

Many different models for stiff-string were created, and their approach is not always the same. In general, the importance of stiff string models was growing when horizontal wells were becoming industry-standard e.g., HWDP and drill collars are being run in compressional sections frequently; the goal was to overcome the poor results of the soft-string model for stiff tubular, high dogleg severity or narrow radial clearance. To name outstanding stiff-string models:

- Inclusion of bending stiffness:
They generally improved the soft-string model by adding BHA specific calculations for stiffness and considering different approaches for directional surveys (Mirhaj, S. A et al., 2016) but still neglecting clearance.
- Inclusion of radial displacement:
Analytical and finite element models that consider both bending stiffness and radial displacement.
Finite element analysis model for the radial displacement of the casing .
- Dynamic stiff string model [Vadim Tikhonov, et al., 2013]

As these models have been discussed in previous publications, a detailed description will not be given at this point.

2.3.1.3 Torque and Drag Simulation

Software tools apply a similar approach of torque and drag modeling, explained in the previous chapter, and are capable of simulating it for multiple scenarios and conditions in a short time. The simulated scenarios may further be updated whilst ongoing operations after input of actual measurements and real-time data in an automated way, which is a clear improvement to the manual approach that was done in the past. A wide variety of simulation tools is available on the market, which makes it easy to generate torque and drag and buckling prediction plots, that can be used for a safe drill string design. In general, the tools use a similar approach based on the fundamental kinematic equations that were explained earlier. An outcrop of simulated torque and drag broomstick plots is shown in Figure 13. The different colored lines are indicating different simulated operational loads and torque in terms of moving the drill string upwards (red), downwards (blue), or rotating it on the bottom (green) for varying friction factors in cased and open hole (varying line formatting).

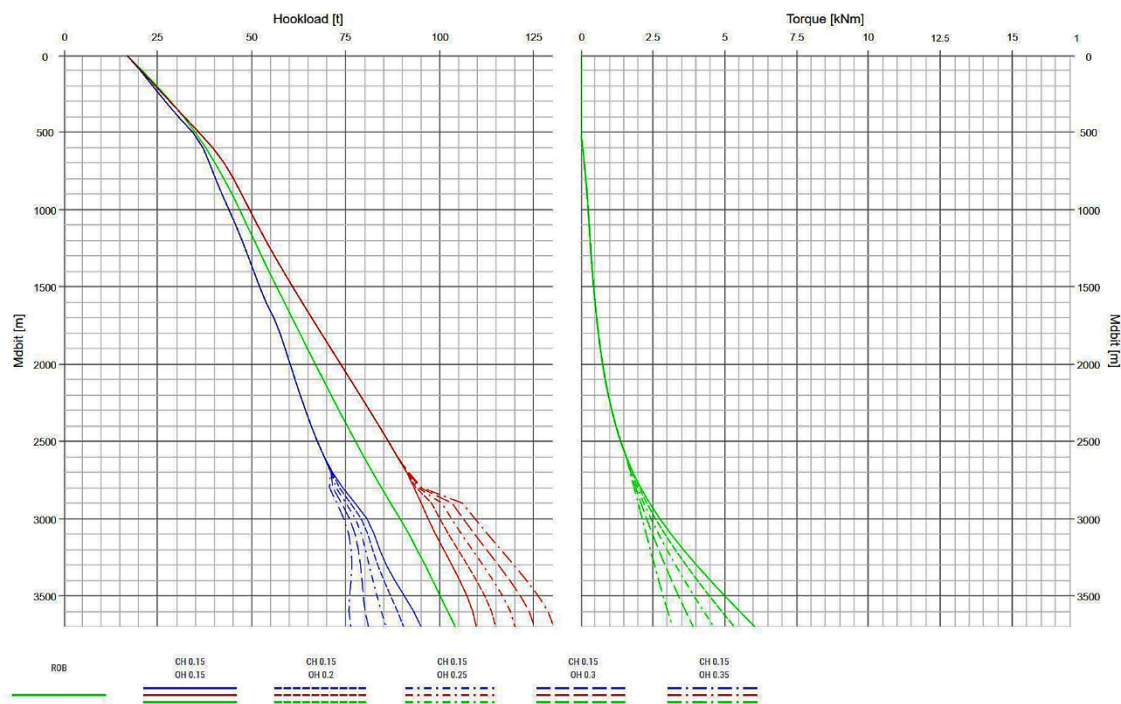


Figure 13: Simulated torque and drag broomstick plots, indicating simulations for RIH (blue), POOH (red), and ROB (green) for the different cased hole (CH) and open hole (OH) friction factors (number beside CH and OH) (©proNova by TDE)

2.3.1.4 Torque and Drag Real-time Monitoring

The simulated curves can be used to monitor and identify abnormal behavior of the sensor data channel trends in real-time. The surface sensor data channels that are available via a standard real-time WITSML data provider setup are:

- Hook-load
- WOB
- Torque (surface)
- SPP
- Flow in

- RPM
- ROP
- Block position
- Bit and hole depth

The following figure shows a monitoring plot of simulated vs. actual sensor data (red, blue, and green markers) and indications for abnormal behavior. It plots frequent sensor data channel points (usually average values) of torque and hook-load for RIH, RIH with rotation, POOH, POOH with rotation, and whilst drilling in real-time. Rig state detection algorithms and alerts are used to notify the personnel of any deviations from the simulated trends. A deviation of torque at a measured depth between approximately 3300m and 3500 m can be spotted for spacing out, picking up, and rotating on the bottom in the example. The simulated curve should be updated as often as possible, and if the deviation is maintaining, the driller should act accordingly in order to prevent possible upcoming incidents.

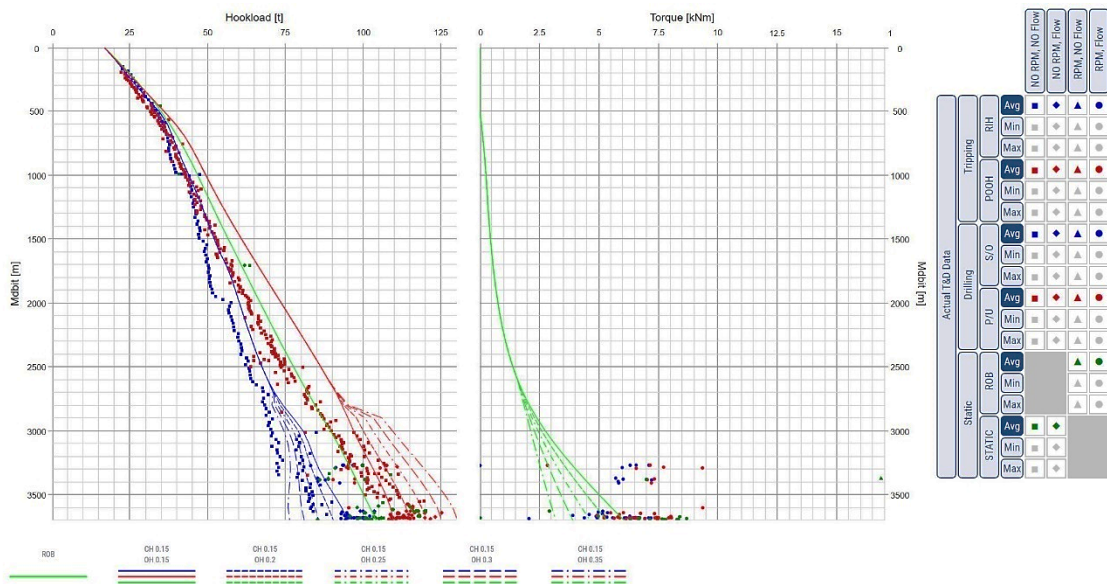


Figure 14: Torque and drag real-time data vs. simulated curves (©proNova by TDE)

There are tools available that update the friction factor based on the measured sensor data frequently and calculate it via iterations, e.g., until the actual HKLD matches the predicted one. This method is called “Torque and Force Method” [Frank Reiber (Baker Hughes Inteq), Bart E. Vos (Baker Hughes Inteq), Svein E. Eide (Statoil), 1999]. Besides, the real-time friction factor calculation for other surface and downhole parameters may be used as input at the rig site and improve the quality of problem indications.

Dogleg severity plots are used in addition to identifying possible obstacles in the wellbore (Figure 15).

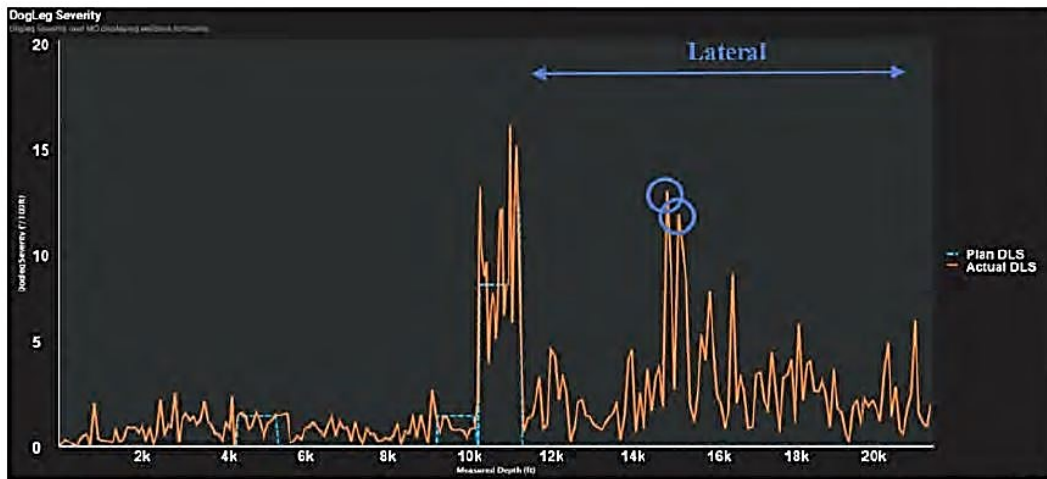


Figure 15: Dogleg severity for entire well - planned vs. actual (Eddie Martinez et al., 2020)

Tests have been performed on models that use downhole measurements (e.g., torque at the bit). However, it needs to be carefully considered that measurements at the bit are highly influenced by downhole conditions, and the error may be high as, e.g., vibrations in the drill string can add up to the measured (real) torque at the bit and therefore make the values useless for HSE-related monitoring purposes. One major problem of nowadays torque and drag monitoring procedures is the dependency on multiple parameters, meaning that there can be significant differences in the predictions and possible misinterpretation of the results (human factor).

2.3.2 Standpipe Pressure as Index for Detecting Downhole Problems

2.3.2.1 Standpipe Pressure Modeling

A proper determination of the pressure drop in the wells system is not only vital for safe planning and realization but also for improvement of drilling performance. The deterministic approach considers onsite measurements of the drilling mud composition, etc. and applies laboratory tests for tracking hydraulic conditions and to monitor pressure losses over the complete period of ongoing well operations. Since annular pressure drop is the critical component of pressure drops to be evaluated and the other components were discussed in detail in previous papers already, the description in this thesis is limited to the methodology of the annular section.

It is critical to consider the correct models and procedures related to the fluid system. The pressure losses vary significantly for different rheological models and equivalent diameter definitions at different operating conditions. The importance of determining the pressure losses during drilling fluid circulation is related to the influence on ECD, as the mud window must not be exceeded.

Considering rather non-newtonian than Newtonian fluids in the wellbore annulus under realistic conditions, the applied rheological models are:

- Bingham Plastic

$$\tau = \tau_0 + \mu_p \times \gamma \quad (16)$$

- Power Law

$$\tau = K \times \gamma^n \quad (17)$$

- Yield Power Law

$$\tau = \tau_0 + k \times \gamma^n \quad (18)$$

where μ_p = Plastic viscosity [cp]

τ_y = Yield point [lbf/100ft²]

γ = Shear rate [s⁻¹]

τ = Shear stress [lbf/ft²]

Which differ basically in their relationship between friction factors, velocities, diameters, shear stress, and shear rate. They also reflect the viscosity of the drilling fluid and its hole cleaning ability.

After the proper model was chosen, the flow regime needs to be defined and is achieved by determination of the critical Reynolds Number (laminar below 2100 or turbulent flow above 2100). For the pressure loss calculation in the annulus, laboratory tests with the rotational viscometer are performed at different rotations per minute (θ) to provide the rheological parameters for the respective model. Where the plastic viscosity and yield point are determined:

$$\mu_p = \theta_{600} - \theta_{300} \quad (19)$$

$$\tau_y = \theta_{300} - \mu_p \quad (20)$$

The power law rheological parameters in the annulus are determined as followed:

- For high shear rate:

$$n_{HS} = 3.32 \log \frac{\theta_{600}}{\theta_{300}} \quad (21)$$

$$K_{HS} = \frac{5.11 \theta_{600}}{1022^{n_{HS}}} \quad (22)$$

- For low shear rate conditions in the annulus:

$$n_{LS} = 0.657 \log \frac{\theta_{100}}{\theta_3} \quad (23)$$

$$K_{LS} = \frac{5.11 \theta_3}{5.11^{n_{LS}}} \quad (24)$$

where

K_{HS} = High shear consistency index [eqcp]

K_{LS} = Low shear consistency index [eqcp]

n_{HS} = High shear flow behavior index [-]

n_{LS} = Low shear flow behavior index [-]

Equivalent diameters are used to perform a comparative comparison of pressure losses of different sections. Annular pressure loss gradients versus flow rates can be determined for each section and further the effect on total pressure loss.

- Hydraulic Diameter:

$$d_e = 4 \times r_H = d_o - d_i \quad (25)$$

- Crittendon⁷ Criteria:

$$d_e = \frac{1}{2} \times \left[\sqrt[4]{d_o^4 - d_i^4 - \frac{(d_o^2 - d_i^2)}{\ln\left(\frac{d_o}{d_i}\right)}} \right] + \frac{1}{2} \times \sqrt{d_o^2 - d_i^2} \quad (26)$$

- Slot Approximation:

$$d_e = 0.816 \times (d_o - d_i) \quad (27)$$

- Lamb¹⁸ Approach:

$$d_e = \sqrt{\left[d_o^2 + d_i^2 - \frac{(d_o^2 - d_i^2)}{\ln\left(\frac{d_o}{d_i}\right)} \right]} \quad (28)$$

where

d_e = Equivalent diameter [in]

d_i = Drill pipe or collar outer diameter [in]

d_o = Wellbore or casing inner diameter [in]

K = d_i/d_o ratio [-]

The frictional pressure loss inside an annulus using the slot approximation:

$$\frac{dP}{dz} = \frac{f_f \times \rho \times v_a^2}{25.81 \times (D_o - D_i)} \quad (29)$$

Where ρ is the static density, v_a is the average annular velocity, and f_f is the friction factor. The friction factor is changing significantly with the flow regime and pipe rotation, respectively. Figure 16 shows a sample plot for determining frictional pressure loss gradients at varying flow rates based on a drill collar section on the explained methodology.

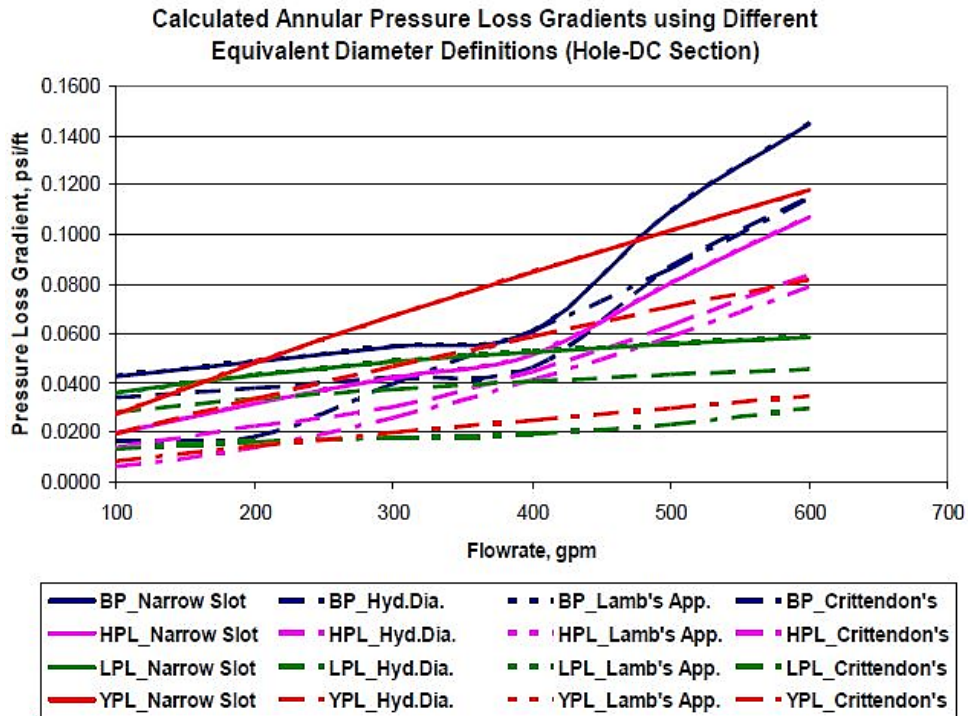


Figure 16: Example for pressure loss gradient analysis at open hole - drill collar annular section ($K=0.735$) (Demirdal, B., & Cunha, J. C. S 2007)

After the determination of the annular pressure loss, the total pressure loss of the system can be calculated by summing up the components.

$$\Delta P = \Delta P_{Hydrostatic} + \Delta P_{DP} + \Delta P_{BHA} + \Delta P_{Bit} + \Delta P_{Annulus} + \Delta P_{Surface\ Tools} \quad (30)$$

The major problem for the deterministic approach is the consistency in the required measurements to be performed (uncertainty of parameters), time, and human factors (misinterpretation). Temperature profiles and alteration of the mud system add up possible errors to the calculation.

2.3.2.2 Standpipe Pressure Simulation

Similar to torque and drag simulation software tools, there are a variety of hydraulics simulators available on the market. The majority use the input parameters similar to the deterministic approach and compute the pressure loss for the desired component. Hence, the computation of the results was digitalized and enhanced.

The computed pressure loss is used for evaluation of the actual pressure readings at the pressure gauges or of the real-time sensor data channel stream. Monitoring and analysis of standpipe pressure provide information on the efficiency of the hole cleaning and may indicate major upcoming drilling problems.

Figure 17 shows calculated pressure loss curves based on the rheological models vs. actual measurements. The curves were computed by a simulator that requires the input well information and parameters from the laboratory (viscometer). The rheological model that fits best with the actual curve can be applied for further downhole condition interpretation and hence for standpipe pressure evaluation in real-time. It can be seen that while at shallow depth, the simulation after Herschel Bulkley (purple) fits best, the power-law model simulation (yellow) is closest to the actual measurements (black) with

advancing measured depth and should therefore be used for further monitoring purpose of the ongoing operations [K. Ayeni, S.O. Osisanya (The University of Oklahoma), 2004].

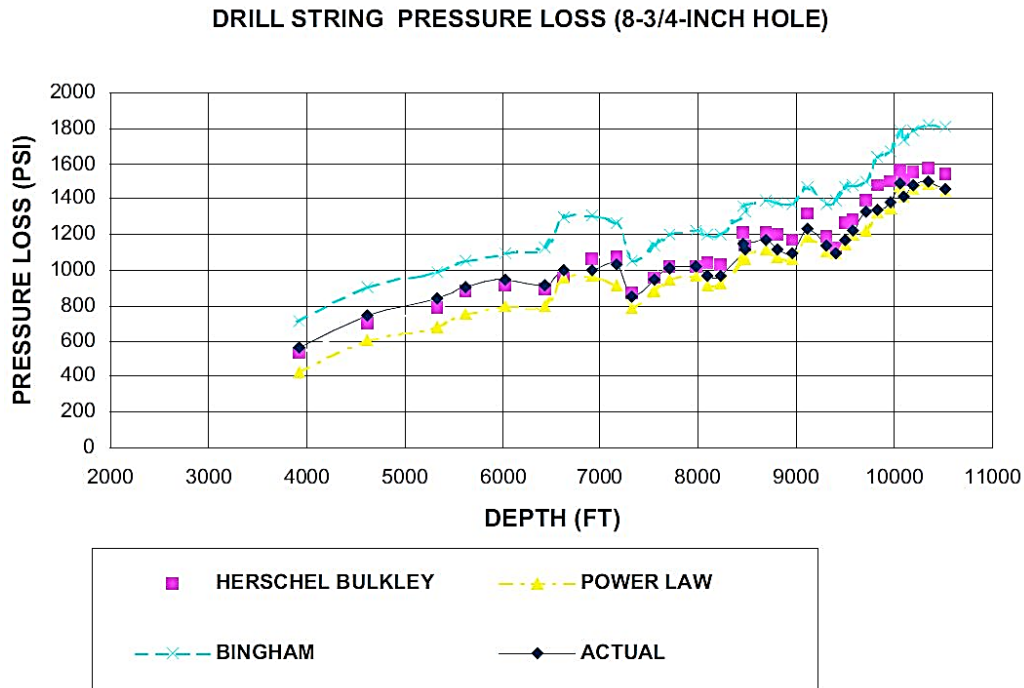


Figure 17: Drill string pressure loss plot for 8 3/4" hole (Ayeni, K., & Osisanya, S. O, 2004)

2.3.2.3 Standpipe Pressure Real-Time Monitoring

Monitoring of standpipe pressure in real-time is further used to evaluate performance-related behavior during routine drilling-related operations (e.g., during Weight to weight connection, slip to slip connection). Pumps-off and pumps-on procedures can be analyzed in detail and improved if necessary. A case study proved that focus on gel breaking related standpipe pressure (SPP) peaks after changing from static conditions to pumps-on can improve performance and prevent damaging the wellbore. “Especially in narrow drill-ability windows, this pressure peak may lead to a fracturing of the formation, lost circulation, kicks or even collapse of the wellbore” (Zoellner, P et al., 2011). Figure 18 shows a pressure peak of 12 bars after starting up the pumps, which led to a significant increase in ECD. The pressure peak in the shown case describes the difference between the highest value and the stabilized pressure value.

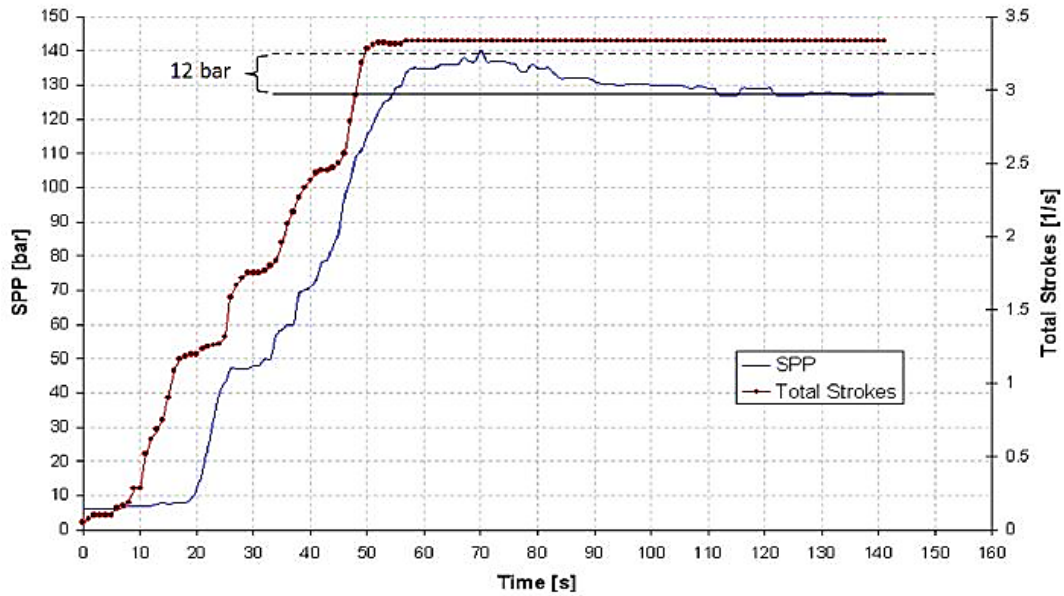


Figure 18: Pressure peak observed during pump start-up (Reitsma, D, 2011)

HSE related alerts may be set, and performance-related timings (Key Performance Indicators) can be measured by implementing algorithms based on the provided sensor data. Additionally, to the standpipe pressure sensor, an annular discharge pressure (ADP) sensor may be installed (e.g., anywhere along with the discharge piping, BOP, etc.) and connected directly to the system on the rig site since the detection of anomalous behavior could be delayed via WITS streaming. This is only applicable for managed pressure drilling (MPD) and underbalanced drilling (UBD) but not at overbalanced conditions. Tests have shown that a lower sensor span can result in significant improvement of the resolution, which enhances the timing for detecting anomalies (Reitsma, D, 2011). Figure 19 shows that normal variations have been removed (corrected) since an anomaly will cause significant changes in the data channels, and a lower frequency will improve visibility.

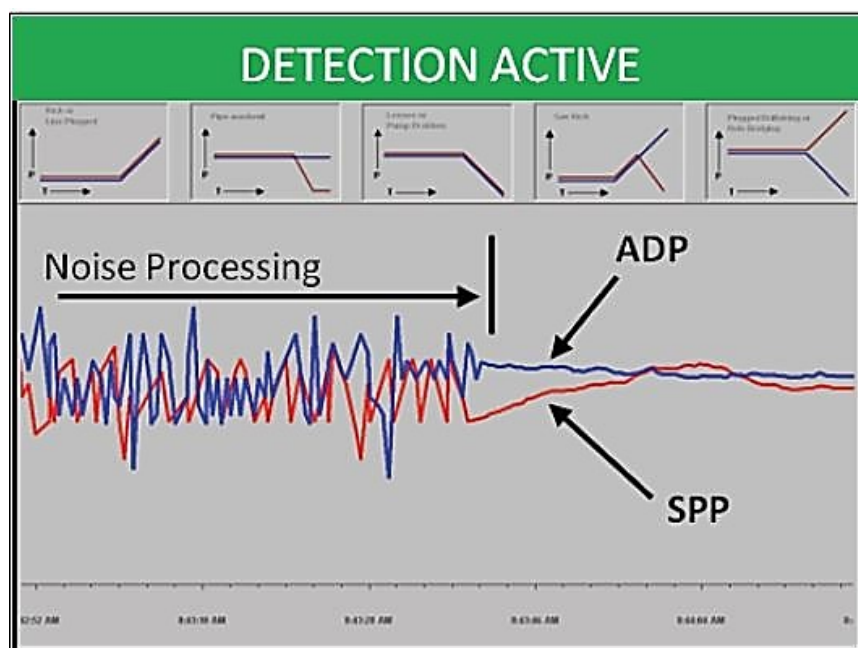


Figure 19: Calibration of SPP vs. ADP monitor (Reitsma, D, 2011)

Once calibrated, this approach is useful to detect a number of issues. Amongst others, besides kicks and losses, leaking equipment and plugging may be indicated by clear changes in the sensor channel data trends.

While Figure 20 shows an indication of a fast kick on the left (an abrupt increase of both channels), on the right, a clear indication of a washout (drill-pipe leak) is given by a decrease in the SPP and a consistent ADP trend at the same time (losses would be indicated by a decrease in both channels).

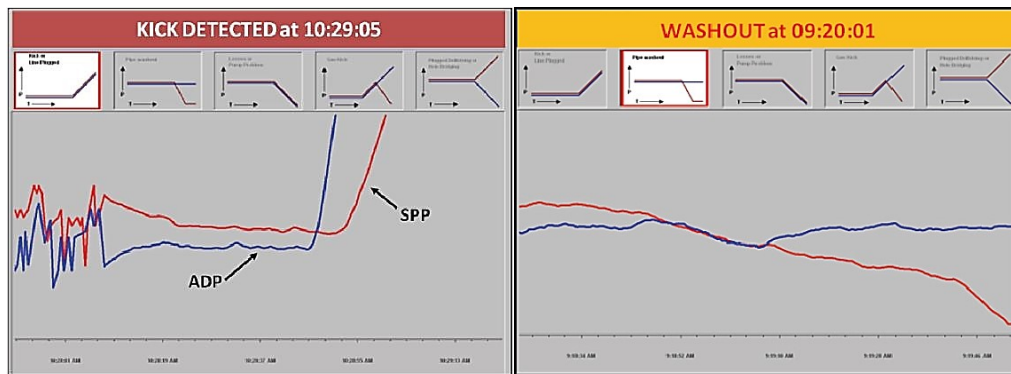


Figure 20: System screen of fast kick test (left) and drill-pipe leak (right) (Reitsma, D, 2011)

A major advantage of this method compared to a Coriolis flowmeter is that kicks can be detected when the well is shut-in. The major disadvantage is missing kick rate and volume calculation. Critical parameters that may influence the behavior of the data trend to misleading view (e.g., downhole torque measurements, heaves, etc.) need to be considered.

Alerts can be improved by preventing false alarms during “ballooning” and “breathing” conditions due to total flow and the continuous total change in volume-related pressure change. Standard alarm settings that are based on the change in total flow (whilst steady-state conditions) may be deactivated during specific periods to avoid false alarms and is critical for HSE. Concluding standpipe pressure real-time monitoring, the simulated standpipe pressure curves by considering varying calculation models can be updated in real-time by the input of actual measurements and compared in terms of pressure trend evaluation in real-time. Most models are limited by the required input parameters, the accuracy of required measurements, and not easy to apply for complex wells.

2.3.3 Delta Flow for Detecting Kicks and Fluid (Matrix) Losses

Flow meters (Coriolis meter) are capable of detecting kicks and losses at the rig site. However, there is a potential error due to vibration sources, and maintenance is required frequently to assure reliability. Downhole measurements (e.g., via downhole pressure sensors) also are limited to a range of uncertainty that is related to the telemetry system and the delay encountered in signal transmission. Pressure sensors (e.g., hysteresis) are smaller and easier to install, and cheaper than flow meters.

2.3.4 Analysis of historical data (offset wells)

The use of historical data for HSE-related simulation and analysis is limited due to varying equipment, procedures, and downhole conditions from well to well. Even at

batch wells and fields with several offset wells, respectively, the changing parameters need to be considered carefully.

Gathered data from offset wells may be used for planning and lessons learned purposes in general but never seen as a correct outlook for upcoming well operations.

Like torque and drag, historical hydraulics data can be used rather than review issues with the equipment at certain conditions than as a reliable reference for simulations and predictions.

As using historical data is critical to make predictions for safe well operations, this approach will not be discussed further in this thesis. To sum it up, historical data may be useful for planning purposes of the well design and to review operational problems (non-productive time) and to analyze performance related to the human factor, equipment, or operational procedure.

2.3.5 Machine Learning Approach

2.3.5.1 Overview

Machine learning approaches are rising in the drilling industry for a couple of years, with wells becoming more challenging, and HSE has priority from planning until competing operations for a well. This section provides an overview and outlook on machine learning trends being established in the near future. It needs to be stated that this summary does not provide a description of all existing machine learning techniques.

Popular machine learning methods are [Noshi, C. I., & Schubert, J. J., 2018]:

- Linear Regression
- Decision Trees (Random Forest)
- Linear Classifiers (Perceptron, Support Vector Machine)
- Artificial Neural Network
- Principal Component Analysis (PCA)
- K-Means Clustering
- Fuzzy Logic (BBN)
- Genetic Algorithms (GA)
- Bayesian Belief Networks (BBN)

2.3.5.2 Machine Learning Approaches Applied for Drilling Parameters

2.3.5.2.1 Statistical Learning Models

Statistical learning models can be supervised by calculating an output from defined inputs or unsupervised by learning trends in data without definite outputs. A supervised model is described in [Hegde, C., 2015], which differs between “normal” and “abnormal” torque via putting the prediction into classes that reflect operational performance.

The model accuracy was determined as followed:

$$MSER = \frac{1}{n} \sum_{j=1}^n (Actual\ Torque - Predicted\ Torque)^2 \quad (31)$$

Where MSER = Mean Squared Error

Modeling techniques differ from regressions, bootstrapping, and random forests to support vector machines (SVM).

Regressions [e.g., Multilinear regression (MLR)] uses linear models for predictions of torque.

$$Torque = \sum_{k=1}^K a_k x_k \quad (32)$$

where k = number of parameters

a = constant determined by MLR algorithm

Bootstrapping returns the uncertainty by sampling the data.

$$Residual = Actual Torque - \sum_{k=1}^K a_k x_k \quad (33)$$

Figure 21 illustrates an example for bootstrapped regression.

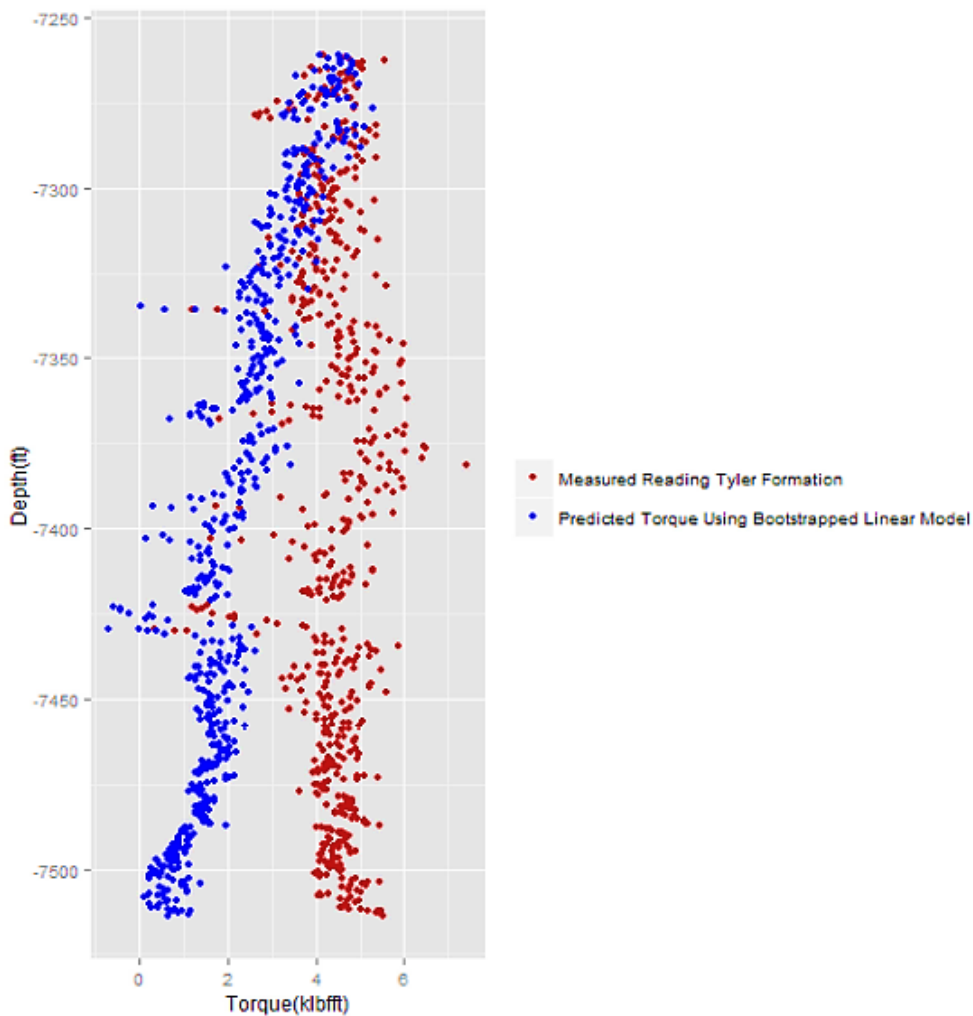


Figure 21: Depth plotted against downhole torque in Tyler formation using Bootstrapped regression (Hegde, C., 2015)

Random Forests use decision trees to capture non-linearity in the data. Random forests use bootstrapping samples to overcome low accuracy and overfitting (Figure 22).

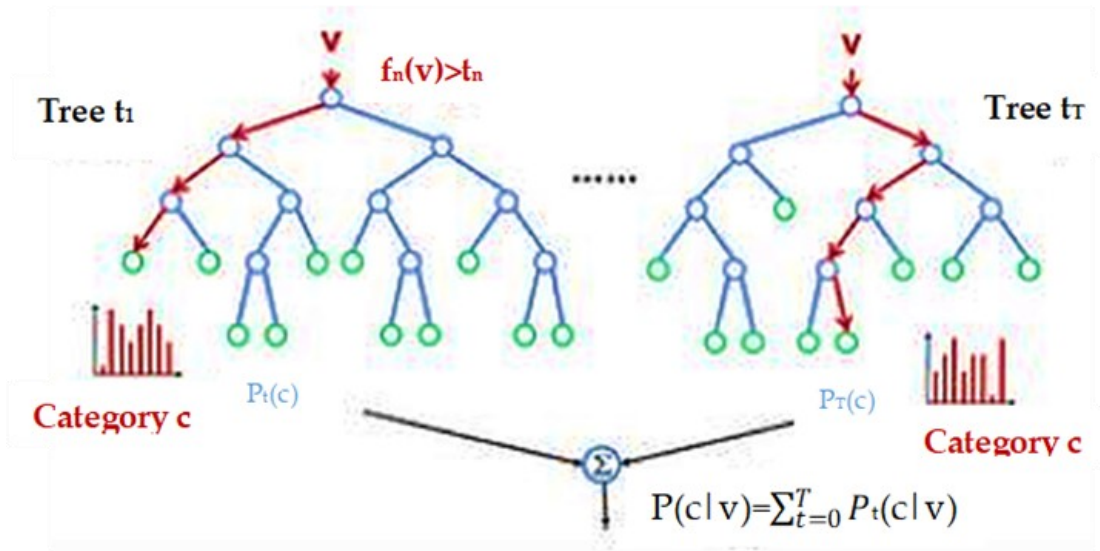


Figure 22: Random forest visualization (Hegde, C., 2015)

Figure 23 illustrates an example for random forest.

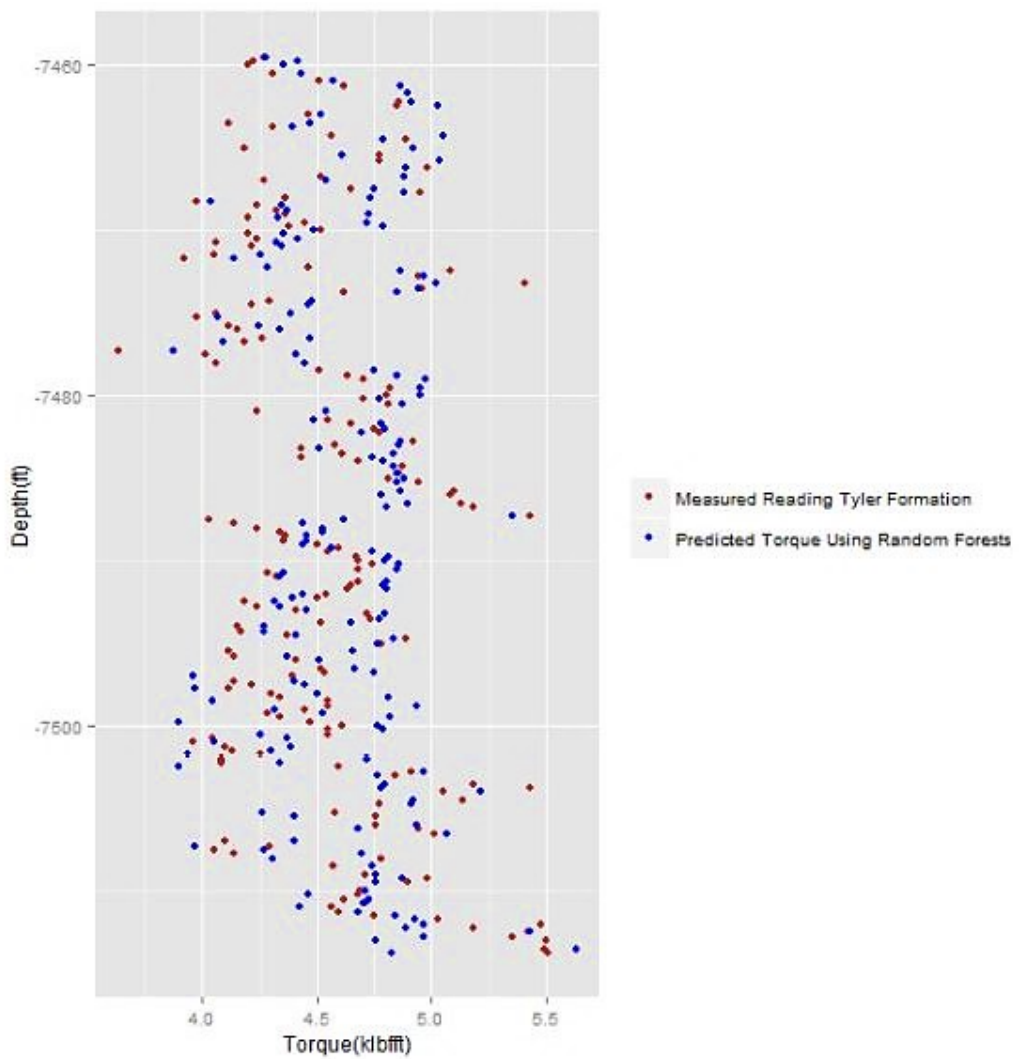


Figure 23: Downhole torque versus depth using random forests with 80% of the data used for training (Hegde, C., 2015)

A moving window linear regression model is shown in Figure 24. A moving window algorithm was developed for different surface data channels. Once torque changes are noticed, the next value is predicted via linear regression and compared to the upcoming actual value, which will provide a possible indication of abnormal behavior. “Evolving differential sticking tendency and poor hole cleaning can be detected and addressed early with this symptom”(Ahmed, O. S., 2019).

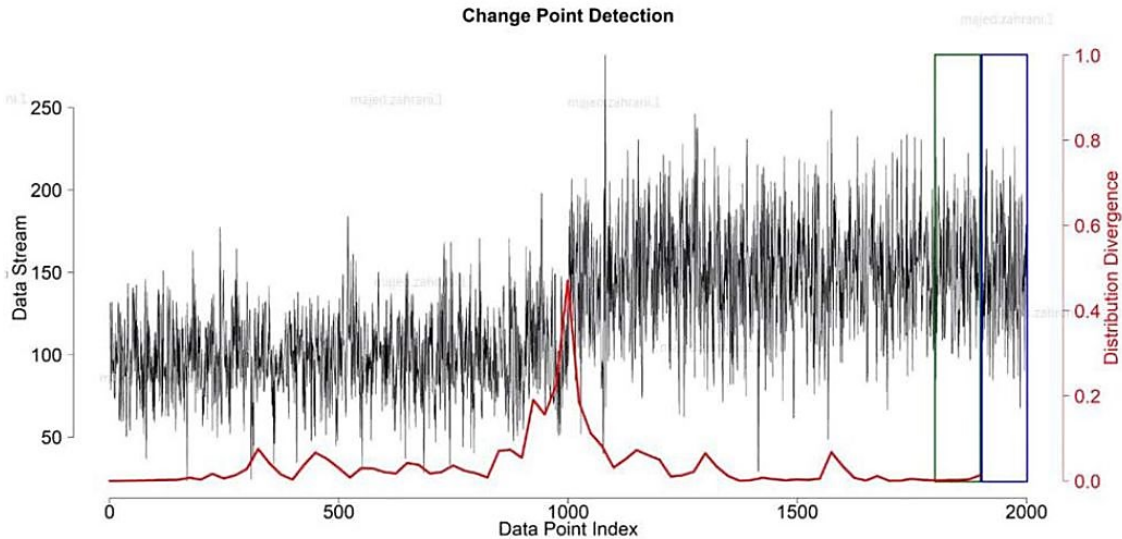


Figure 24: Change Point Detection algorithm. The black line is the input data stream, the green, and blue boxes are the right and left sliding window, respectively, and the red line is the calculated distribution divergence distance for data from both sliding windows evaluated at their adjacent point (Ahmed, O. S., 2019)

SVMs use non-linear classification boundaries for classification and pattern recognition of the torque trend (Table 2). Pre-processing the input and target data (e.g., normalization) is necessary to improve the predicted results, and different types of kernel functions are used.

Total Population	Condition Positive	Condition Negative
Test Outcome Positive	True Positive	False Positive
Test Outcome Negative	False Negative	True Negative
Accuracy = $\frac{\sum \text{True Positive} + \sum \text{True Negative}}{\sum \text{Total Population}}$		

Table 2: Confusion matrix used to evaluate the accuracy of classification algorithms in machine learning (Hegde, C., 2015)

The method splits the two classes by a hyperplane (Figure 25).

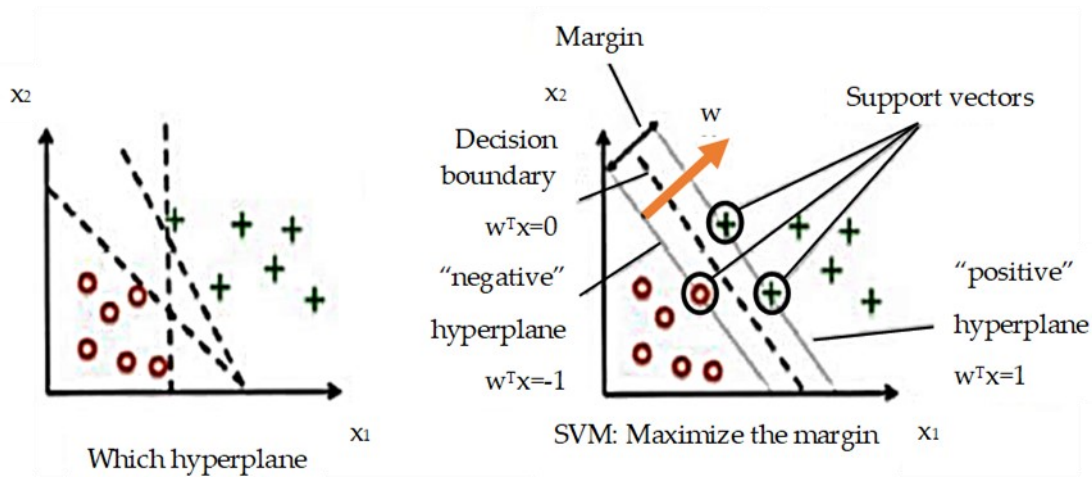


Figure 25: Hyperplane in SVM (Mishra and Datta-Gupta, 2017)

The method being used depends highly on the run time for processing the data as it may be used for real-time alerting applications.

2.3.5.2.2 Deep Learning for Torque Predictions

Artificial neural networks use input, hidden, and output layers that are linked via transfer functions for predictions. The methods vary from feed-forward to recurrent networks. Feedforward backpropagation is a supervised learning method, whereas Levenberg-Marquard training function is probably the best-known learning algorithm for ANNs [Abbas, A. K et al., 2019]. Figure 26 illustrates the basic structure of an artificial neural network (ANN).

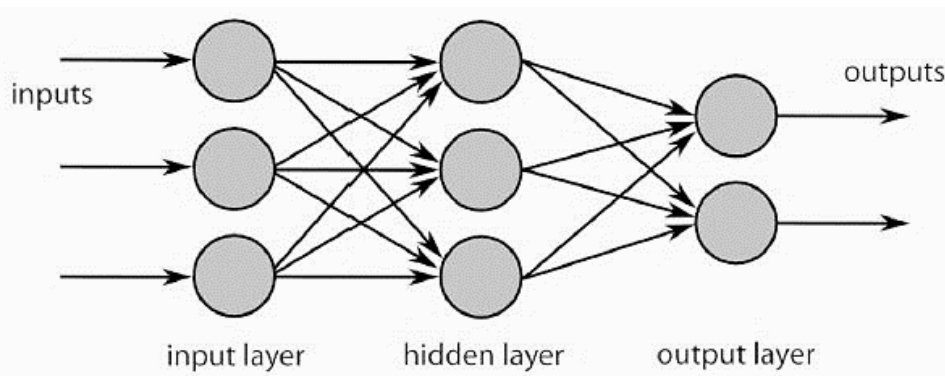


Figure 26: ANNs structure with one hidden layer (Abbas, A. K et al., 2019)

The ANNs used in this project will be explained further in the “Methodology” chapter of the thesis. The following deep neural network (DNN) contains several additional layers between the input and output layers (Figure 27). The network was trained with 42287 samples and a sample rate of 5 seconds/sample, including block position (BPOS), hook load (HKLD), pressure (SPPA), surface torque (STOR), RPM, and pumping rate (SPM1). The training was carried out for 200 epochs and reached an accuracy of 98%, using the mean-square error function.

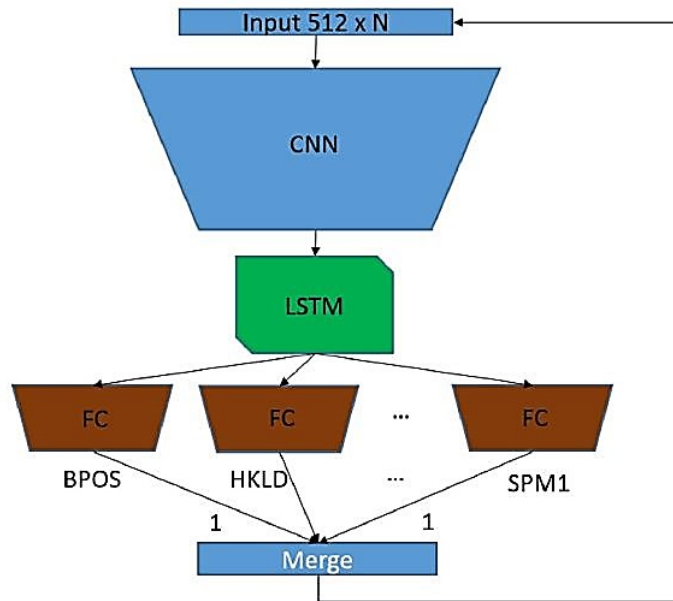


Figure 27: Overall architecture of the proposed DNN model (Yu, Y., Chambon, S., et al., 2018). N is the number of channels, CNN convolutional layers, LSTM long short-term memory layer and FC are fully connected layers

As a result, over 10000 timestamps were simulated recursively (Figure 28). It has to be considered that depth data was not considered for the model, which may lead to increasing errors in the predictions.

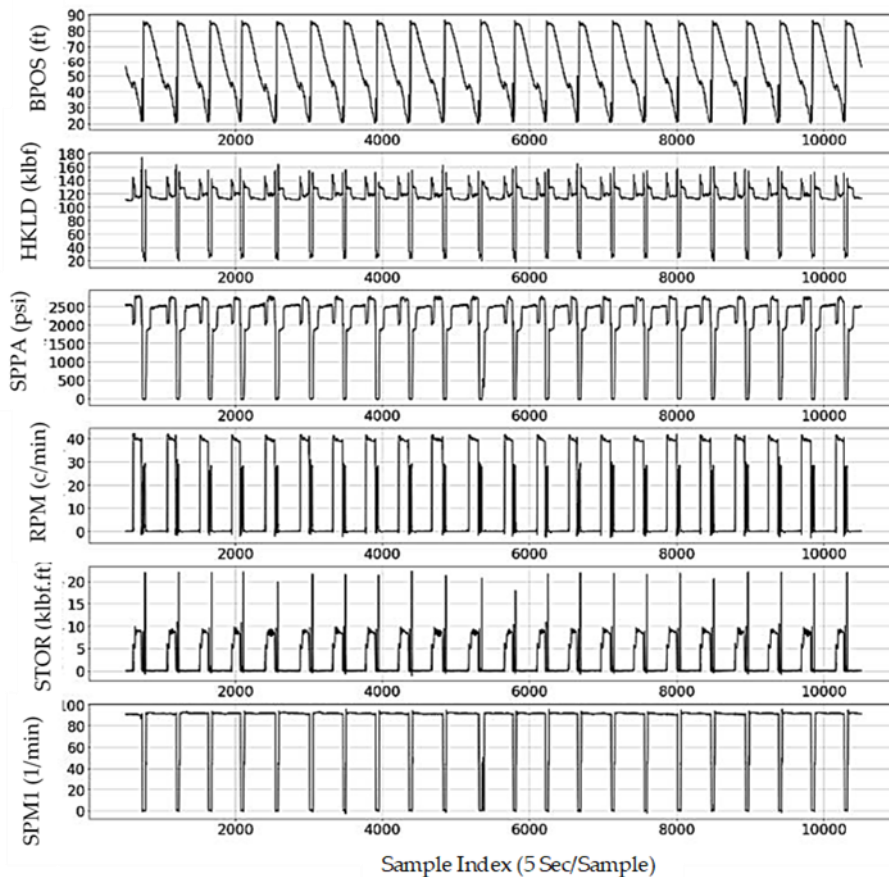


Figure 28: Simulated time sequence by the proposed DNN (Yu, Y., Chambon, S., et al., 2018)

2.3.5.2.3 Lost Circulation Prediction Via Deep Learning

A neural network approach was proposed based on data acquired from the Yingqiong Basin in the southern Chinese sea, which is known for a narrow safe drilling mud density window (Figure 29). Hence the loss of circulation is a serious issue in the mentioned region.

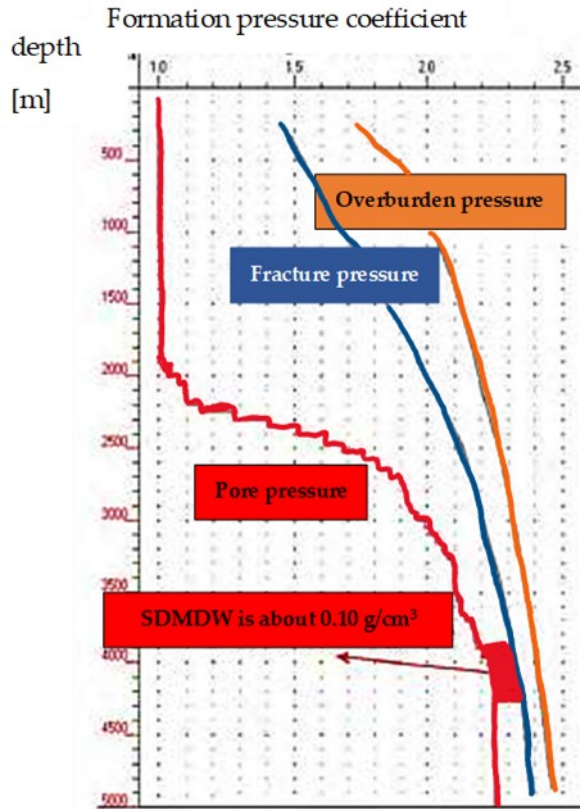


Figure 29: Illustration of the safe drilling mud window (SDMDW) in Yingqiong Basin (Hou, X. et al., 2020)

The data was selected by consideration of drilling parameters of available surface sensor data channels (e.g., TQA, SPP, MD, WOB, etc.), geological parameters (e.g., lithology, pore pressure, formation fracture pressure, etc.), and drilling fluid properties (e.g., yield point, mud weight, etc.). After selection, the data was pre-processed in terms of data outliers, qualitative features, and normalization (34).

$$x'_i = \frac{x_i - \text{Min}_i}{\text{Max}_i - \text{Min}_i} \quad (34)$$

Where

x'_i is the value of i -th feature after normalization

x_i is the original value i -th feature

Max_i is the maximum of i -th feature

Min_i is the minimum of i -th feature

The ANN was a supervised learning model, using rectified linear unit (ReLU) as activation function, L₂-Norm for regularization and hidden neurons number N_h (35).

$$N_h = \sqrt{m + n} + a \quad (35)$$

Where

m is the neuron number of input layers

n is the neuron number of output layers (loss risk type)

a is a constant within 1-10

The model was evaluated using the cross-entropy loss function J (36).

$$J = -\sum_{i=1}^K y_i \log(p_i) \quad (36)$$

Where

K is the number of class

y is label, that is, if class is i, $y_i=1$, otherwise $y_i=0$

p is the output of the ANN

The architecture of the ANN is illustrated below.

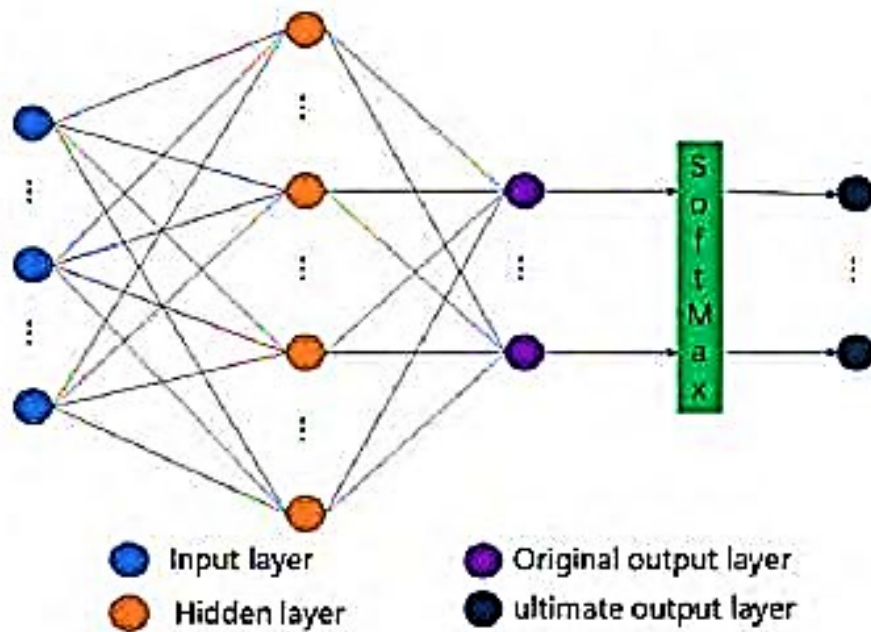


Figure 30: Architecture of lost circulation prediction ANN (Hou, X. et al., 2020)

Accuracy and loss during training and testing are illustrated in Figure 31. It can be seen that the accuracy during both testing and training is exceeding 0.9 after 10 epochs and the loss is decreasing below 0.2 after 10 epochs.

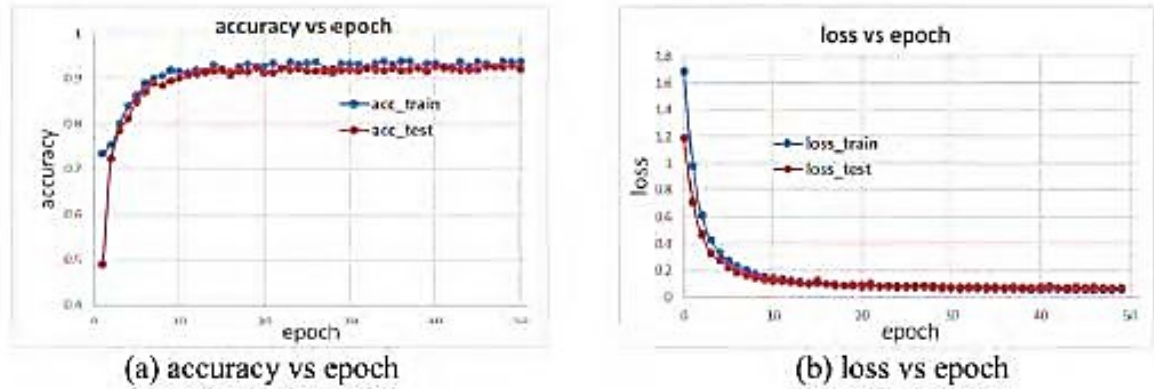


Figure 31: Accuracy (a) and loss (b) on training and testing set (Hou, X. et al., 2020)

The results showed no overfitting issues and an accuracy of 91% (mean) after 50 epochs (Table 3).

Loss risk type	Precision
No loss	0.86
Micro loss	0.90
Small loss	0.95
Middle loss	0.95
Large loss	0.89
Severe loss	0.93
Mean	0.91

Table 3: Metrics of six loss types (Hou, X. et al., 2020)

Generally, the classification results of the proposed circulation lost risks prediction method agree with the practical engineering situation, satisfy the needs of drilling engineering, and can provide guidance for the estimation of lost circulation risks. This method can be applied to other fields if the required data is available (Hou, X. et al., 2020).

2.3.5.2.4 Drilling Hydraulic Optimization Via Deep Learning

A model that is capable of predicting pump pressure versus depth (in similar formations) and in real-time was proposed in 2015 (Wang, Y., & Salehi, S. 2015). It was built in MATLAB by using the fitting tool. The ANN used 12 input parameters (Table 4).

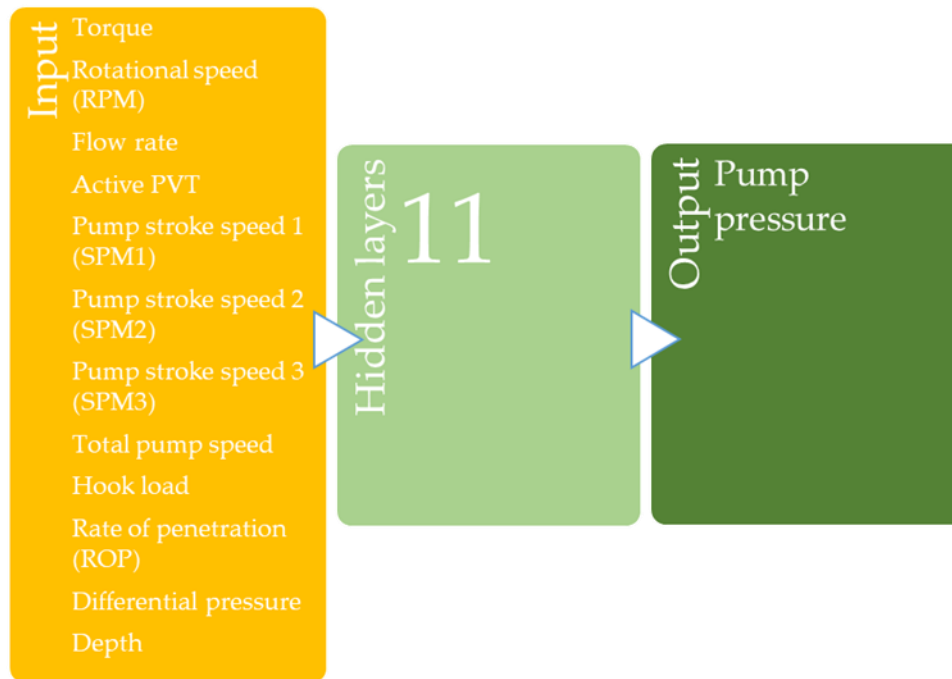


Table 4: Input and output parameters (Wang, Y., & Salehi, S. 2015)

The data was pre-processed by normalizing before training the model, whereas the mean squared error function was used for scaling. The number of hidden layers was determined after the heuristic approach. The data was split into 75% for training, 15% for validation, and 10% for testing. Overfitting is prevented by the determination of the minimum validation error in general (MSE).

One hundred twenty networks were created and evaluated. The best results were provided by a three-layered network with 11 hidden neurons in the hidden layer. A feed-forward network with 'tansig' activation function, 'purelin' output layer function, and Levenberg-Marquand function (back-propagation) has been used for training.

To evaluate the impact of each data channel on the error of prediction, a forward regression (heuristic approach) was undertaken. Single channels were considered as the input layer, and 1440 networks were created to identify the ranking after MSE (Figure 32). It turned out that depth has the most impact on the model.

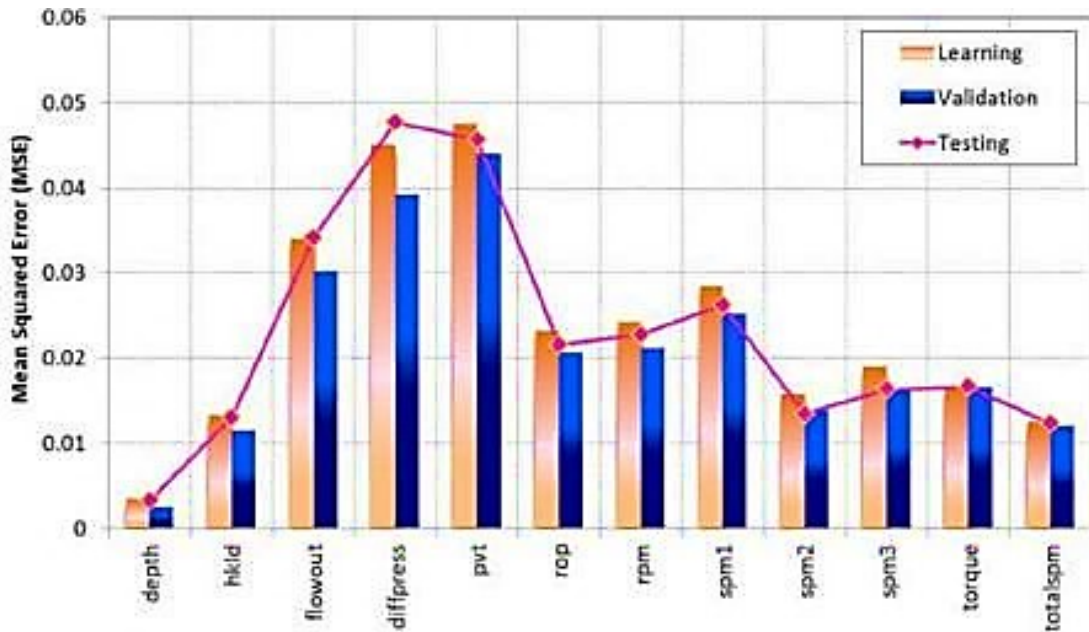


Figure 32: Ranking of model input, one input channel (Wang, Y., & Salehi, S. 2015)

Afterward, the other channels were used in combination with the depth channel as input. The pump speed (total spm) showed the lowest error together with depth. The final step was using depth, pump speed in combination with the other channels, showing differential pressure as the next best fit, etc. up to 9360 networks in total (Figure 33).

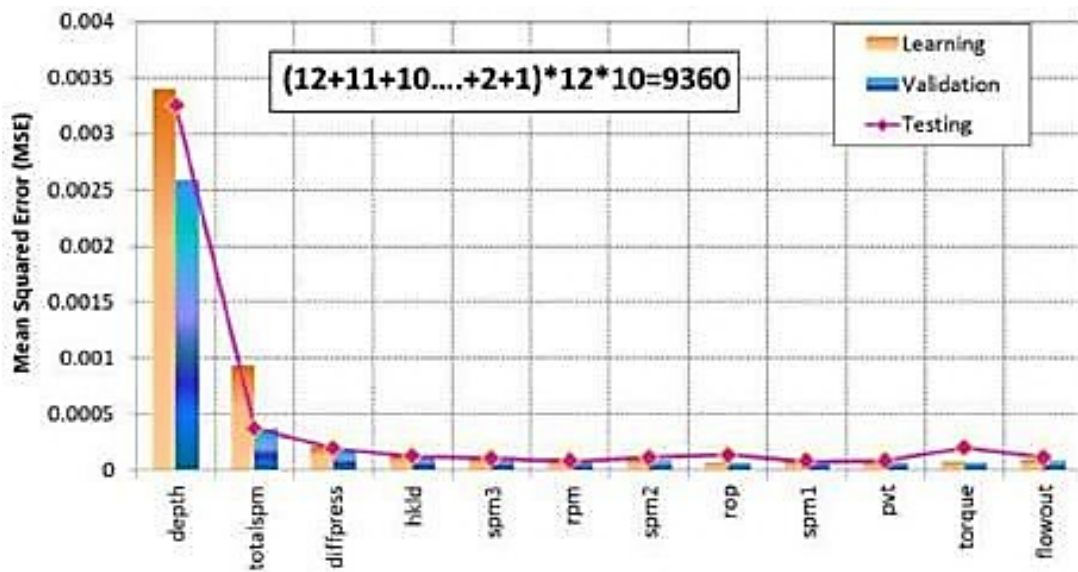


Figure 33: Ranking of model input (Wang, Y., & Salehi, S. 2015)

A regression of the simulated pump pressure vs. measured pump pressure is illustrated in Figure 34 and shows good results.

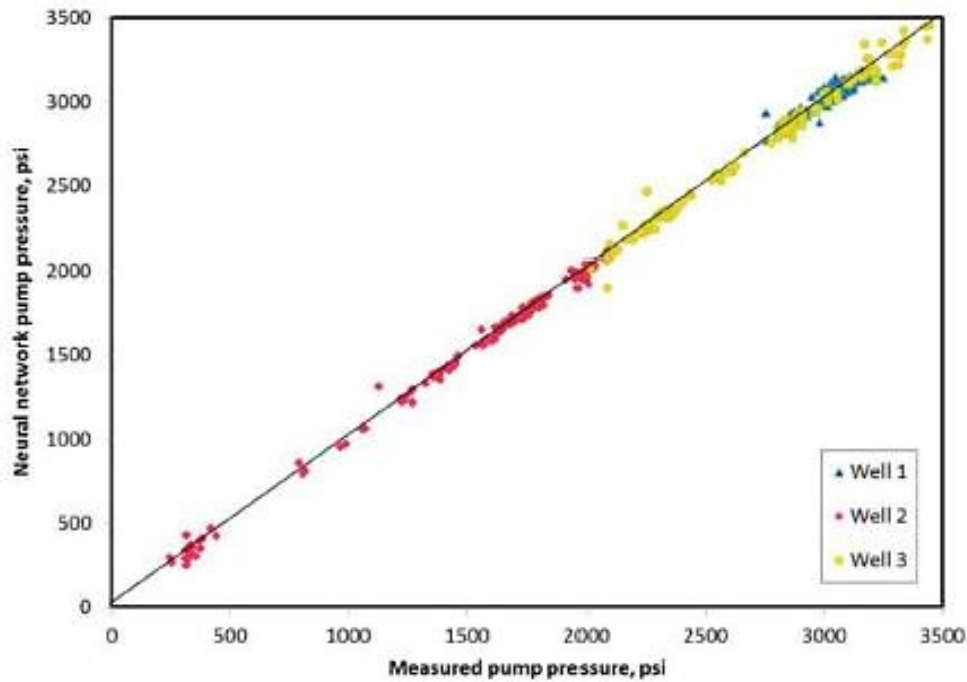


Figure 34: Regression of the overall simulation results for three wells (Wang, Y. & Salehi, S. 2015)

The review of the discussed papers provided the base for the neural network approach developed during this thesis project, in which the methodology is introduced in the next chapter.

2.3.5.3 Limitations of Machine Learning for Predicting Torque and Standpipe Pressure

The main limitation of the discussed machine learning methods is that they are only considering the prediction of abnormalities of a single data channel. The input parameters often need to be manipulated, or manual work has to be done to fit the requirements of the existing approaches and may not be set up quickly or require frequent updates of specific manual measurements.

The developed hybrid model analyses torque and standpipe pressure behavior at the same time and can easily be integrated at any system that is gathering a standard set of surface sensor data without changing settings or preparing the configuration of the parameters manually. It provides an easy approach in addition to existing methods that are used in the field in order to verify false alarms that are e.g. caused by inaccurate simulations of curves, leading to confusion amongst the drilling personnel.

Chapter 3 Developed Methodology to Detect Anomalies in Drilling Behaviors

3.1 Background

In this chapter, a detailed description of the steps undertaken to develop a hybrid model that provides better accuracy in the detection of abnormal behaviors of measured drilling parameters is provided. The terminus “hybrid model” is related to the different sets of neural networks that are used at the same time to identify the critical behavior of a specific data channel. For each data channel, three networks are used to predict the actual and future values and trends. After importing and filtering the sensor data, the networks will be trained, and the algorithms for predicting the data will be applied once new sensor data is available. In order to reduce the impact of uncertainty of the prediction models, an uncertainty window is constructed. It is calculated based on statistical evaluation of the error between the predicted and the actual data. Therefore, the standard deviation of the mean squared error between the actual and predicted data is used. Once a predefined number of actual data points is shown to be outlying the window of uncertainty, alerts will be triggered accordingly.

The following flow chart (Figure 35) illustrates the undertaken development steps for creating the hybrid model.

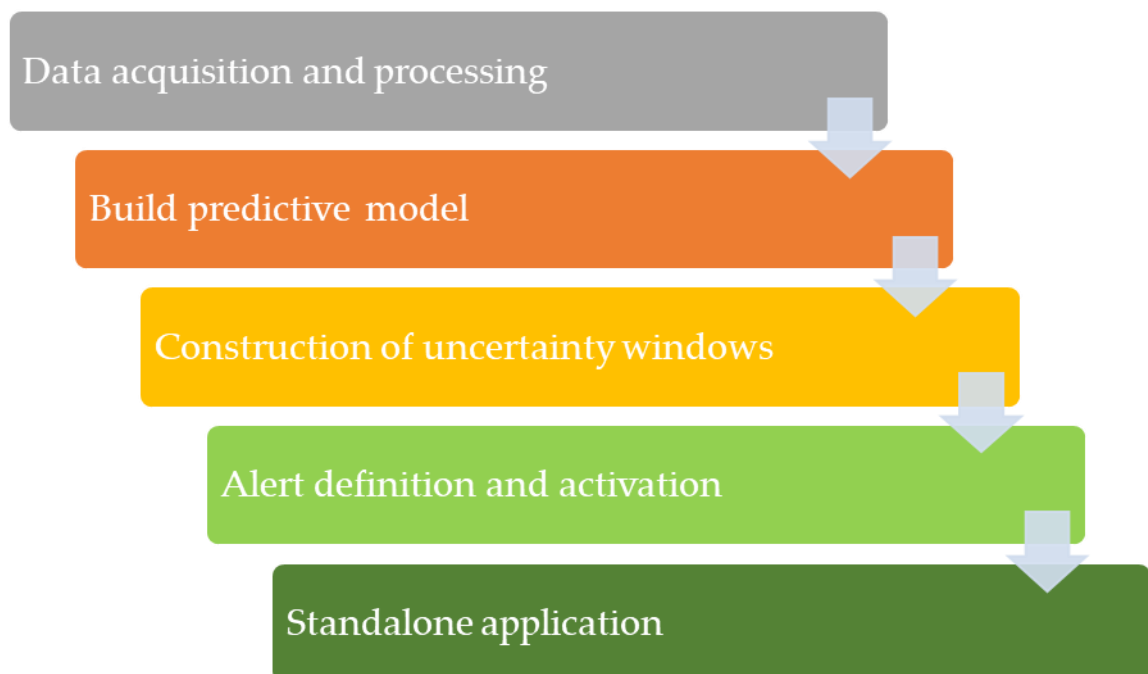


Figure 35: Flow chart of undertaken development steps for creating the hybrid model

3.2 Data Processing

The procedure of data acquisition and pre-processing is illustrated in Figure 36.

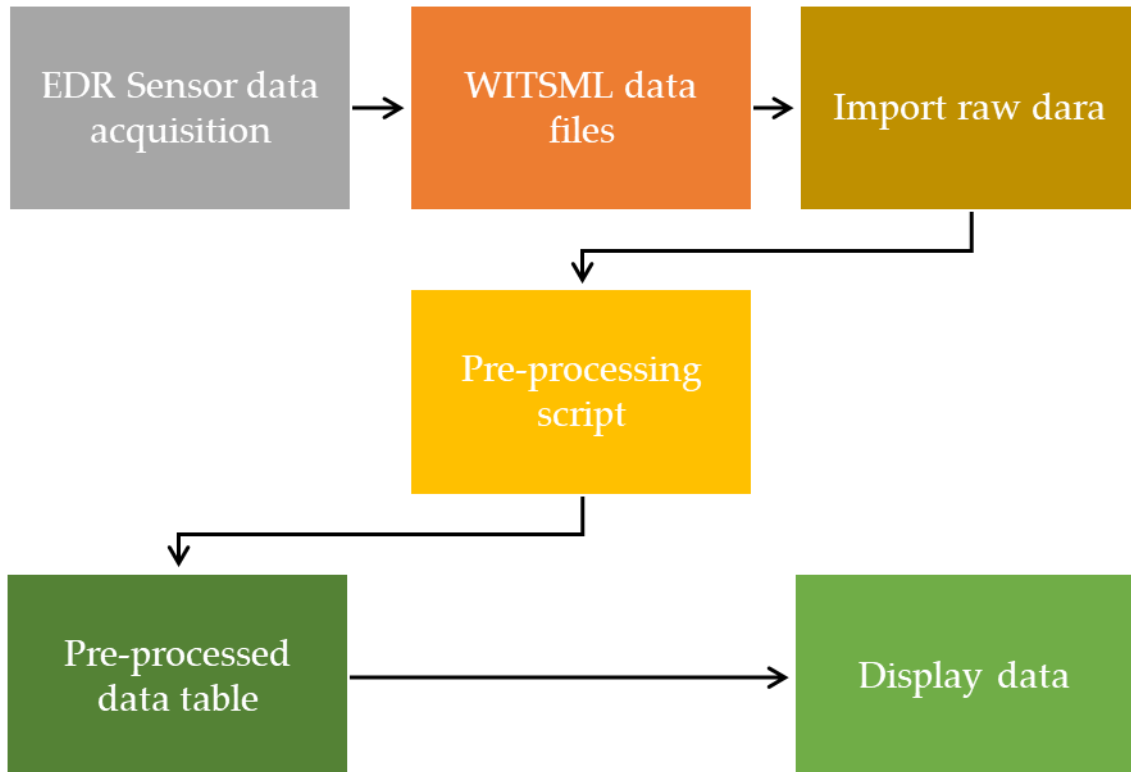


Figure 36: Data acquisition and pre-processing procedure

3.2.1 Data Acquisition

The data acquisition is conducted via standard EDR surface sensor and MWD/LWD data, provided via WITSML files via a setup server connection, usually called the WITSML bridge. The WITSML data is converted into .csv format by a developed Python script to ease data import into Matlab. A sample file of the WITSML data and converted import table file can be found in the Appendix.

The available well data contain varying amounts of data channels, but the desired surface sensor data channels are available as per standard data provider companies of the drilling industry in general. The minimum required surface sensor data channels for developing the presented hybrid model are:

- TIME
- TQA (Surface average torque)
- SPPA (Standpipe pressure average)
- DBTM (Measured bit depth)
- DMEA (Measured hole depth)
- RPM (Rotation)
- SPM 1 (Pump rate 1)
- SPM2 (Pump rate 2)
- SPM3 (Pump rate 3)
- BPOS (Block position)

- HKLD (Hook load)
- TFLO (Flow in)
- SWOB (Surface weight on bit)
- ROP (Rate of penetration)

3.2.2 Data Selectivity

In order to provide the best possible input for training the hybrid model that intends to predict abnormal drilling behavior in real-time, it is necessary to meet the minimum requirements to the data set, which are:

- Minimum of 3 hours bit on bottom drilling or at least one completed stand of drilling.
- Sufficient period of drilling without issues.
- Sufficient data quality.
- Available daily drilling reports (DDR) to verify potentially identified issues.
- Available “issue data” to test the hybrid model for feasibility in terms of industrial requirements.

3.2.3 Data Handling

The data of the explained surface sensor data channels are imported into Matlab and pre-processed in order to meet the requirements of machine learning purposes. Pre-processing of the data is important, as inaccurate measurements, such as outlying datapoints, missing data, or small variations in the data intervals (heaving), will lower the quality and validity of the trained hybrid model.

3.2.3.1 Outliers, Data Gaps, and Conversions

Outliers of specific data channels are being removed via threshold rules applied and filled afterward by linear regression. Data gaps are filled by the available linear regression (fill missing indices functions), and outliers are removed and replaced via outlier threshold functions in Matlab. The data of the output layers is further smoothed (via an available smoothing function in Matlab), as removing small variations (heaves) in the curves will reduce overfitting later at creating the ANNs. Every filtering process influences the results in terms of distortion; hence filtering (removal of outliers and smoothing data curves) should be kept at a minimum level and according to necessity. Specific data channel units are converted to improve visualization in the plots. The pump stroke parameters (often three mud pumps at rig site) are merged due to the fact that not always the similar pumps are operating at the same time, and the pumps that are inactive would show zero values and falsify the results.

The pre-processing and cleaning of the data is achieved by the implementation of additional functions and plots that will provide the user an overview of the filtered data points compared to the raw data points of each channel that was received via WITSML data stream. The pre-processed data channels were merged into a new table, whereas the filtering functions are displayed in Table 5.

Processing function/Surface sensor data channel	TIME	filteredTQA2	filteredSP2	filteredRPM2	filled_Output DMEA	filled_Output DBTM	filled_SWOB	filled_ROP	filled_TFLO	filled_HKLD	filled_BPOS	filled_SPM1	filled_SPM2	filled_SPM3
Fill missing indices	-	linear	linear	linear	linear	linear	linear	linear	linear	linear	linear	linear	linear	linear
Outlier threshold factor	-	15	200	-	-	-	50	-	-	-	-	-	-	-
Miscellaneous calculations	-	-	Pa to bar	-	x(-1)	x(-1)	-	-	-	-	-	Σ SPM = SPM total		

Table 5: Applied filtering functions of the merged filtered data table

3.2.3.2 Raw versus Filtered Data

Figure 37 illustrates an outcrop of the major raw surface sensor data of interest after import into Matlab. Where the blue line indicates the torque channel data and the red line the rotations per minute, missing data (empty intervals at both channels) and outliers (peaks to approximately -400, -600, and -800 in the blue line) can be found.

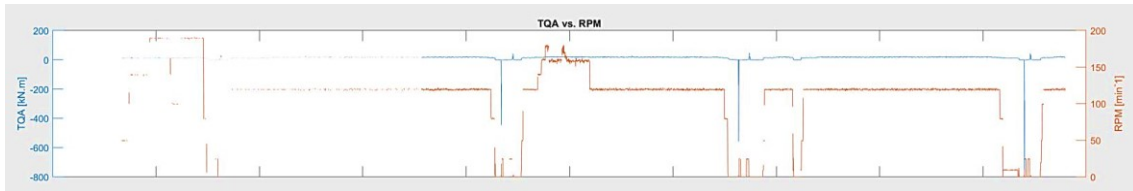


Figure 37: Outcrop of raw surface sensor data, rig Maersk Inspire, well NO 15/9-F-15 A

Figure 38 illustrates an outcrop of pre-processed data (red line) in comparison to the raw torque data of the surface sensors (blue line), where the missing data points shown in the previous plot are being filled, and outliers are being removed at the TQA channel.

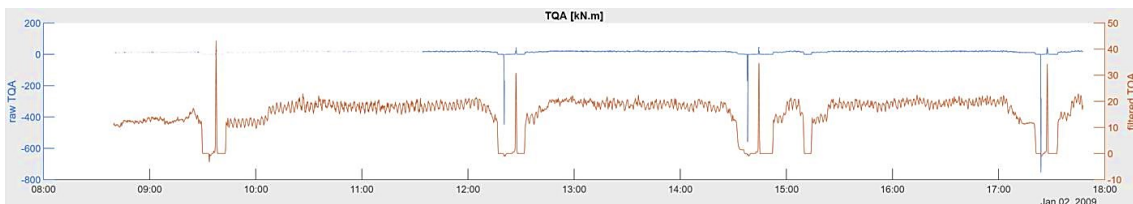


Figure 38: Outcrop of pre-processed surface sensor data, rig Maersk Inspire, well NO 15/9-F-15 A

3.3 Building Predictive Model

The hybrid model was designed to be able to predict abnormal behavior based on actual time input parameters and to provide an expectation of the behavior of the data in the future. It is comparing a future prediction that is done via a delay between input and output parameters during training to a future trend that is simulated via a closed-loop network of an input parameter.

Since the input data is provided in timestamps and to meet the purpose of training a model to predict future timestamps, usage of neural network times series application in Matlab was chosen. However, the models will be independent of data frequency since the models will predict for similar intervals between data points. This means that similar

timestamps as actual datapoints (actual network) and 50 timestamps in the future, with similar data frequency as the input parameter, will be predicted.

The hybrid model will be trained for two separate input parameters (One for Torque and one for SPP); hence Data Handlingence six artificial neural networks will be generated (Figure 39).

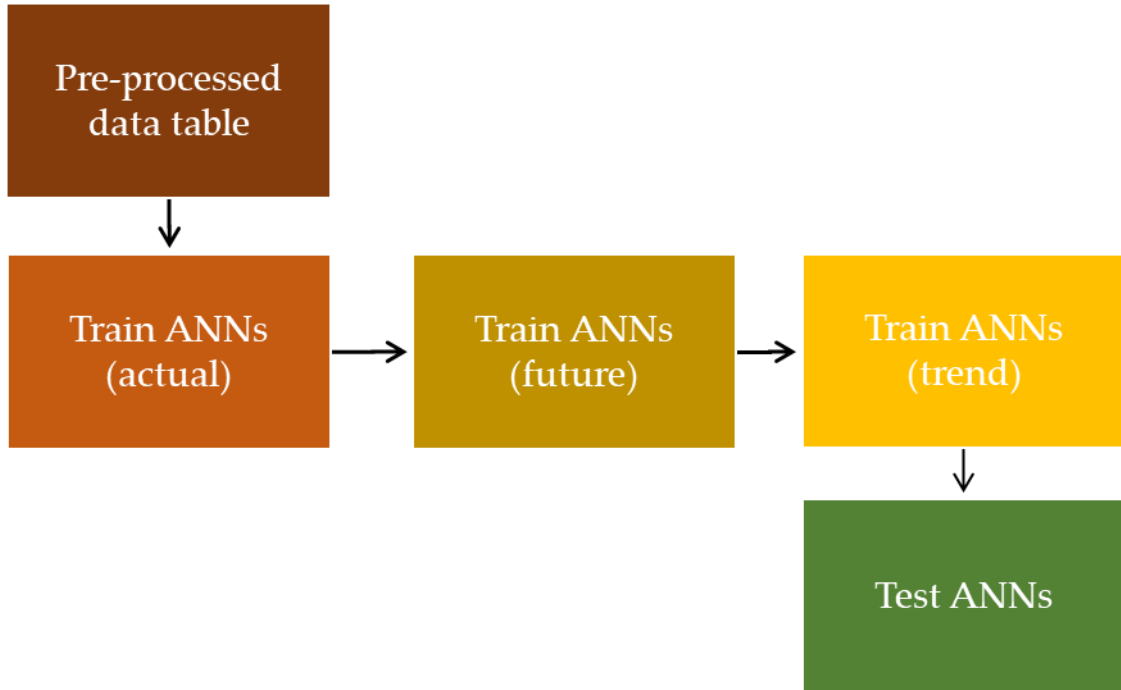


Figure 39: Predictive models creation workflow

3.3.1 ANN for Actual Time Prediction

The neural networks for the hybrid model predicting the actual time series were created via the neural network time series application in Matlab and use the Levenberg-Marquardt backpropagation as training function. The non-linear autoregressive network with external input (“NARX”) was constructed with the determination of the network’s hyper-parameters, such as 1:50 input delays, 1:50 feedback delays, and 1 hidden layer. The division of data is set to 70% for training, 15% for validation, and 15% for testing. The performance was evaluated using the mean squared error (MSER) function.

The time series for input and output use similar timestamps of data points. It predicts series $y(t)$ given d past values of $y(t)$ and another series $x(t)$ (Matlab R2019b).

The architecture of the actual prediction networks was constructed, as shown in the following example figure. The input parameters are streamed into a single hidden layer with 10 hidden neurons and used to train the network based on one output layer.

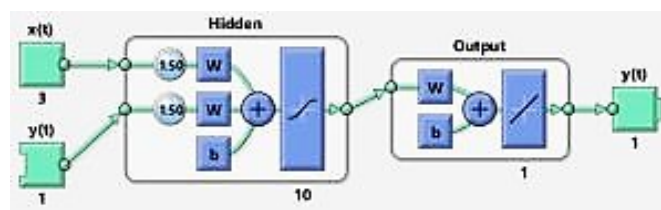


Figure 40: NARX Neural Network architecture, prediction of actual time series

3.3.2 ANN for Future Prediction

The neural networks for the hybrid model predicting the future time series were created via the neural network time series application in Matlab and use the Levenberg-Marquardt backpropagation as training function. The non-linear autoregressive network with external input (“NARX”) was constructed with the determination of the network’s hyper-parameters, such as 1:50 input delays, 1:50 feedback delays, and 1 hidden layer. The division of data is set to 70% for training, 15% for validation, and 15% for testing. The performance was evaluated using the mean squared error (MSER) function.

The timestamps of the output time series are 50 timestamps delayed to the future of the input time series timestamps. This allows creating a network for a prediction of 50 timestamps ahead. It predicts series $y(t+50)$ given d past values of $y(t+50)$ and another series $x(t)$ (Matlab R2019b).

The architecture of the actual prediction networks was constructed, as shown in the following example figure. The input parameters are streamed into single hidden layer with 10 hidden neurons and used to train the network based on one output layer.

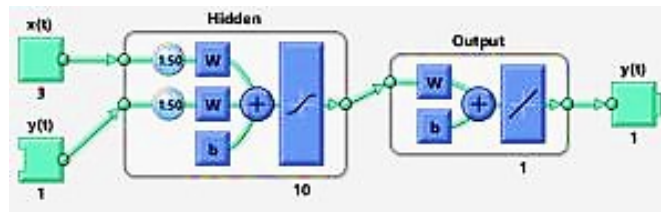


Figure 41: NARX Neural Network architecture, prediction of future time series

3.3.3 ANN for Future Trend Prediction

The neural networks for the hybrid model predicting the future time trends were created via the neural network time series application in Matlab and use the Levenberg-Marquardt backpropagation as training function. The non-linear autoregressive network (“NAR”) considers 1:50 feedback delays and one hidden layer. The division of data is set to random. The performance was evaluated using the mean squared error (MSER) function.

The architecture of the open-loop network is illustrated in Figure 42.

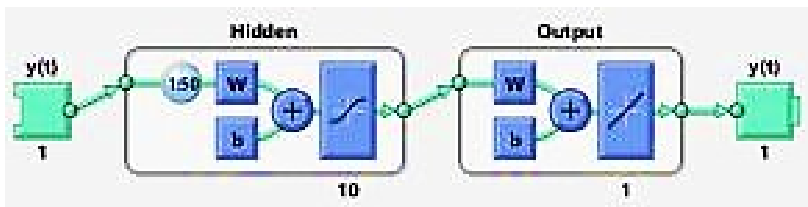


Figure 42: NAR Neural Network architecture, trend prediction, open loop

After simulating the open-loop network, the network is being closed and will predict the future trend of the input channel for 50 timestamps into the future (Figure 43). The output is used as further input to the network after closing the loop.

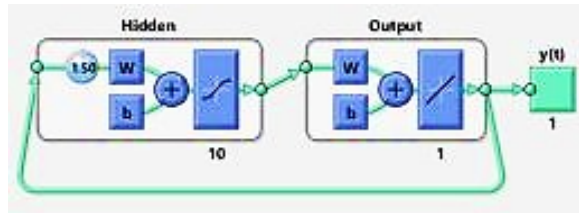


Figure 43: NAR Neural Network architecture, trend prediction, closed-loop

Table 6 shows the models of prediction and their functions in the context of the entire model and for defining the abnormality.

Predictive Model	Function	Purpose
ANN for Actual Time Prediction	Predicts datapoints based on actual channel data input.	Comparison of actual and predicted datapoints to identify abnormalities.
ANN for Future Prediction	Predicts datapoints with 50 timestamps offset into the future based on actual channel data input.	Comparison of predicted future datapoints and the predicted future trend of a single data channel in order to provide drilling behavior forecasts.
ANN for Future Trend Prediction	Predicts the trend of a single data channel input with 50 timestamps offset into the future.	

Table 6. Models of prediction description

3.4 Construction of Uncertainty Windows

3.4.1 Overview

The main purpose of triggering alerts is achieved by calculating a predictive window of uncertainty (safety window) and detection of outlier data points. Once data points are identified as outliers from the window that is being generated by calculating the MSER and considering the standard deviation of it, alerts are going to be triggered accordingly (Figure 44).

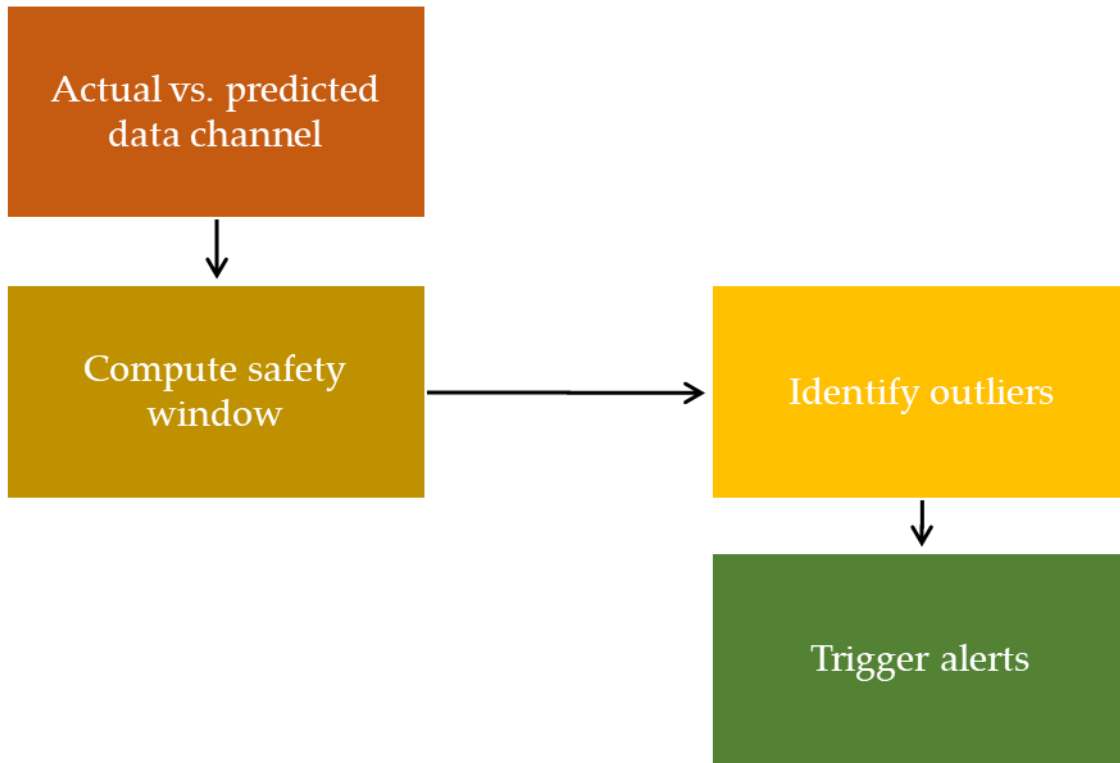


Figure 44: Workflow of safety window creation and triggering alerts

The sketch in Figure 45 illustrates the principle of identifying outliers (abnormal behavior of a data channel). The window is created by considering the MSER function and standard deviation of each timestamp of the investigated range of data. A similar principle is applicable for the future prediction of the channels compared to the predicted future trend of a single channel.

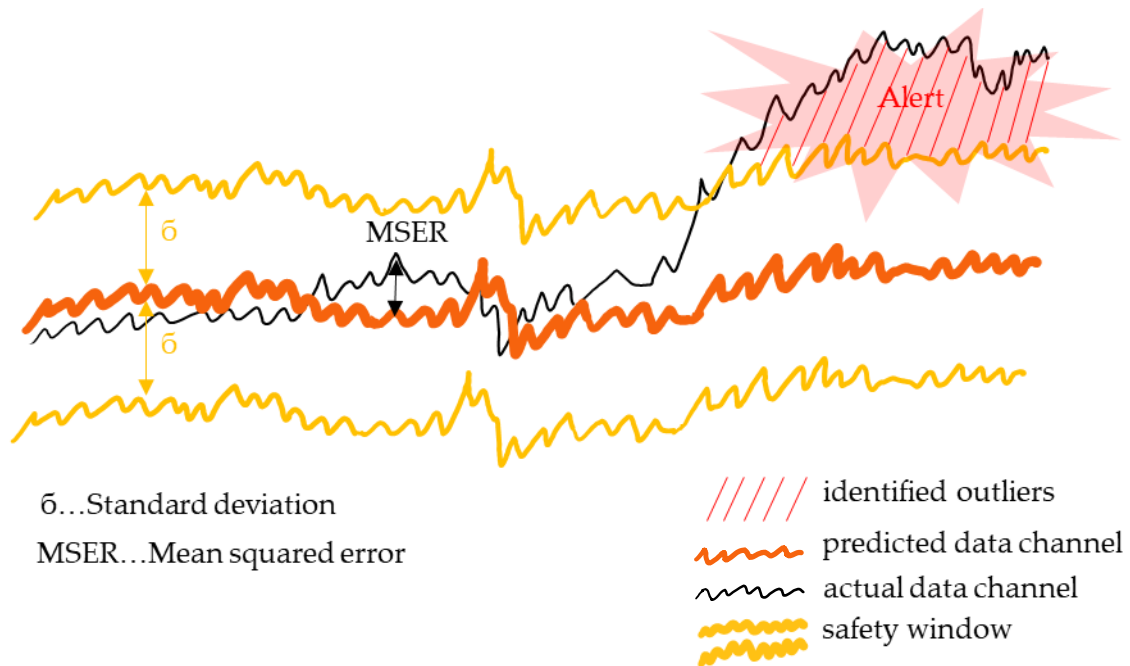


Figure 45: Principal of identifying outliers, in other words, abnormal behavior of the specific data channel

3.4.2 Extraction of Actual and Predicted Data

After applying the models of predicting the torque and standpipe pressure, the data points can be extracted for further calculations.

3.4.3 Compute Mean Squared Error (MSER)

After simulating the curves for TQA and SPPA the error between the predicted and actual data and between the future prediction and trend lines respectively can be calculated. The mean squared error function was applied to each timestamp.

$$MSER = \sqrt{(P_{actual} - P_{predicted})^2} \quad (37)$$

3.4.4 Obtain Standard Deviation

The standard deviation of the calculated MSER can be computed by the statistical approach. The error histogram in the figure shows the distribution of the MSER and the standard deviation in theory. The data samples (MSER of each timestamp) are plotted against their density (occurrence). By evaluating the mean, the standard deviation (of the normally distributed histogram) is defined to the left and right.

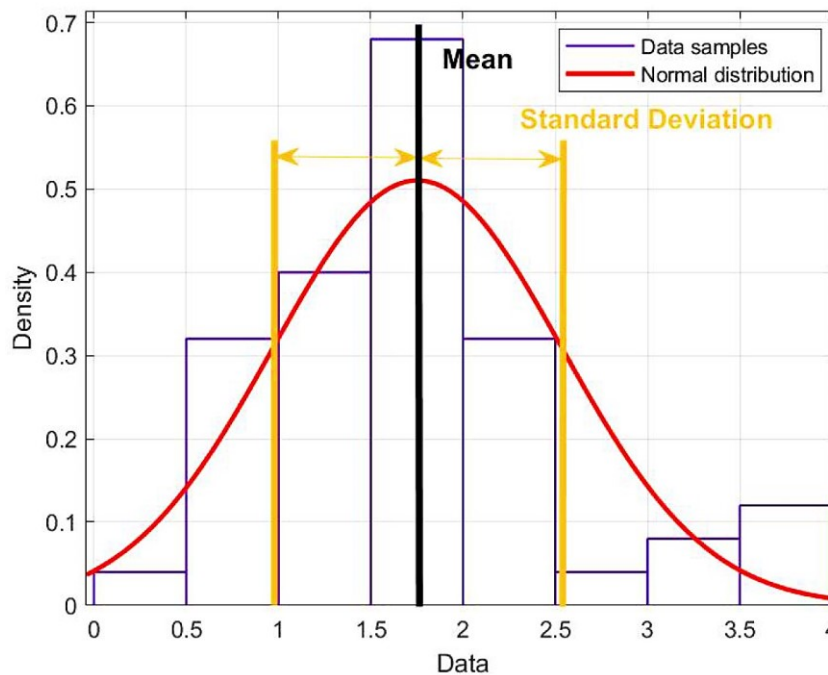


Figure 46: Normal distributed histogram of data samples (MSER of each timestamp), indicating mean and standard deviation

The standard deviation for a sample is calculated as followed.

$$\sigma = \sqrt{\frac{\sum_{i=1}^n (x_i - x_{mean})^2}{(n-1)}} \quad (38)$$

where

σ is the Standard Deviation

x_i is the value of the sample

n is the total number of sample elements

x_{mean} is the sample mean

$$x_{mean} = \frac{\sum_{i=1}^n x_i}{n} \quad (39)$$

3.4.5 Create Windows

After obtaining the overall standard deviation explained earlier, the windows can be created once new predictions based on new data input were calculated.

3.4.6 Compare Actual Data with Predictive Windows

The actual data will be compared to the predictive windows. If the actual data is within the window, the situation is expected to be safe, and no alert will be triggered. In case the actual data is detected to be outside the window, alerts will be triggered accordingly.

3.5 Alert Level Definition and Activation

Once a specific amount of data point is identified as an outlier from the window of uncertainty, alerts are triggered accordingly. The main purpose is to indicate any potential evolving issue and to draw attention to the drilling personnel at an early stage of a possible problematic situation, but not to classify the reason at this point (more explanation will be given in the future work chapter).

The thresholds for the specific alerts were defined as followed:

- 50 data points of actual TQA above upper window border: potential packoff, stuck pipe
- 50 data points of actual TQA below lower window border: potential twist off
- 50 data points of actual SPPA above upper window border: potential packoff, plugged equipment (bit balling) or kick
- 50 data points of actual SPPA below lower window border: potential losses or washout of equipment

3.6 Standalone Application

The aim was to create a simple user interface (UI), which is capable of performing pre-processing, training algorithms, and operational evaluation of the imported data at the same time, without adding additional afford to the drilling personnel. The application was designed specifically for analyzing the behavior of surface torque (TQA) and standpipe pressure (SPPA). Figure 47 illustrates a flow chart of the methodology behind the developed standalone application.

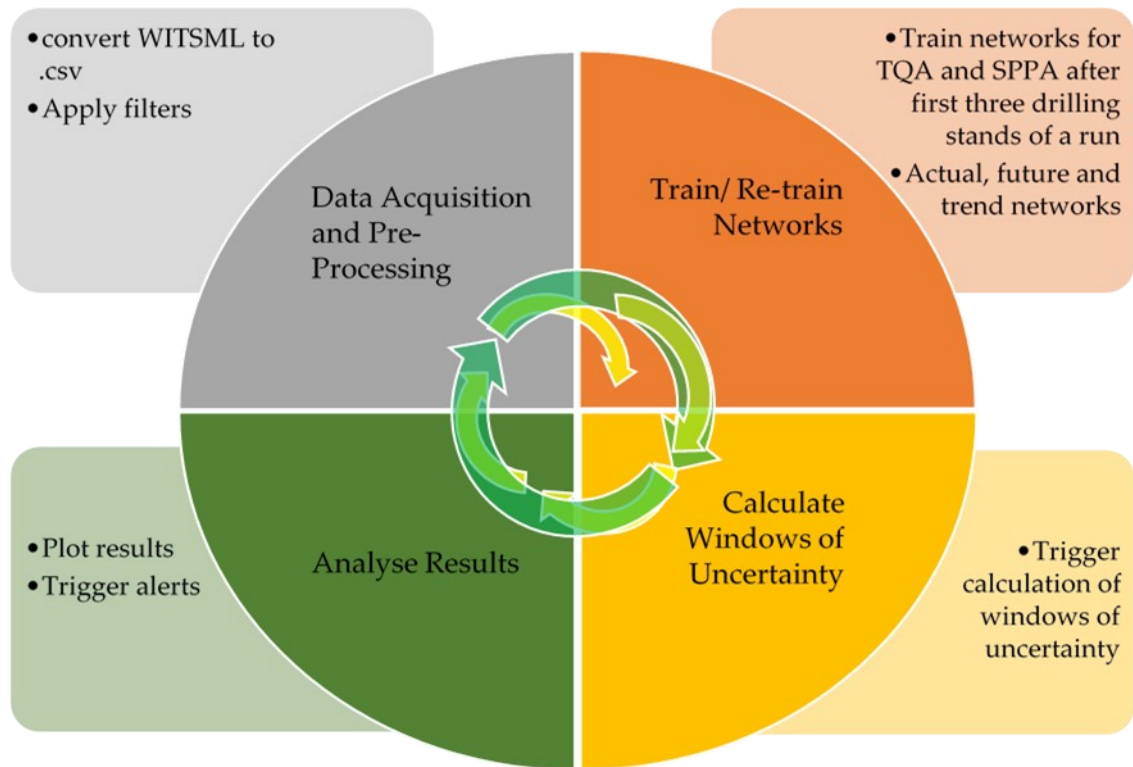


Figure 47: Outlook of the developed standalone application

The overview of the standalone application shows an indication of a critical torque after the comparison of actual versus predicted values of actual timestamps and predicted future timestamps versus future trends of TQA and SPPA (Figure 48).

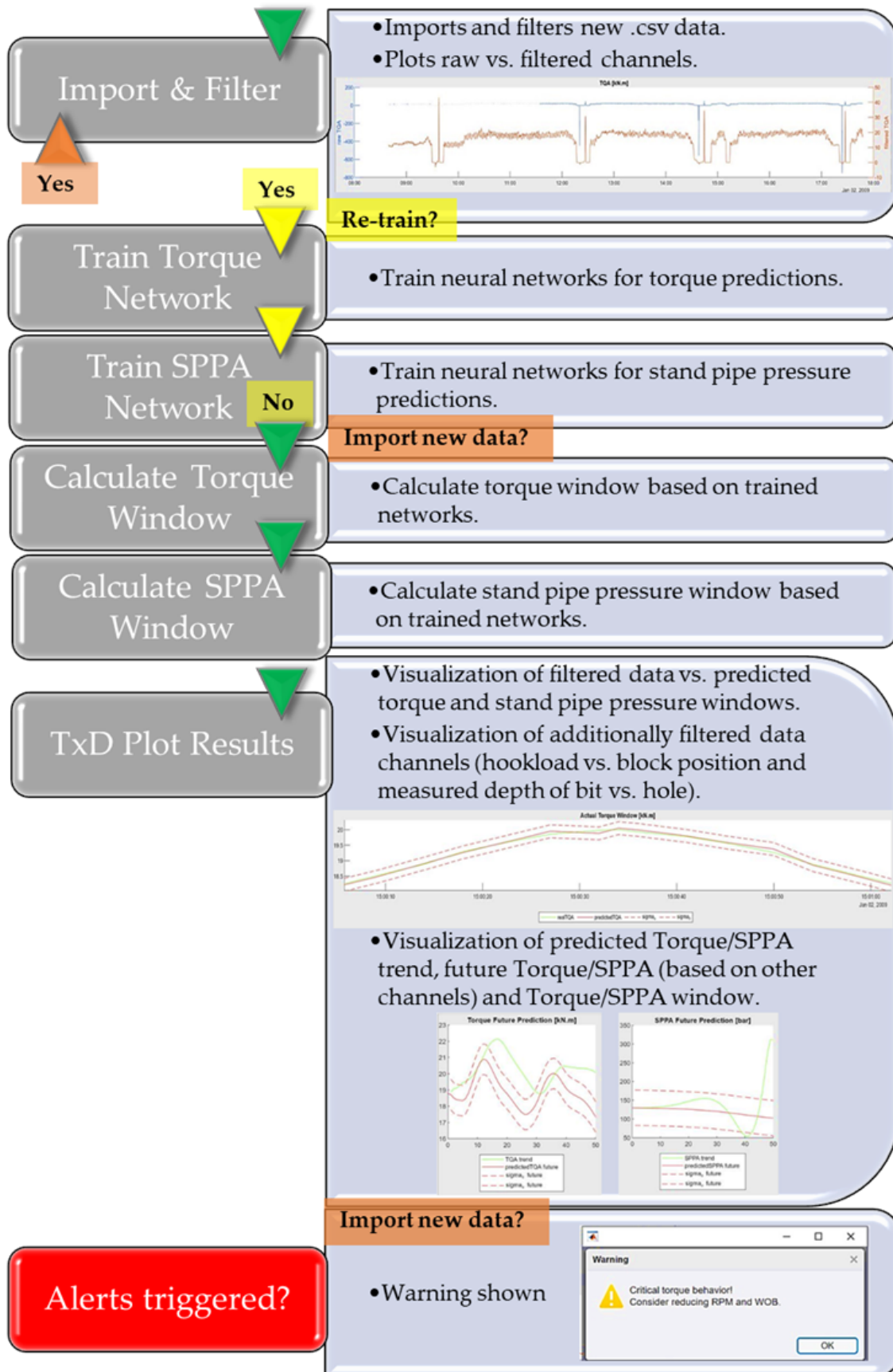


Figure 48: Workflow of the developed Standalone Application

3.6.1 Data Import and Filter

By pushing the data import and filter button, the folder which contains the new (actual) data sample can be selected. The format of the import data needs to be in “csv,” and the channel mapping of the sample data table needs to be adjusted accordingly in the script upfront. Usually, the channel mapping does not change during a well operation; hence once a standard mapping was applied, no further changes need to be done.

The software imports the raw data and applies pre-defined filters for filling missing data points and replacing outlier data values. The data is visualized once the filtering process was completed (Figure 49).

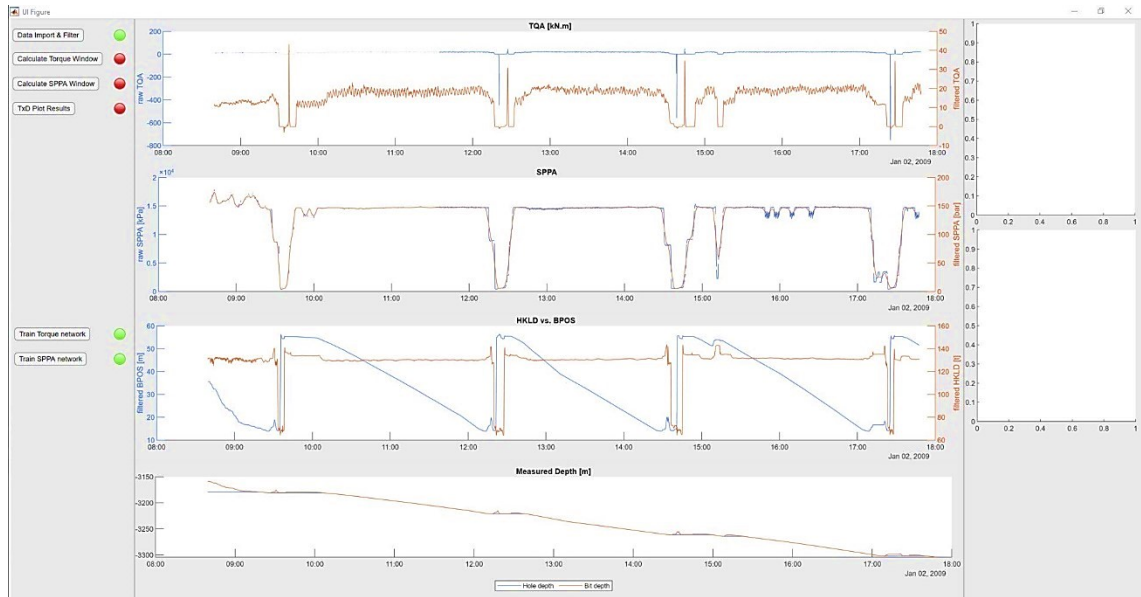


Figure 49: Visualization of the imported raw and filtered actual data in standalone application charts (well NO 15/9-F-15 A)

3.6.2 Train Torque Network

By pushing “train torque network,” training of the three torque prediction networks for a chosen time range is triggered. The start time and end time of the training data can be entered by the user (Figure 50).

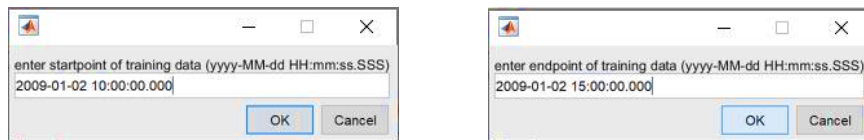


Figure 50: Enter the start point (start time) and endpoint (end time) of training data (well NO 15/9-F-15 A)

3.6.2.1 ANN for Actual TQA

The architecture of the ANN is illustrated in Figure 51.

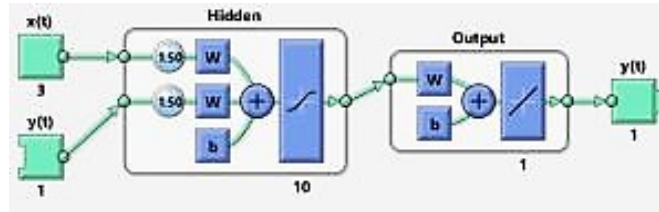


Figure 51: NARX Neural Network architecture, prediction of actual TQA time series

The ANN for predicting the actual torque values uses the input parameters shown in Table 7 for training.

Input time series $x(t)$			Target time series (output) $y(t)$
filtered_RPM2	filtered_SWOB	filled_HKLD	filtered_TQA2

Table 7: ANN for actual TQA prediction, data selection

3.6.2.2 ANN for future TQA prediction

The architecture of the ANN is illustrated in Figure 52.

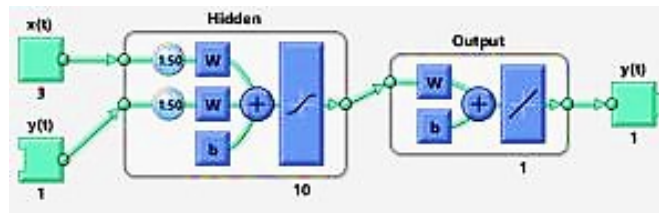


Figure 52: NARX Neural Network architecture, prediction of future TQA time series

The ANN for predicting the actual torque values uses the input parameters shown in Table 8 for training.

Timestamp	Input time series $x(t)$			Timestamp	Target time series (output) $y(t+50)$
t	filtered_RPM2	filtered_SWOB	filled_HKLD	t+50	filtered_TQA2

Table 8: ANN for future TQA prediction, data selection

3.6.2.3 ANN for Future Trend Prediction

The target time series, defining the desired outputs of the trend prediction, are stated in Table 9.

NAR Neural Network	Target time series (output) $y(t)$
TQA future trend	filtered_TQA2
SPPA future trend	filtered_SPP2

Table 9: ANNs for TQA and SPPA future trend prediction, data selection

Training the torque networks reached a sufficient performance after a small number of iterations and short durations:

- Training the actual torque prediction network took 12 iterations (20 seconds) with a performance of $1.45 \cdot 10^{-3}$.
- Training the future torque prediction network took 17 iterations (32 seconds) with a performance of $1.19 \cdot 10^{-3}$.
- Training the torque trend prediction network took 78 iterations (9 seconds) with a performance of $1.62 \cdot 10^{-3}$.

3.6.3 Train SPPA Network

By pushing “train torque network” training of the three standpipe pressure prediction networks as described in chapter 2.3 for a chosen time range. The start time and end time of the training data can be entered by the user (Figure 53).



Figure 53: Enter start point (start time) and endpoint (end time) of training data (well NO 15/9-F-15 A)

3.6.3.1 ANN for actual SPPA

The architecture of the ANN is illustrated in Figure 54.

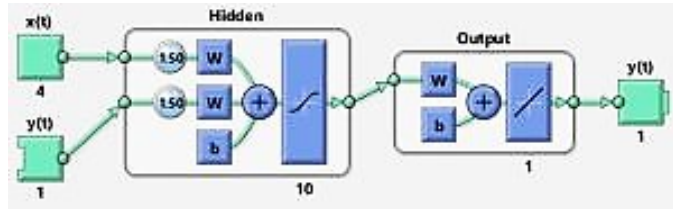


Figure 54: NARX Neural Network architecture, prediction of actual SPPA time series

The ANN for predicting the actual standpipe pressure values uses the input parameters shown in Table 10 for training.

Input time series x(t)					Target time series (output) y(t)
filled_ TFLO	filled_ SPM1	filled_ SPM2	filled_ SPM3	filled_Output DMEA	filtered_SPP2
SPM total					

Table 10: ANN for actual SPPA prediction, data selection

3.6.3.2 ANN for Future SPPA Prediction

The architecture of the ANN is illustrated in Figure 55.

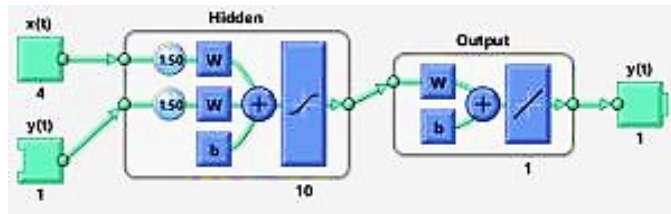


Figure 55: NARX Neural Network architecture, prediction of future SPPA time series

The ANN for predicting the actual standpipe pressure values uses the input parameters shown in Table 11 for training.

Timestamp	Input time series $x(t)$					Timestamp	Target time series (output) $y(t+50)$
	filled_TFLO	filled_SPM1	filled_SPM2	filled_SPM3	filled_Output DMEA		
t	filled_TFLO	filled_SPM1	filled_SPM2	filled_SPM3	filled_Output DMEA	t+50	filtered_SPP2
		SPM total					

Table 11: ANN for future SPPA prediction, data selection

The big difference to the torque networks in iterations of the training processes can be explained by the different training modes and the bit depth channel used as an input channel, which is gradually changing and, therefore, will not lead to steady gradients. The training processes were stopped after sufficient performance was reached.

- Training the actual SPPA prediction network took 600 iterations (manually stopped after 35 minutes 34 seconds) with a (sufficient) performance of $1.21 \cdot 10^{-8}$.
- Training the future SPPA prediction network took 325 iterations (manually stopped after 23 minutes 41 seconds) with a (sufficient) performance of $2.50 \cdot 10^{-7}$.
- Training the SPPA trend prediction network took 1000 iterations (2 minutes 7 seconds) with a performance of $4.05 \cdot 10^{-5}$.

Re-training of the networks should be performed at the start of a new drilling run once the first stands have been drilled without issues, or after a longer period of missing sensor data (an outage of sensor measurements) and drilling ahead of the required stands for sufficient amount of training data.

3.6.4 Calculate Torque Window

“Calculate Torque Window” will perform the statistical calculations for the construction of the torque windows of uncertainty, as described in chapter 2.4.

The histogram of the mean squared error of predicting the actual torque values is illustrated in Figure 56. The standard deviation can be evaluated after the normal distribution. The majority of error values was ranging between 0 and 0.4.

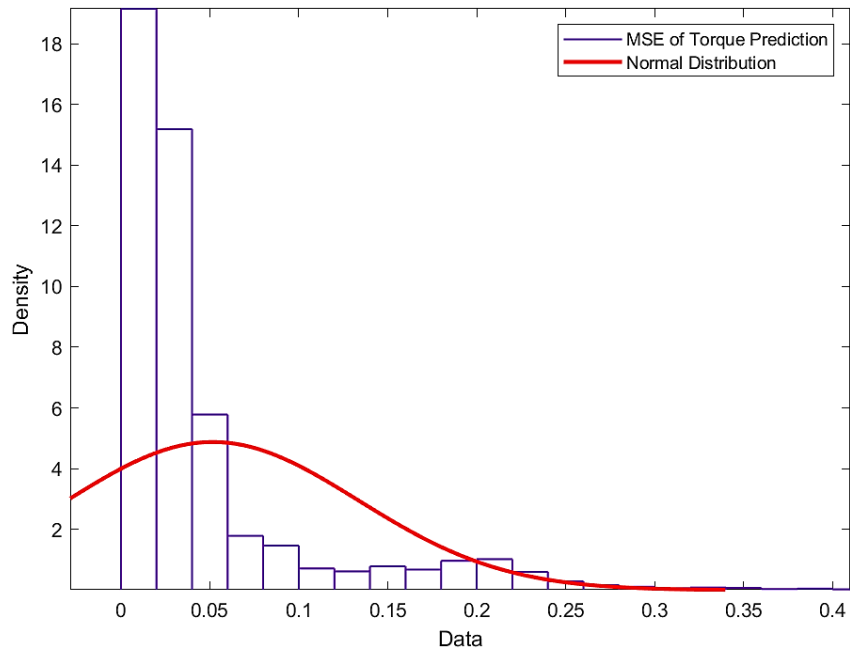


Figure 56: Mean squared error (MSER) of actual torque prediction (TQA), Histogram

3.6.5 Calculate SPPA Window

“Calculate SPPA Window” will perform the statistical calculations for the construction of the standpipe pressure windows of uncertainty, as described in chapter 2.4.

The histogram of the mean squared error of predicting the actual standpipe pressure values is illustrated in Figure 57. The standard deviation can be evaluated after the normal distribution. The majority of error values was ranging between 0 and below 0.05.

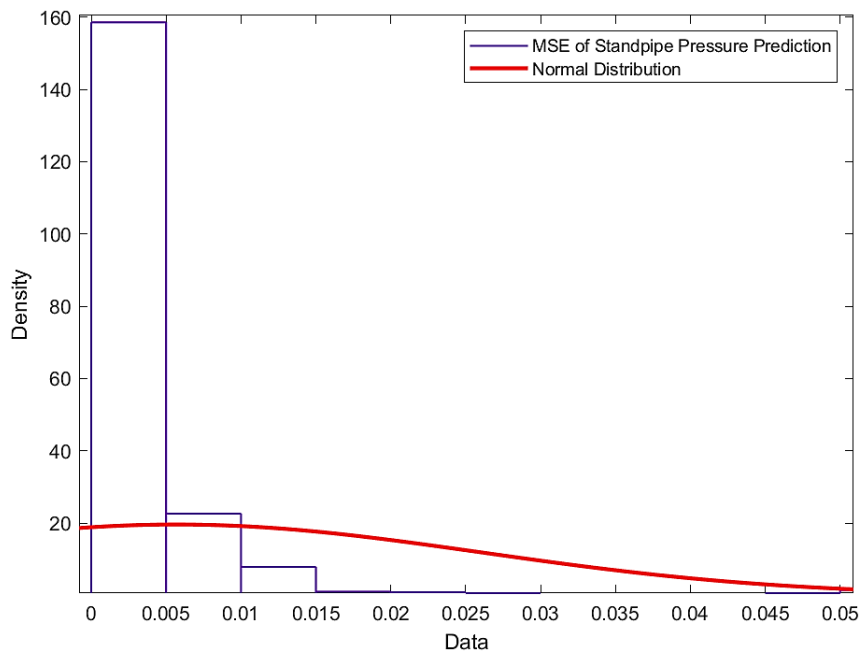


Figure 57: Mean squared error (MSER) of actual standpipe pressure prediction (SPPA), Histogram

3.6.6 TxD Plot Results

The final results are plotted by pushing the “TxD Plot Results” button. The charts area of the standalone application will change to visualize the actual vs. actual predicted windows of uncertainty, and future trend vs. future predicted windows of uncertainty. Figure 58 shows the visualization of the predicted data and windows of uncertainty in the actual data charts section (the predictions after timestamp 15:00:00 vary from the real values since the data was not included in the training data set). Additionally, the future predictions (50 timestamps after the last available real data point) are visualized in the right-hand charts section.

It has to be mentioned that future predictions potentially indicate upcoming problems by comparing the future trends of the channels to the predicted future uncertainty windows, but due to the insufficient testing period of the software, it is not considered for triggering alerts at this stage.

The outcrop in Figure 58 shows that the actual data channels (green line) stay inside the predicted actual windows of uncertainty (dashed red lines). Therefore no alerts will be triggered.

The future predictions show that the torque trend (green line) tends to exceed the upper boundary of the window ($\sigma_{0, \text{future}}$) partly over the next 50 timestamps and the standpipe pressure trend to stay within the window (between $\sigma_{u, \text{future}}$ and $\sigma_{o, \text{future}}$) over the next 40 timestamps with a sudden increase afterward. Both channels should be monitored closely for the new imported actual data (does actual data reflect a similar trend?) as well as updated future predictions for a potential indication of upcoming problems in such cases (Figure 59).

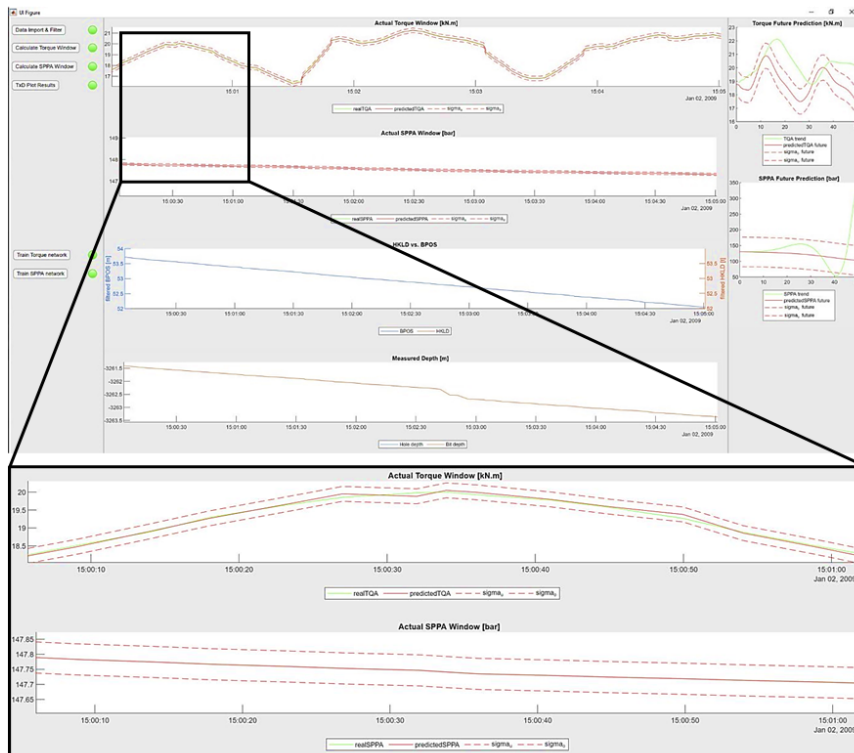


Figure 58: Visualization of the actual results in the standalone application (well NO 15/9-F-15 A).

Developed Methodology to Detect Anomalies in Drilling Behaviors

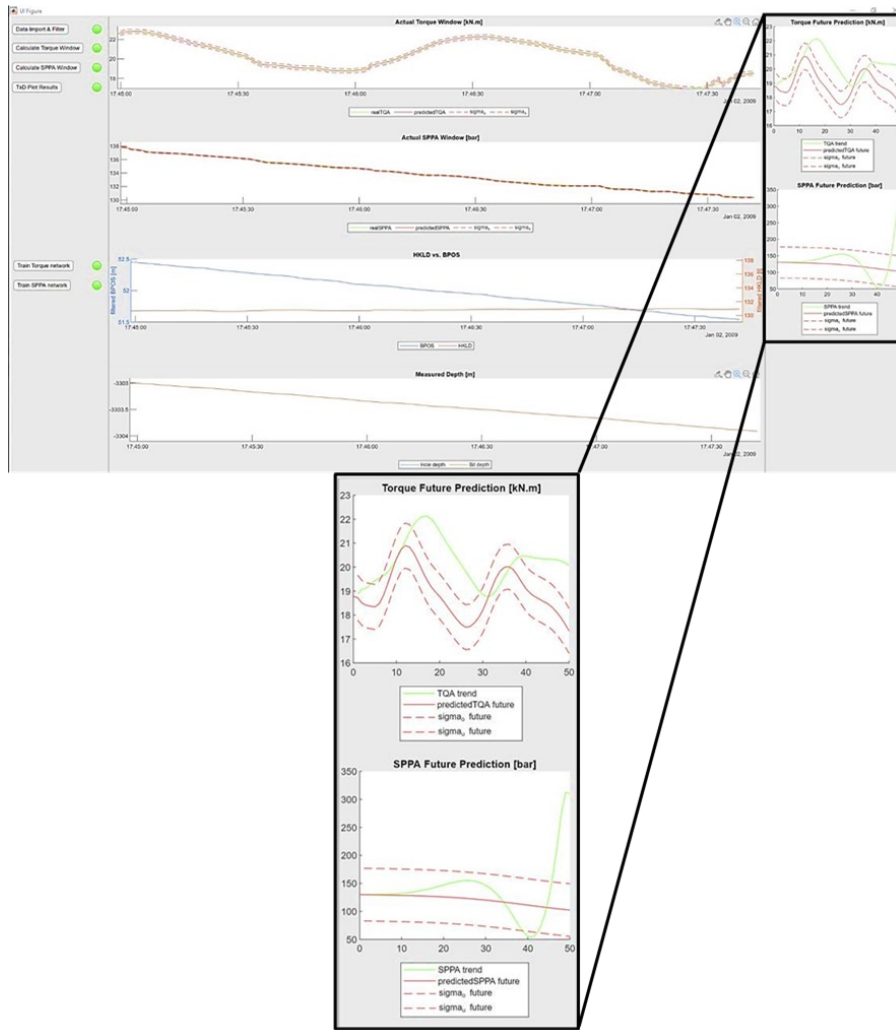


Figure 59: Visualization of the future results in the standalone application (well NO 15/9-F-15 A).

Alerts will be triggered accordingly after importing new sample data, recalculating the windows, and plotting the results. It is important that the new sample data contains the previous imported time range, hence continuously updating data similar to real-time mode. The real-time mode is not available in the developed application.

3.6.7 Advantages and Limitations of The Standalone Application

Table 12 compiles the advantages and disadvantages of the standalone application.



 <p data-bbox="236 763 300 1106">Advantages</p> <ul data-bbox="320 555 683 1077" style="list-style-type: none">• quick and easy to use import and filter• independent from data frequency• re-training of networks for desired time interval and calculation of results without re-start• illustration of desired actual data channels and results• warning signs shown immediately in case of pre-defined alert case• preview of future predictions (50 timestamps)	 <p data-bbox="818 689 882 1106">Disadvantages</p> <ul data-bbox="903 555 1249 936" style="list-style-type: none">• no real-time mode• .csv data format required• no direct configuration of data file mapping, network and alert settings• no specific classification of abnormality available (alert level)• no parallel zoom of charts (to show similar time interval)
---	---

Table 12: Advantages and disadvantages of the standalone application

Chapter 4 Case Studies

In order to examine the functionality of the developed standalone application, made-up scenarios based on manipulated data are created. The Data from Volve (well NO 15/9-F-15 A) was manipulated in terms of deviating torque and standpipe pressure data measurements to provide sufficient data for case studies evidence.

4.1 Model Definition

Similar network settings in terms of hyperparameters, as described in chapter 3.6 have been used to test the standalone application. The tests were performed after manipulating the original raw data set to provide the different test scenarios. After re-training was performed, a similar data file, including manipulated data points after 17:47 was imported to test the standalone application. The networks have been re-trained based on wells NO 15/9-F-15 A time interval from 2009-Jan-02 8:39 to 2009-Jan-02 17:47 (Figure 60).

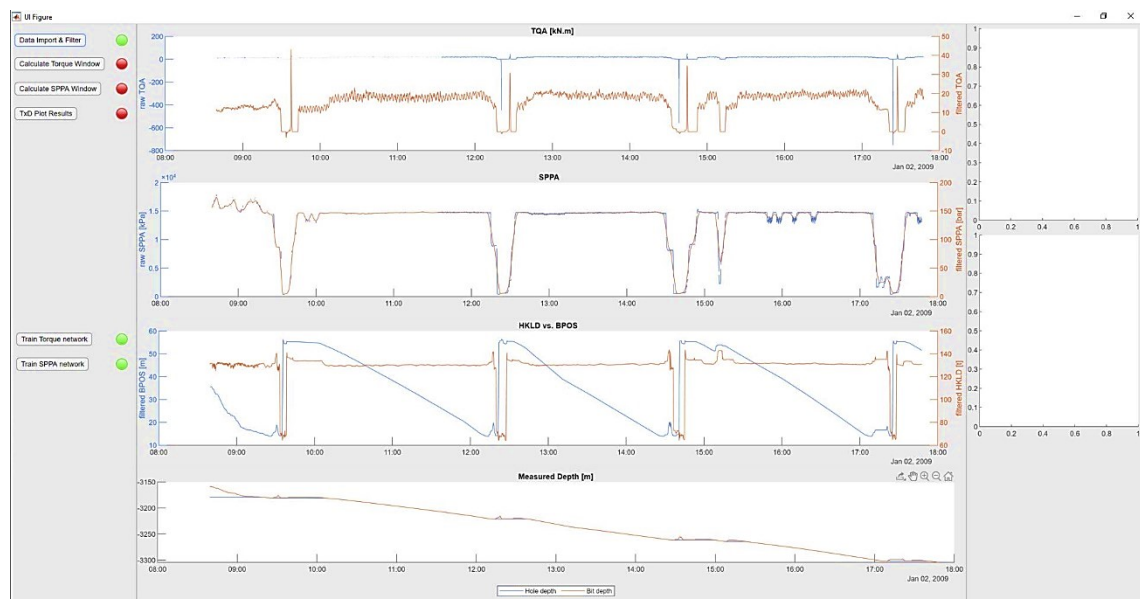


Figure 60: Standalone application view of the actual data training interval, imported, filtered, and trained networks, well NO 15/9-F-15 A

To demonstrate that the application requires a short amount of time for training, in order to provide feasibility of handling during ongoing drilling operations (e.g. whilst performing a weight to weight connection) and without adding additional effort to the drilling personnel, the performance of training the system is given:

- Training the actual torque prediction network took 35 iterations (1 minute 26 seconds) with a performance of $1.40 \cdot 10^{-3}$.
- Training the future torque prediction network took 39 iterations (1 minute 34 seconds) with a performance of $1.41 \cdot 10^{-3}$.
- Training the torque trend prediction network took 199 iterations (26 seconds) with a performance of $1.30 \cdot 10^{-3}$.

- Training the actual SPPA prediction network took 45 iterations (manually stopped after 3 minutes 00 seconds) with a (sufficient) performance of $1.2 \cdot 10^{-5}$.
- Training the future SPPA prediction network took 35 iterations (manually stopped after 3 minutes 00 seconds) with a (sufficient) performance of $2.81 \cdot 10^{-3}$.
- Training the SPPA trend prediction network took 1000 iterations (3 minutes 13 seconds) with a performance of $4.09 \cdot 10^{-4}$.

4.2 Performed Scenarios

The standalone application has been trained for the following scenarios:

- Excessive torque
- Decreasing torque
- Excessing standpipe pressure
- Decreasing standpipe pressure.

4.2.1 Excessive Torque

To test the alerting for excessive torque, the dataset for upcoming test import (100 timestamps) was manipulated by increasing the actual torque values (raw datapoints inside red square) by 5 kN.m (Figure 61).

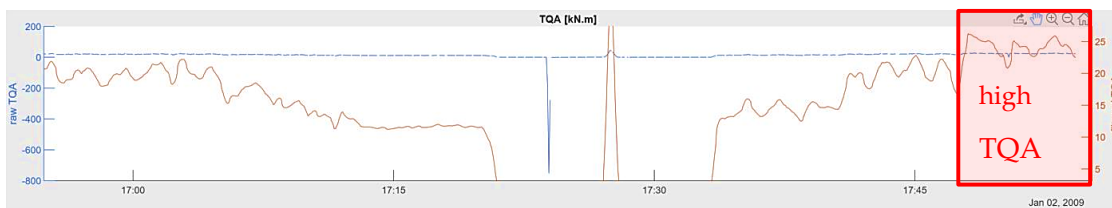


Figure 61: Manipulated input data, excessive torque

Figure 62 shows an increase of actual torque after importing new timestamps (after approx. 17:48) and the actual (real TQA - in green) exceeding the predicted window (σ_0 - in red). Hence a warning for excessive torque was triggered.

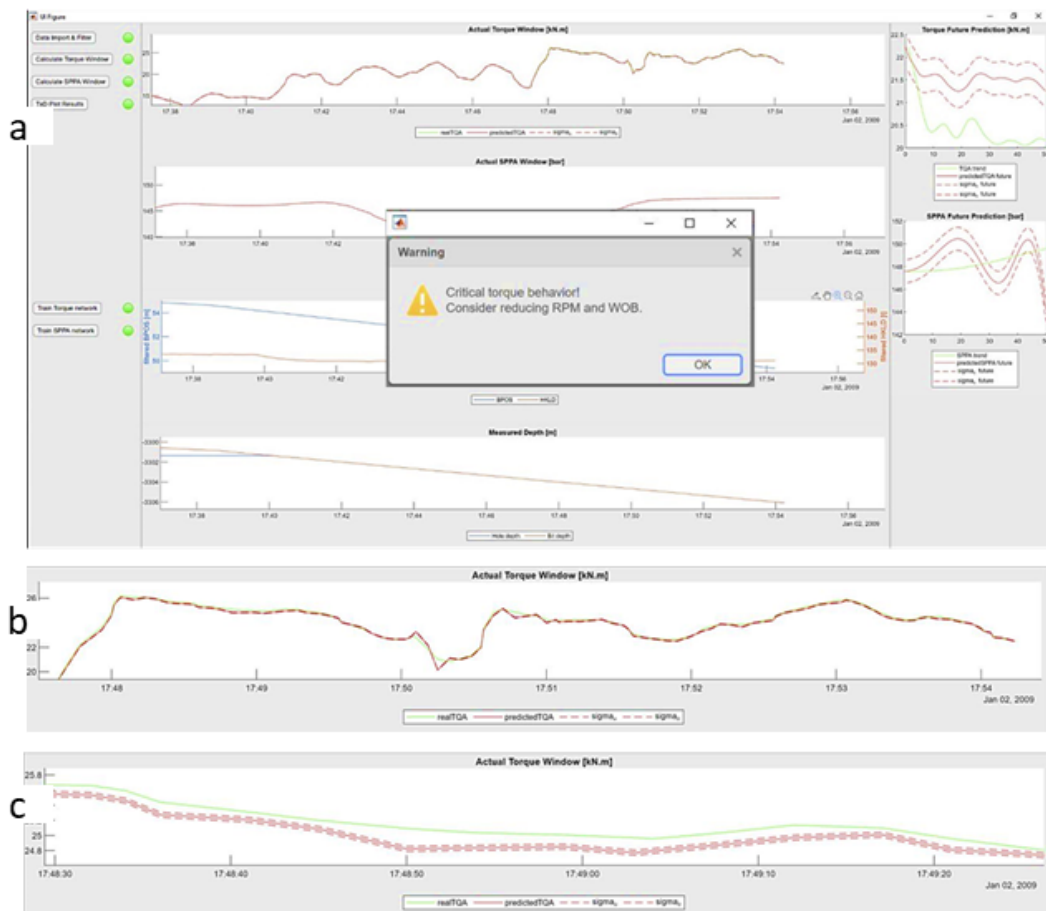


Figure 62: Performed Scenario to identify excessive torque behavior, manipulated well data (NO 15/9-F-15 A). a.) Standalone application view shows a warning message shown b.) Zoomed “Actual Torque Window” view indicates the actual outlier data in green from the predicted window in red c.) Zoomed “Actual Torque Window” view (II) provides a closer look into the outlier data range, whereas the actual TQA data in green is clearly exceeding the predicted window of uncertainty (upper border) in red.

The application detected abnormal torque behavior based on the increased values by five kN.m accordingly; hence the networks can be considered as sufficient models. However, for advanced detection, a classification of the specific issue, additional data channels should be implemented as network training references [directional drilling data (e.g., inclination, dogleg severity)].

4.2.2 Decreased Torque

To test the alerting for decreased torque, the dataset for upcoming test import (100 timestamps) was manipulated by decreasing the actual torque values (raw datapoints inside red square) by 5 kN.m (Figure 63).

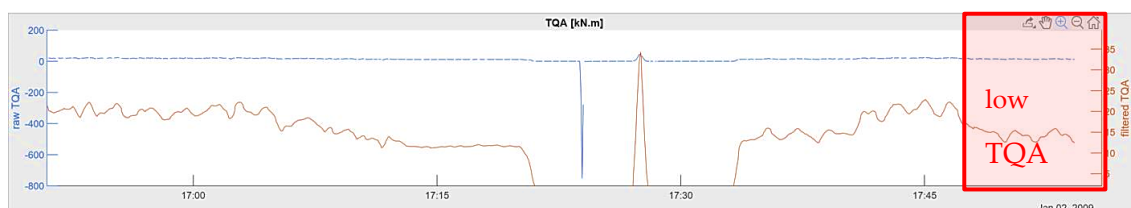


Figure 63: Manipulated input data, decreased torque

Figure 64 shows a decrease of actual torque after importing new timestamps (after approx. 17:48) and the actual (real TQA – in red) exceeding the predicted window (σ_{u} – in red); hence a warning for decreased torque was triggered.

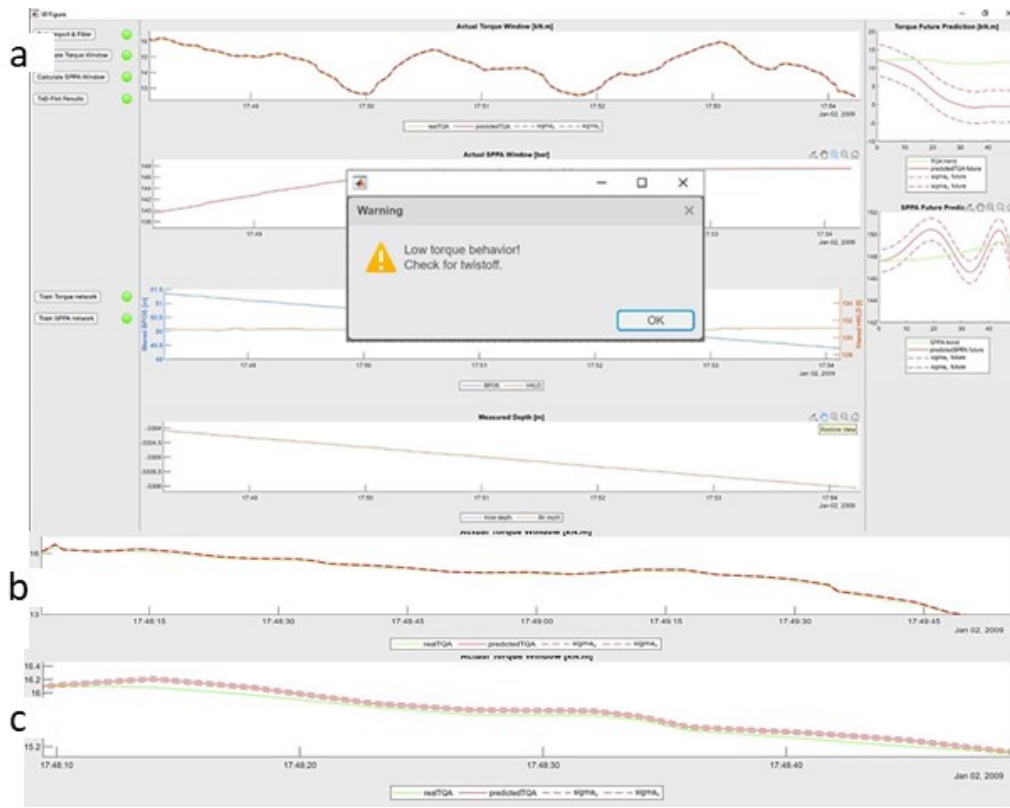


Figure 64: Performed Scenario to identify decreased torque behavior, manipulated well data (NO 15/9-F-15 A). a.) Standalone application view shows a warning message shown b.) Zoomed “Actual Torque Window” view indicates the outlier actual data in green from the predicted window in red c.) Zoomed “Actual Torque Window” view (II) provides a closer look into the outlier data range, whereas the actual TQA data in green is clearly exceeding the predicted window of uncertainty (lower border) in red.

The application detected abnormal torque behavior based on the decreased values by 5 kN.m accordingly, hence the networks can be considered as sufficient models. Similar approach for potential improvement of the models as for excessive torque should be considered in the future.

4.2.3 Excessive Standpipe Pressure

To test the alerting for excessive standpipe pressure, the dataset for upcoming test import (100 timestamps) was manipulated by increasing the actual SPPA values (raw datapoints inside red square) by 10000 kPa (100 bar) (Figure 65).

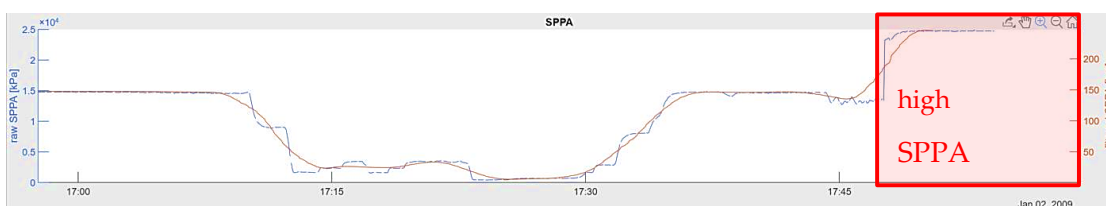


Figure 65: Manipulated input data, excessive standpipe pressure

Figure 66 shows significant increase of actual SPPA after importing new timestamps (after approx. 17:48) and the actual (realSPPA – in green) exceeding the predicted window (sigma₀ – in red), hence a warning for excessive SPPA was triggered.

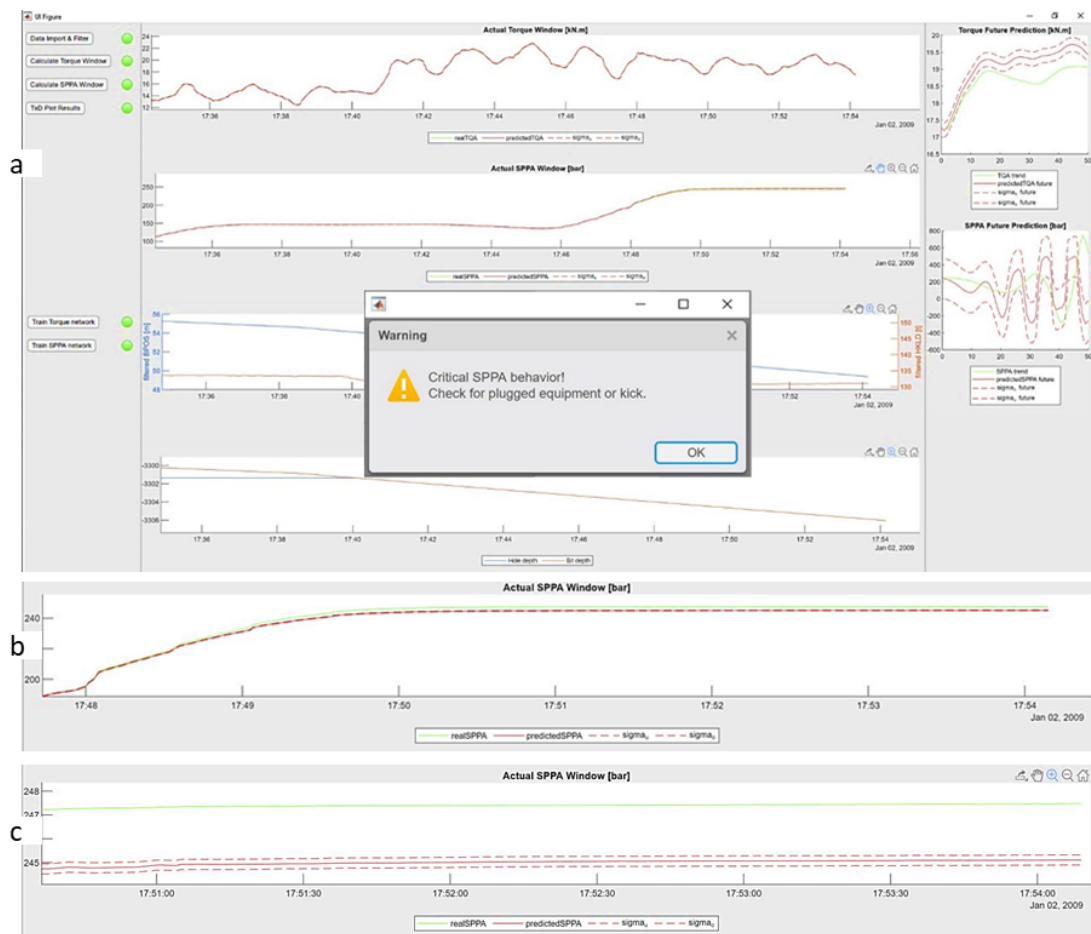


Figure 66: Performed Scenario to identify excessive SPPA behavior, manipulated well data (NO 15/9-F-15 A). a.) Standalone application view shows a warning message shown b.) Zoomed “Actual SPPA Window” view indicates the outlier, actual data in green from the predicted window in red c.) Zoomed “Actual SPPA Window” view (II) provides a closer look into the outlier data range, whereas the actual SPPA data in green is clearly exceeding the predicted window of uncertainty (upper border) in red.

While the tests performed based on manipulated standpipe pressure data provided evidence for abnormal SPPA behavior for significantly higher values (>50 bar increase), detection was showing less reliability with decreasing values added, hence potential miss of detection (and therefore warnings) could be induced after slight increase of SPPA. The miss of detecting slight increased SPPA values could lead to delayed recognition of severe problems like equipment failure.

Output of the SPPA networks could be improved by implementation of additional data channels for training input. In other words, discharge pressure, ECD and implementation of formation data classification would improve detection of abnormal standpipe pressure.

4.2.4 Decreased Standpipe Pressure

To test the alerting for decreased standpipe pressure, the dataset for upcoming test import (100 timestamps) was manipulated by decreasing the actual SPPA values (data points inside red square) by 10000 kPa (100 bar) (Figure 67).

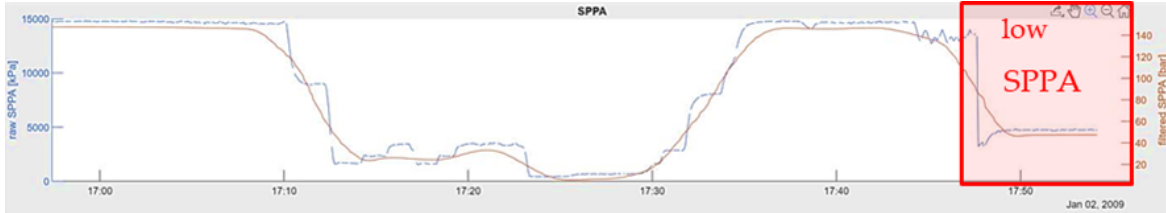


Figure 67: Manipulated input data, decreased standpipe pressure

Figure 68 shows a significant decrease of actual SPPA after importing new timestamps (after approx. 17:48) and the actual (realSPPA – in green) exceeding the predicted window (sigma_u – in red); hence a warning for decreased SPPA was triggered.

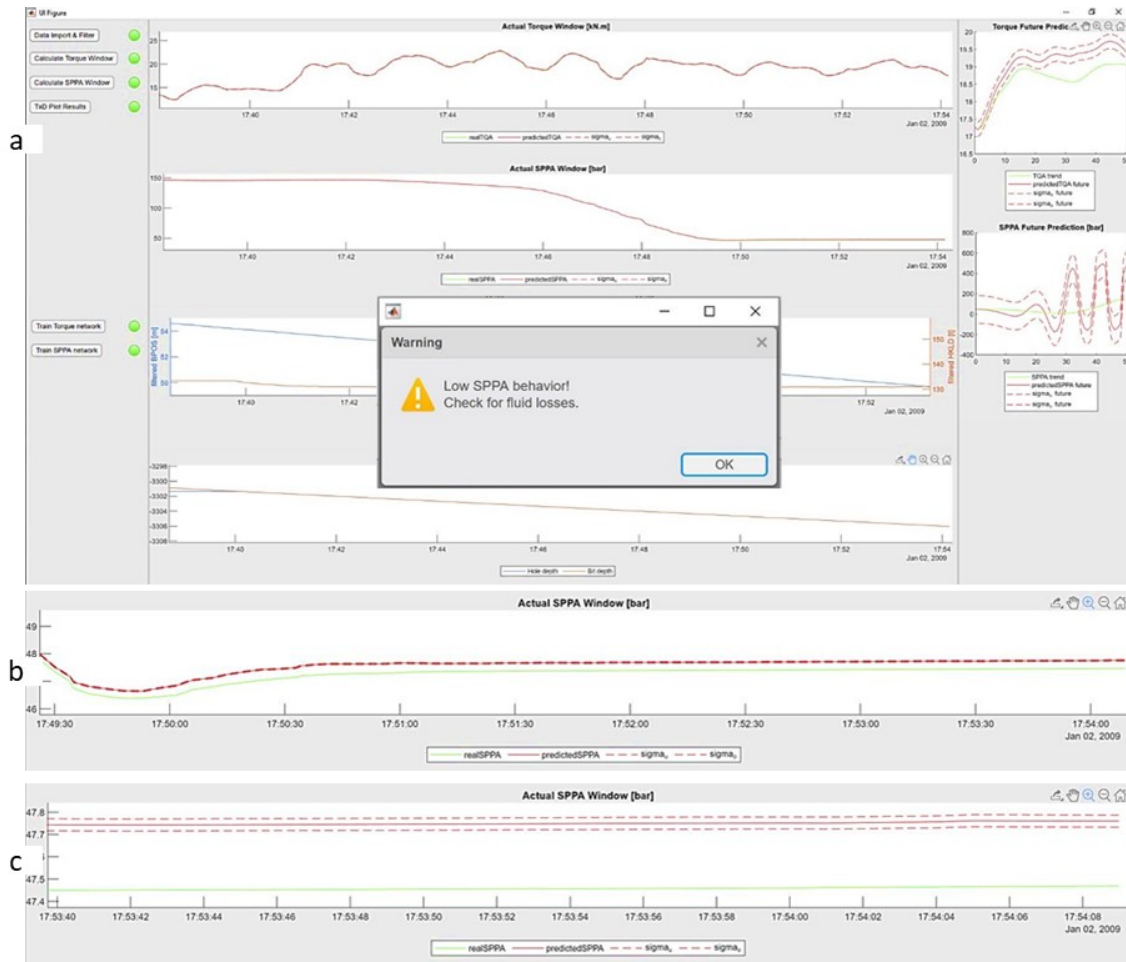


Figure 68: Performed Scenario to identify decreased SPPA behavior, manipulated well data (NO 15/9-F-15 A). a.) Standalone application view shows a warning message shown b.) Zoomed “Actual SPPA Window” view indicates the actual outlier data in green from the predicted window in red c.) Zoomed “Actual SPPA Window” view (II) provides a closer look into the outlier data range, whereas the actual SPPA data in green is clearly exceeding the predicted window of uncertainty (lower border) in red.

While the tests performed based on manipulated standpipe pressure data provided evidence for abnormal SPPA behavior for significantly lower values (>50 bar decrease), the detection was showing less reliability with decreasing values removed, hence potential miss of detection (and therefore warnings) could be induced after slight decrease of SPPA. The miss of detecting slightly decreased SPPA values could lead to delayed recognition of severe problems like severe fluid losses to the formation or washouts.

A similar approach for potential improvement of detecting abnormal behavior as for excessive standpipe pressure should be considered in the future.

4.3 Case Study Conclusion

After undertaking the study on the provided scenarios in this chapter, the standalone application has proven its user-friendliness by an easy approach of performing analysis on input data.

The application showed a short timeframe between configuring the models (training the networks), importing new data into the program, and showing valuable results, for instance, warning messages, in case abnormal drilling behavior was detected. The accuracy of the predictions was sufficient after short training intervals, although results could be improved by considering additional data channels.

Aside from the proven functionalities of the developed standalone application, a number of limitations still appear. The import data needs to be converted from WITSML to csv format externally before it can be imported into the application; therefore real-time streaming without manual input is not applicable yet. A direct configuration in the standalone application is not possible and needs to be handled by the administrator in case changing conditions and considerations is desired.

Chapter 5 Conclusions and Future Work

5.1 Conclusions

The main conclusion of the presented work can be summarized in the following points.

1. The major drilling problems that appear during routine operations are related to pipe sticking (differential sticking or mechanical sticking), tight hole conditions, bit balling, losses, kicks, or the equipment being used.
2. Today a lot of simulation programs are available for torque and standpipe pressure calculations and are used for real-time monitoring purposes. The actual trend of the data can be compared to the simulated expected values. Hence drilling problems can be noticed by deviating trends but can potentially be missed due to human factors.
3. Often historical data is being used for planning purposes and to review the performance at previous well operations of a similar field. This can be a useful approach for choosing the equipment and creation of the drilling program. However, previous theses have shown that this is not applicable for detecting drilling problems as minor changes in the setup or downhole conditions will lead to a completely different scenario.
4. Since the age of machine learning also reached the oil business a decade ago, various machine learning approach concepts for minimizing health, safety, and environmental risks and improving drilling performance have been proposed, developed, and tested to the industry. Amongst various statistical learning models, artificial neural networks for torque and drag predictions and lost circulation, as well as drilling hydraulic optimization related to standpipe pressure prediction, have been introduced and discussed in this thesis.
5. Up to now, simulating torque and drag and standpipe pressure after standard principals are still state of the art and most used approaches at the drilling rig.
6. The developed hybrid model compiles six artificial neural networks, whereas three are used for predictions of a single data channel (e.g. torque or standpipe pressure). The actual data channel values are predicted based on a set of related data channels and are compared to the actual data afterward. Additionally, future values are predicted based on related actual data channels, and the future trend of a specific data channel is predicted based on the actual values. Windows of uncertainty are calculated based on the mean squared error between actual and predicted values to identify outliers (deviations from the trend) and, therefore, potential drilling-related problems. The standard deviation is used to create the windows. Alerts are being triggered once a pre-defined number of outliers was identified, and warning signs are shown.

7. The created standalone application provides an easy user interface to ease data import & filter, training the networks, calculation, and visualization of the results and to provide warning messages related to the type of the issue. The advantages of the application include quick and easy usage, independence from the data frequency, re-training of networks for the desired time interval, and calculation of results without restarting it. The illustration of the actual data channels and results, warning signs being shown, and a preview of future predictions (50 timestamps) also add up to a plus. Potential future work and disadvantages of the app can be seen in the missing real-time mode, the required data format (.csv), and that a direct configuration of the data file mapping, network, and alert settings, as well as parallel zoom of the charts, is not available yet.
8. Based on the results of the conducted scenarios, the following points can be considered as main findings.
 - The planned laboratory tests at UFES Brazil (mini drilling rig) could not be performed due to the COVID-19 situation, hence data from Volve (well NO 15/9-F-15 A) was manipulated in terms of exceeding torque and standpipe pressure data measurements to provide sufficient data for case studies evidence.
 - Performed Scenarios have been performed on four main scenarios, i.e. excessive torque, decreased torque, excessive standpipe pressure, and decreased standpipe pressure.
 - The outcome of the case studies was that while abnormal torque behavior could be detected properly at small deviations from the safety windows, abnormal standpipe pressure tends to be detected the easier, the larger the deviation of the actual values from the predicted. In other words, the standpipe pressure model provides the potential for improvement.
 - It is recommended to consider additional input data channels for predicting torque and standpipe pressure and to perform further tests in real-time and on the rig site, respectively.

5.2 Future work

General future work should be done on the main developed hybrid model:

- Real-time mode for automated data import (direct import and conversion of WITSML data)
- Classification of alert level and issue type (e.g. loss rate or kick rate could be calculated)
- Improve actual networks and therefore, alert timing by consideration of additional input data channels for torque (e.g. inclination, DLS) and standpipe pressure predictions (e.g. discharge pressure, ECD, formation classification).
- Improve future networks and therefore alert timing by consideration of additional input data channels and neural network settings (e.g. type, parameters)

- Additional tests based on real issue data and in real-time (data stream at or from rig site)

The following implementations should be done to the standalone application to improve capabilities, independent from administrators (easier user handling) and alert timing:

- Allow for direct configuration of data format and input, networks training parameters and alerts.
- Parallel zoom option of charts
- Mark outlier regions of actual data from windows of uncertainty in the results charts
- Improve preview of future predictions (show information about changing upcoming trends)

Appendix A

Developed Scripts

A.1.1 Python Script

Incoming WITSML data is converted from WITSML to CSV format via a python script.

```
- <logData>
<mnemonicList>TIME,GRID CORR,SHKLV,GS_SPM3,ROP30s,MWIN,MTF_RT,DLREF,PMAX_RT,SGY,GS_TV06,DCRNT,ETSL,MSP6,ECD_MW_IN,MBOT,HV,CRS4,OSTM,MS1(
<unitList>s,dega,unitless,1/min,m/h,mS/m,dega,rpm,kPa,m/s2,m3,A,s,unitless,g/cm3,unitless,unitless,unitless,s,unitless,ohm.m,m,unitless,m3,m,unitless,h,unitles
<data> 2009-01-
21T00:36:32.000Z,,0,,0.9906,,,,,65.47104,,,,,2794.52832,,,,,39.93,,2794.52832,8.0400004336052,,23.91,0,,60,,0,,30,55.0891107724152,5616,,,,,247.78,,
20,,,,,1,,2794.52832,44928,,,,,0,,,,,0,,19501.8899512996,,,,,248.38,,0,293.88816,0,,4.182626318,50.92,,,,,3,78,,156.3759695575,,,,,1,0,,153,,,,
<data> 2009-01-
21T00:36:36.000Z,,0,,0.646176,,,,,65.47104,,,,,2794.52832,,,,,39.93,,2794.52832,10.277100048352,,23.91,0,,60,,0,,30,0.5616,,,,,247.78,,,,0,168,32.1740
20,,,,,1,,2794.52832,44928,,,,,0,,,,,0,,19501.8899512996,,,,,248.38,,0,293.88816,0,,4.182626318,50.92,,,,,3,78,,156.4122569471,,,,,1,0,,153,,,,
<data> 2009-01-
21T00:36:40.000Z,,0,,0.24384,,,,,65.47104,,,,,2794.52832,,,,,39.93,,2794.52832,11.6871507146167,,23.91,0,,60,,0,,30,0.5616,,,,,247.78,,,,0,168,32.1740
20,,,,,1,,2794.52832,44928,,,,,0,,,,,0,,19501.8899512996,,,,,248.38,,0,293.88816,0,,4.182626318,50.92,,,,,3,78,,156.4394724893,,,,,1,0,,153,,,,
<data> 2009-01-
21T00:36:44.000Z,,0,,0.070104,,,,,65.47104,,,,,2794.52832,,,,,39.93,,2794.52832,12.5684323810321,,23.91,0,,60,,0,,30,0.5616,,,,,247.78,,,,0,168,32.174
20,,,,,1,,2794.52832,44928,,,,,0,,,,,0,,19501.8899512996,,,,,248.38,,0,293.88816,0,,4.182626318,50.92,,,,,3,78,,156.48936765,,,,,1,0,,153,,,,
<data> 2009-01-
21T00:36:48.000Z,,0,,0,,65.47104,,,,,2794.52832,,,,,39.93,,2794.52832,39.1017896298776,,23.91,0,,60,,0,,30,0.5616,,,,,247.78,,,,0,168,32.1740486,,
20,,,,,1,,2794.52832,44928,,,,,11,,,,,0,,19534.2953105775,,,,,248.38,,0,293.88816,0,,4.182626318,50.93,,,,,3,78,,156.580086124,,,,,1,0,,153,,,,
<data> 2009-01-
21T00:36:52.000Z,,0,,0,,65.47104,,,,,2794.52832,,,,,39.93,,2794.52832,44.6742013975197,,23.91,0,,60,,0,,30,0.5616,,,,,247.78,,,,0,168,32.1740486,,
20,,,,,1,,2794.52832,44928,,,,,11,,,,,0,,19534.2953105775,,,,,248.38,,0,293.88816,0,,4.182626318,50.93,,,,,3,78,,156.6073016662,,,,,1,0,,153,,,,
<data> 2009-01-
21T00:36:56.000Z,,0,,0,,65.47104,,,,,2794.52832,,,,,39.94,,2794.52832,54.1513688563561,,23.91,0,,60,,0,,30,75.4286447872619,5616,,,,,247.78,,,,0,1
20,,,,,1,,2794.52832,44928,,,,,0,,,,,0,,19593.9349611634,,,,,248.38,,0,293.88816,0,,4.182626318,50.93,,,,,3,78,,156.670804598,,,,,1,0,,153,,,,
<data> 2009-01-
21T00:37:00.000Z,,0,,0,,65.47104,,,,,2794.52832,,,,,39.94,,2794.52832,67.256865962041,,23.91,0,,60,,0,,30,75.4286447872619,5616,,,,,247.78,,,,0,1
20,,,,,1,,2794.52832,44928,,,,,0,,,,,0,,19593.9349611634,,,,,248.38,,0,293.88816,0,,4.182626318,50.93,,,,,3,78,,156.7206997587,,,,,1,0,,153,,,,
```

Figure 69: WITSML (.xml) Well Data Outcrop before format conversion to CSV (.csv)

```
import glob
z=glob.glob(r"C:\Users\Andi\OneDrive\Uni\Master Thesis\data collection\Norway-StatoilHydro-15_$47$-9-F-15A_converted\1\log\DateTime\850\1\*.xml')
3
4
5def xml_to_csv(input_):
6    with open(input_,"r") as file:
7        raw = file.read()
8
9    import xmltodict
10    data = xmltodict.parse(raw)
11    #print(data)
12
13
14    import pandas as pd
15    df = pd.DataFrame(data["logs"])
16    #df.head()
17
18
19    dl=data["logs"]["log"]
20
21    logData=dl["logData"]
22    logDl=logData["data"]
23
24
25    #columns=["TIME","MTOA","TVCA","TCHR","TV14","DBTM","TV04","Bit_RPM","TV05","TV11","G_NC4","RSDX","DCHV","HKLD","G_C1","TV10","FVOC","TV03","T
26
27    df = pd.DataFrame([sub.split(",") for sub in logDl])
28    #df.columns=columns
29
30
31    # =====
32    # import itertools
33    # key = lambda sep: sep == ','
34    # zz=[list(group) for is_key, group in itertools.groupby(list(LogData['mnemonicList']), key) if not is_key]
35
36    # import itertools
37    # key = lambda sep: sep == '_'
38    # zz=[list(group) for is_key, group in itertools.groupby(zz, key) if not is_key]
39
40    #
41    # =====
42    output=input_[0:-4]+str(".csv")
43    df.to_csv(output, sep=";")
44
45
46#List2 = [list(group) for key, group in groupby(LogData['mnemonicList'], lambda x: x == ",",) if not key]
47
48li=["00003.xml"]
49]
50for andreas in z:
51    xml_to_csv(andreas)
```

Figure 70: Python script, xml to csv converter

```

1 ;0;1;2;3;4;5;6;7;8;9;10;11;12;13;14;15;16;17;18;19;20;21;22;23;24;25;26;27;28;29;30;31;32;33;34;35;36;37;38;39;40;41;42;43;44;45;
2 0;2009-01-21T00:36:32.000Z;;0;;0.9906;;65.47104;;2794.52832;;39.93;;2794.52832;8.0400004336052;;23.91;0;;60;0;;30;
3 1;2009-01-21T00:36:36.000Z;;0;;0.646176;;65.47104;;2794.52832;;39.93;;2794.52832;10.277100048352;;23.91;0;;60;0;;
4 2;2009-01-21T00:36:40.000Z;;0;;0.24384;;65.47104;;2794.52832;;39.93;;2794.52832;11.6871507146167;;23.91;0;;60;0;;
5 3;2009-01-21T00:36:44.000Z;;0;;0.070104;;65.47104;;2794.52832;;39.93;;2794.52832;12.5684323810321;;23.91;0;;60;0;
6 4;2009-01-21T00:36:48.000Z;;0;;0;;65.47104;;2794.52832;;39.93;;2794.52832;39.1017896298776;;23.91;0;;60;0;;30;0;56
7 5;2009-01-21T00:36:52.000Z;;0;;0;;65.47104;;2794.52832;;39.93;;2794.52832;44.6742013975197;;23.91;0;;60;0;;30;0;56
8 6;2009-01-21T00:36:56.000Z;;0;;0;;65.47104;;2794.52832;;39.94;;2794.52832;54.1513688563561;;23.91;0;;60;0;;30;75.4
9 7;2009-01-21T00:37:00.000Z;;0;;0;;65.47104;;2794.52832;;39.94;;2794.52832;67.2756865962041;;23.91;0;;60;0;;30;75.4
10 8;2009-01-21T00:37:04.000Z;;0;;0;;65.47104;;2794.52832;;39.94;;2794.52832;74.5564289787437;;23.91;0;;60;0;;30;0;56
11 9;2009-01-21T00:37:08.000Z;;0;;0;;65.47104;;2794.52832;;39.94;;2794.52832;76.0478287219083;;-47.81;0;;60;0;;30;0;51
12 10;2009-01-21T00:37:12.000Z;;0;;0;;65.47104;;2794.52832;;39.94;;2794.52832;62.1100202130615;;-47.81;0;;60;0;;30;8;
13 11;2009-01-21T00:37:16.000Z;;0;;0;;65.47104;;2794.427736;;39.94;;2794.52832;55.5614195226208;;-47.81;0;;60;0;;30;0;
14 12;2009-01-21T00:37:20.000Z;;0;;0;;65.47104;;2794.321056;;39.94;;2794.52832;43.481081602988;;-46.41;0;;60;0;;30;0;
15 13;2009-01-21T00:37:24.000Z;;0;;0;;65.47104;;2794.321056;;39.94;;2794.52832;29.3127840429249;;-46.41;0;;60;0;;30;2
16 14;2009-01-21T00:37:28.000Z;;0;;0;;65.47104;;2794.321056;;39.94;;2794.52832;3.30819579392862;;-46.41;0;;60;0;;30;1
17 15;2009-01-21T00:37:32.000Z;;0;;0;;65.47104;;2794.308864;;39.94;;2794.52832;3.14549764012885;;-46.41;0;;60;0;;30;0;
18 16;2009-01-21T00:37:36.000Z;;0;;0;;65.47104;;2794.107696;;39.94;;2794.52832;2.26421597371344;;-46.41;0;;60;0;;30;0;
19 17;2009-01-21T00:37:40.000Z;;0;;0;;65.47104;;2794.077216;;39.94;;2794.52832;1.19311979453163;;-46.41;0;;60;0;;30;3;
20 18;2009-01-21T00:37:44.000Z;;0;;0;;65.47104;;2794.077216;;39.94;;2794.52832;0;;-46.41;0;;60;0;;30;0;5616;;247.78;;

```

Figure 71: CSV Well Data Outcrop after format conversion

A.1.2 Matlab Scripts

Before running the standalone application and importing files, the script needs to be adjusted to the well data file columns header.

```

IMPORT_RAW_data_and_FILTER.m x RESULTS_TIME_PLOT.m x Torque_trend_prediction_VERSION_1.m x
%% Setup the Import Options
opts = delimitedTextImportOptions("NumVariables", 253);

% Specify range and delimiter
ots.DataLines = [2,Inf];
opts.Delimiter = ";";

% Specify column names and typ
opts.VariableNames = ["Line", "TIME", "BHFG", "P28H_ECO_RT", "DMEA", "TQA", "CRS_C",
opts.VariableTypes = ["double", "string", "double", "double", "double", "double",
opts = setvaropts(opts, 2, "WhitespaceRule", "preserve");
opts = setvaropts(opts, 2, "EmptyFieldRule", "auto");
opts.ExtraColumnsRule = "ignore";
opts.EmptyLineRule = "read";

%import latest data file from directory

startingFolder = pwd; % Whatever.
folder = uigetdir(startingFolder);
% Now get .csv files
filePattern = fullfile(folder, '*.csv');

```

Figure 72: Import and filter data script, outcrop, heada parameters to be adjusted

1	2	3	4	5	6	7	8	9	10	11	12	13	14	
TIME	filteredTQA2	filteredSP2	filteredRPM2	filled_OutputDME/filled_OutputDBTV	filled_SWOB	filled_ROP	filled_TFLO	filled_HKLD	filled_BPOS	filled_SPM1	filled_SPM2	filled_SPM3		
1	2009-01-02T08:39:27.014Z	11.0884	155.9437	49	-3.1794e+03	-3.1589e+03	0	332.5900	2.1374e+03	130.6868	35.6100	48	0	48
2	2009-01-02T08:39:27.965Z	11.0897	156.1446	49.5000	-3.1794e+03	-3.1589e+03	0	332.5900	2.1373e+03	131.2069	35.6100	48	0	48
3	2009-01-02T08:39:32.026Z	11.0925	156.3470	50	-3.1794e+03	-3.1589e+03	0	332.5900	2.1372e+03	131.7269	35.6100	48	0	48
4	2009-01-02T08:39:36.000Z	11.0878	156.5507	50	-3.1794e+03	-3.1589e+03	0	332.5900	2.1371e+03	131.7235	35.6100	48	0	48
5	2009-01-02T08:39:39.974Z	11.0750	156.7557	50	-3.1794e+03	-3.1589e+03	0	332.5900	2.1371e+03	131.7201	35.6100	48	0	48
6	2009-01-02T08:39:41.011Z	11.0970	156.9621	50	-3.1794e+03	-3.1589e+03	0	332.5900	2.1371e+03	131.7167	35.6100	48	0	48
7	2009-01-02T08:39:44.035Z	11.1419	157.1698	49.5000	-3.1794e+03	-3.1589e+03	0	332.5900	2.1369e+03	131.7167	35.6100	48	0	48
8	2009-01-02T08:39:44.986Z	11.2091	157.3786	49	-3.1794e+03	-3.1589e+03	0	332.5900	2.1368e+03	131.7167	35.6100	48	0	48
9	2009-01-02T08:39:48.010Z	11.3143	157.5886	49	-3.1794e+03	-3.1589e+03	0	332.5900	2.1371e+03	131.7218	35.6100	48	0	48
10	2009-01-02T08:39:49.997Z	11.4426	157.7997	49	-3.1794e+03	-3.1589e+03	0	332.5900	2.1375e+03	131.7269	35.6100	48	0	48
11	2009-01-02T08:39:51.984Z	11.5652	158.0117	49.5000	-3.1794e+03	-3.1589e+03	0	332.5900	2.1374e+03	131.5485	35.6100	48	0	48
12	2009-01-02T08:39:53.971Z	11.6405	158.2246	50	-3.1794e+03	-3.1589e+03	0	332.5900	2.1374e+03	131.3700	35.6100	48	0	48
13	2009-01-02T08:39:55.958Z	11.6215	158.4383	49.5000	-3.1794e+03	-3.1589e+03	0	332.5900	2.1371e+03	131.4465	35.6100	48	0	48
14	2009-01-02T08:39:58.982Z	11.4766	158.6528	49	-3.1794e+03	-3.1589e+03	0	332.5900	2.1369e+03	131.5230	35.6100	48	0	48
15	2009-01-02T08:40:00.019Z	11.2278	158.8678	49.3333	-3.1794e+03	-3.1589e+03	0	332.5900	2.1369e+03	131.4652	35.6100	48	0	48
16	2009-01-02T08:40:03.994Z	10.9795	159.0834	49.6667	-3.1794e+03	-3.1589e+03	0	332.5900	2.1368e+03	131.4074	35.6100	48	0	48
17	2009-01-02T08:40:07.968Z	10.8349	159.2994	50	-3.1794e+03	-3.1589e+03	0	332.5900	2.1368e+03	131.3496	35.6100	48	0	48
18	2009-01-02T08:40:12.029Z	10.8090	159.5157	49	-3.1794e+03	-3.1589e+03	0	332.5900	2.1374e+03	131.5230	35.6100	48	0	48
19	2009-01-02T08:40:16.003Z	10.8633	159.7323	49	-3.1794e+03	-3.1589e+03	0	332.5900	2.1374e+03	131.5281	35.6100	48	0	48
20	2009-01-02T08:40:17.040Z	10.9257	159.9489	49	-3.1794e+03	-3.1589e+03	0	332.5900	2.1375e+03	131.5332	35.6100	48	0	48
21	2009-01-02T08:40:19.978Z	10.9361	160.1656	49	-3.1794e+03	-3.1589e+03	0	332.5900	2.1374e+03	131.5332	35.6100	48	0	48
22	2009-01-02T08:40:21.014Z	10.8891	160.3822	49	-3.1794e+03	-3.1589e+03	0	332.5900	2.1374e+03	131.5332	35.6100	48	0	48
23	2009-01-02T08:40:24.038Z	10.8093	160.5986	49	-3.1794e+03	-3.1589e+03	0	332.5900	2.1371e+03	131.5485	35.6100	48	0	48
24	2009-01-02T08:40:26.026Z	10.7240	160.8148	49	-3.1794e+03	-3.1589e+03	0	332.5900	2.1369e+03	131.5638	35.6100	48	0	48
25	2009-01-02T08:40:28.013Z	10.6501	161.0305	49	-3.1794e+03	-3.1589e+03	0	332.5900	2.1370e+03	131.6114	35.6100	48	0	48
26	2009-01-02T08:40:31.987Z	10.6191	161.2458	49	-3.1794e+03	-3.1589e+03	0	332.5900	2.1371e+03	131.6590	35.6100	48	0	48
27	2009-01-02T08:40:35.011Z	10.6647	161.4605	49	-3.1794e+03	-3.1589e+03	0	332.5900	2.1372e+03	131.7065	35.6100	48	0	48
28	2009-01-02T08:40:35.962Z	10.7390	161.6747	49	-3.1794e+03	-3.1589e+03	0	332.5900	2.1373e+03	131.6658	35.6100	48	0	48
29	2009-01-02T08:40:38.986Z	10.7287	161.8881	49	-3.1794e+03	-3.1589e+03	0	332.5900	2.1375e+03	131.6250	35.6100	48	0	48
30	2009-01-02T08:40:40.022Z	10.6288	162.1007	49	-3.1794e+03	-3.1589e+03	0	332.5900	2.1374e+03	131.5689	35.6100	48	0	48

Figure 73: Imported and filtered data table

Training parameters of the neural network models may also be calibrated after the users desire upfront (administrator). The scripts will prepare the table parameters and create a matrix for each input and output table before training of the models will be triggered.

```

TQA_NEW_NETWORK_ACTUAL_2.m
5 % This script assumes these variables are defined:
6 %
7 % X_no_problem_24 - input time series.
8 % T_no_problem_24 - feedback time series.
9 Input_Data_X_TQA_train_timetable = table(Merged_well_filtered_data.filteredRPM2,Merged_well_filtered_data
10 Input_Data_X_TQA_train_timetable.TIME = datetime(Merged_well_filtered_data.TIME,'Format','yyyy-MM-dd HH:m
11 Input_Data_X_TQA_train_timetable.Properties.VariableNames(4) = 'TIME';
12 Input_Data_X_TQA_train_timetable.Properties.VariableNames(1) = 'filteredRPM2';
13 Input_Data_X_TQA_train_timetable.Properties.VariableNames(2) = 'filled_SWOB';
14 Input_Data_X_TQA_train_timetable.Properties.VariableNames(3) = 'filled_HKLD';
15
16 Input_Data_X_TQA_train_timetable=table2timetable(Input_Data_X_TQA_train_timetable);
17
18 Input_Data_X_TQA_train_timetable=Input_Data_X_TQA_train_timetable(TR,:);
19
20 Input_Data_X_TQA_train = table(Input_Data_X_TQA_train_timetable.filteredRPM2,Input_Data_X_TQA_train_timet
21 Input_Data_X_TQA_train.Properties.VariableNames(1) = 'filteredRPM2';
22 Input_Data_X_TQA_train.Properties.VariableNames(2) = 'filled_SWOB';
23 Input_Data_X_TQA_train.Properties.VariableNames(3) = 'filled_HKLD';
24
25 Input_Data_X_TQA_matrix_train = Input_Data_X_TQA_train(:,:);
26
27 Input_Data_T_TQA_train_timetable = table(Merged_well_filtered_data.filteredTQA2);
28 Input_Data_T_TQA_train_timetable.TIME = datetime(Merged_well_filtered_data.TIME,'Format','yyyy-MM-dd HH:m
29 Input_Data_T_TQA_train_timetable.Properties.VariableNames(2) = 'TIME';
30 Input_Data_T_TQA_train_timetable.Properties.VariableNames(1) = 'filteredTQA2';
31
32 Input_Data_T_TQA_train_timetable=table2timetable(Input_Data_T_TQA_train_timetable);
33
34 Input_Data_T_TQA_train_timetable=Input_Data_T_TQA_train_timetable(TR,:);
35
36 Input_Data_T_TQA_train = table(Input_Data_T_TQA_train_timetable.filteredTQA2);

```

Figure 74: Actual Torque Prediction Script, outcrop, input parameters

```

TQA_NEW_NETWORK_ACTUAL_2.m x +
28- Input_Data_T_TQA_train_timetable.TIME = datetime(Merged_well_filtered_data.TIME,'Format','yyyy-MM-dd HH:mm:ss');
29- Input_Data_T_TQA_train_timetable.Properties.VariableNames(2) = 'TIME';
30- Input_Data_T_TQA_train_timetable.Properties.VariableNames(1) = 'filteredTQA2';
31
32- Input_Data_T_TQA_train_timetable=table2timetable(Input_Data_T_TQA_train_timetable);
33
34- Input_Data_T_TQA_train_timetable=Input_Data_T_TQA_train_timetable(TR,:);
35
36- Input_Data_T_TQA_train = table(Input_Data_T_TQA_train_timetable.filteredTQA2);
37- Input_Data_T_TQA_train.Properties.VariableNames(1) = 'filteredTQA2';
38
39- Input_Data_T_TQA_matrix_train = Input_Data_T_TQA_train(:,:,);
40
41- X = tonndata(Input_Data_X_TQA_matrix_train,false,false);
42- T = tonndata(Input_Data_T_TQA_matrix_train,false,false);
43
44- X=X(1:end);
45- T=T(1:end);
46
47 % Choose a Training Function
48 % For a list of all training functions type: help nntrain
49 % 'trainlm' is usually fastest.
50 % 'trainbr' takes longer but may be better for challenging problems.
51 % 'trainscg' uses less memory. Suitable in low memory situations.
52- trainFcn = 'trainlm'; % Levenberg-Marquardt backpropagation.
53
54 % Create a Nonlinear Autoregressive Network with External Input
55- inputDelays = 1:50;
56- feedbackDelays = 1:50;
57- hiddenLayerSize = 10;
58- NEW_NET_TQA_ACTUAL_2 = narxnet(inputDelays,feedbackDelays,hiddenLayerSize,'open',trainFcn);
59
<

```

Figure 75: Actual Torque Prediction Script, outcrop, training parameters

Input_Data_X_TQA				Input_Data_X_TQA_matrix			
10000x3 table				10000x3 double			
	1	2	3		1	2	3
	filteredRPM2	filled_SWOB	filled_HKLD				
1	0	0	69.4529	1	0	0	69.4529
2	0	0	69.6262	2	0	0	69.6262
3	0	0	69.7996	3	0	0	69.7996
4	0	0	70.0953	4	0	0	70.0953
5	0	0	70.0137	5	0	0	70.0137
6	0	0	69.6568	6	0	0	69.6568
7	0	0	69.7792	7	0	0	69.7792
8	0	0	70.0647	8	0	0	70.0647
9	0	0	69.7996	9	0	0	69.7996
10	0	0	69.4835	10	0	0	69.4835
11	0	0	69.7486	11	0	0	69.7486
12	0	0	69.7486	12	0	0	69.7486
13	0	0	70.0137	13	0	0	70.0137
14	0	0	69.8353	14	0	0	69.8353
15	0	0	69.6568	15	0	0	69.6568
16	0	0	69.7486	16	0	0	69.7486
17	0	0	69.9933	17	0	0	69.9933
18	0	0	69.7792	18	0	0	69.7792
19	0	0	70.0647	19	0	0	70.0647
20	0	0	69.9933	20	0	0	69.9933

Figure 76: Input data for Actual Torque Prediction, outcrop, table (left) and matrix (right)

```

SPPA_NEW_NETWORK_2.m x +
1  % Solve an Autoregression Problem with External Input with a NARX Neural Network
2  % Script generated by Neural Time Series app
3  Input_Data_X_SPPA_train_timetable = table(Merged_well_filtered_data.filled_TFLO,Merged_well_filtered_data.filled_SPM1,t
4  Input_Data_X_SPPA_train_timetable.TIME = datetime(Merged_well_filtered_data.TIME,'Format','yyyy-MM-dd HH:mm:ss.SSS');
5  Input_Data_X_SPPA_train_timetable.Properties.VariableNames(7) = 'TIME';
6  Input_Data_X_SPPA_train_timetable.Properties.VariableNames(1) = 'filled_TFLO';
7  Input_Data_X_SPPA_train_timetable.Properties.VariableNames(2) = 'filled_SPM1';
8  Input_Data_X_SPPA_train_timetable.Properties.VariableNames(3) = 'filled_SPM2';
9  Input_Data_X_SPPA_train_timetable.Properties.VariableNames(4) = 'filled_SPM3';
10 Input_Data_X_SPPA_train_timetable.Properties.VariableNames(5) = 'filled_OutputDMEA';
11 Input_Data_X_SPPA_train_timetable.Properties.VariableNames(6) = 'filteredRPM2';
12
13 Input_Data_X_SPPA_train_timetable=table2timetable(Input_Data_X_SPPA_train_timetable);
14
15 Input_Data_X_SPPA_train_timetable=Input_Data_X_SPPA_train_timetable(TR,:);
16
17 Input_Data_X_SPPA_train= table(Input_Data_X_SPPA_train_timetable.filled_TFLO,Input_Data_X_SPPA_train_timetable.filled_C
18 Input_Data_X_SPPA_train.Properties.VariableNames(1) = 'filled_TFLO';
19 Input_Data_X_SPPA_train.Properties.VariableNames(2) = 'filled_OutputDMEA';
20 Input_Data_X_SPPA_train.Properties.VariableNames(3) = 'filteredRPM2';
21 Input_Data_X_SPPA_train.Properties.VariableNames(4) = 'filled_SPM1';
22 Input_Data_X_SPPA_train.Properties.VariableNames(5) = 'filled_SPM2';
23 Input_Data_X_SPPA_train.Properties.VariableNames(6) = 'filled_SPM3';
24
25 Input_Data_X_SPPA_matrix_train = Input_Data_X_SPPA_train{:,:};
26 Input_Data_X_SPPA_matrix_train(:,4:6)=sum(Input_Data_X_SPPA_matrix_train(:,4:6),4);
27 Input_Data_X_SPPA_matrix_train=Input_Data_X_SPPA_matrix_train(:,1:4);
28
29 Input_Data_T_SPPA_train_timetable = table(Merged_well_filtered_data.filteredSPP2);
30 Input_Data_T_SPPA_train_timetable.TIME = datetime(Merged_well_filtered_data.TIME,'Format','yyyy-MM-dd HH:mm:ss.SSS');
31 Input_Data_T_SPPA_train_timetable.Properties.VariableNames(2) = 'TIME';
32 Input_Data_T_SPPA_train_timetable.Properties.VariableNames(1) = 'filteredSPP2';

```

Figure 77: Actual Standpipe Pressure Prediction Script, outcrop, input parameters

```

SPPA_NEW_NETWORK_2.m x +
49  % Choose a Training Function
50  % For a list of all training functions type: help nntrain
51  % 'trainlm' is usually fastest.
52  % 'trainbr' takes longer but may be better for challenging problems.
53  % 'trainscg' uses less memory. Suitable in low memory situations.
54  trainFcn = 'trainlm'; % Levenberg-Marquardt backpropagation.
55
56  % Create a Nonlinear Autoregressive Network with External Input
57  inputDelays = 1:50;
58  feedbackDelays = 1:50;
59  hiddenLayerSize = 10;
60  NEW_NET_SPPA_ACTUAL_2 = narxnet(inputDelays,feedbackDelays,hiddenLayerSize,'open',trainFcn);
61
62  % Prepare the Data for Training and Simulation
63  % The function PREPARETS prepares timeseries data for a particular network,
64  % shifting time by the minimum amount to fill input states and layer
65  % states. Using PREPARETS allows you to keep your original time series data
66  % unchanged, while easily customizing it for networks with differing
67  % numbers of delays, with open loop or closed loop feedback modes.
68  [x_sppa_act,xi_sppa_act,ai_sppa_act,t_sppa_act] = preparets(NEW_NET_SPPA_ACTUAL_2,X_sppa_act,[],T_sppa_act);
69
70  % Setup Division of Data for Training, Validation, Testing
71  NEW_NET_SPPA_ACTUAL_2.divideParam.trainRatio = 70/100;
72  NEW_NET_SPPA_ACTUAL_2.divideParam.valRatio = 15/100;
73  NEW_NET_SPPA_ACTUAL_2.divideParam.testRatio = 15/100;
74
75  % Train the Network
76  [NEW_NET_SPPA_ACTUAL_2,tr] = train(NEW_NET_SPPA_ACTUAL_2,x_sppa_act,t_sppa_act,xi_sppa_act,ai_sppa_act);
77
78  % Test the Network
79  yNEW_ACTUAL_SPPA_2 = NEW_NET_SPPA_ACTUAL_2(x_sppa_act,xi_sppa_act,ai_sppa_act);
80  e_sppa_act = subtract(t_sppa_act,yNEW_ACTUAL_SPPA_2);

```

Figure 78: Actual Standpipe Pressure Prediction Script, outcrop, training parameters

Note: The channels for pump strokes are being compiled to a single channel since there are not always the same pumps active, which would falsify the results.

Input_Data_X_SPPA					Input_Data_X_SPPA_matrix		
10000x4 table					10000x2 double		
	1	2	3	4		1	2
	filled_TFLO	filled_SPM1	filled_SPM2	filled_SPM3	1	0	0
1	0	0	0	0	2	0	0
2	0	0	0	0	3	0	0
3	0	0	0	0	4	0	0
4	0	0	0	0	5	0	0
5	0	0	0	0	6	0	0
6	0	0	0	0	7	0	0
7	0	0	0	0	8	0	0
8	0	0	0	0	9	0	0
9	0	0	0	0	10	0	0
10	0	0	0	0	11	0	0
11	0	0	0	0	12	0	0
12	0	0	0	0	13	0	0
13	0	0	0	0	14	0	0
14	0	0	0	0	15	0	0
15	0	0	0	0	16	0	0
16	0	0	0	0	17	0	0
17	0	0	0	0	18	0	0
18	0	0	0	0	19	0	0
19	0	0	0	0	20	0	0
20	0	0	0	0			

Figure 79: Input data for Actual Standpipe Pressure Prediction, outcrop, table (left) and matrix (right)

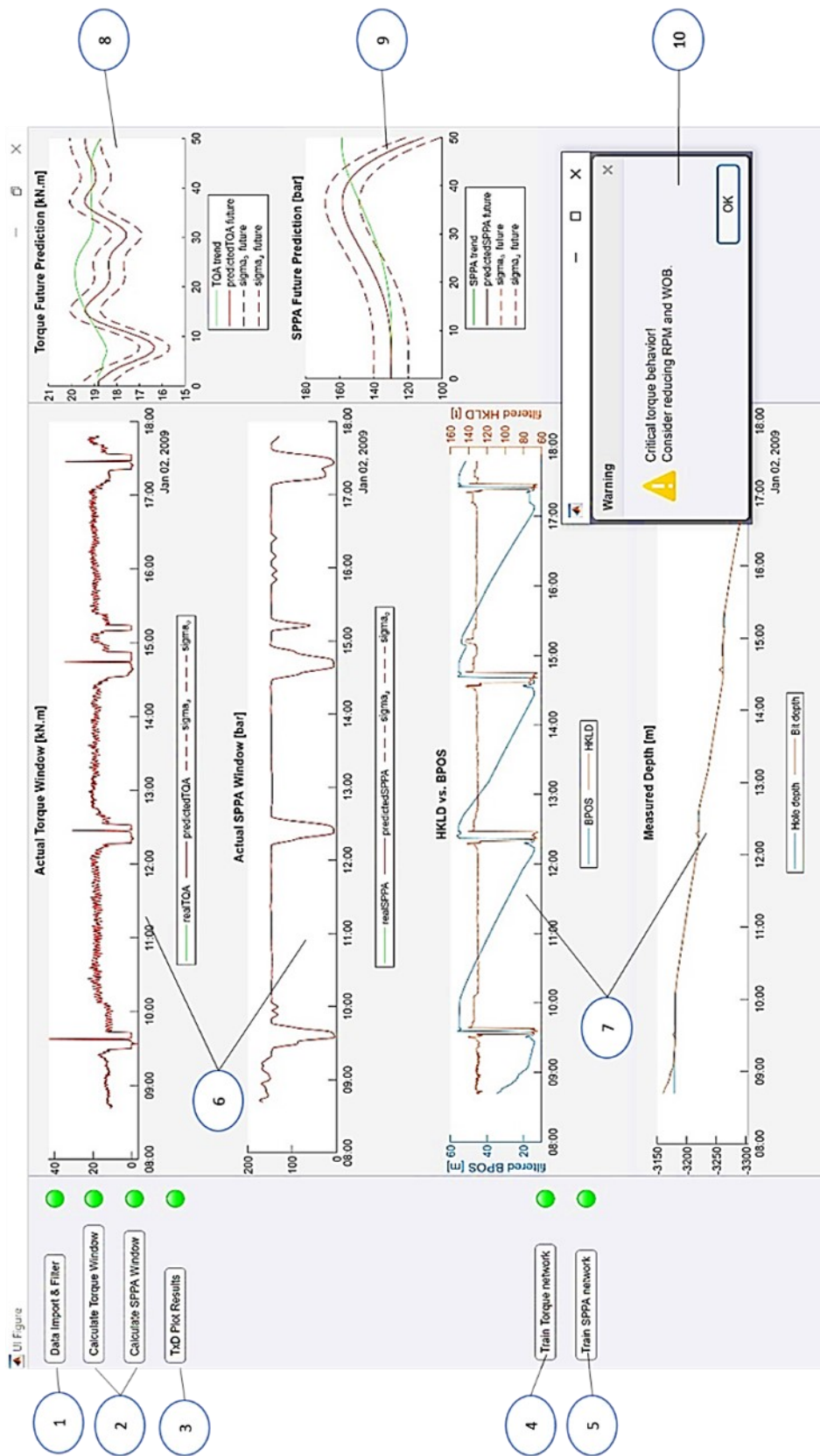


Figure 80: Graphical User Interface for Developed Standalone Application

#	Description and Function
1	Imports and filters new data sample.
2	Calculate torque and standpipe pressure windows based on trained networks.
3	Visualizes results in the specific plot sections.
4	Train neural networks for torque predictions
5	Train neural networks for standpipe pressure predictions
6	Visualization of actual raw data vs. filtered data, predicted torque and standpipe pressure windows
7	Visualization of additionally filtered data channels (hookload vs. block position and measured depth of bit vs. hole).
8	Visualization of predicted torque trend, future torque (based on other channels) and torque window.
9	Visualization of predicted SPPA trend, future SPPA (based on other channels) and SPPA window.
10	Warning shown by alert trigger functions.

Table 13. Detailed Description of the GUI Panel

Bibliography

1. Prichard, S., Roye, J. and Espnoza-Gala, L. M. (2012). Real-time data offers critical tool to redefine well control safety. *Drilling Contractor*, November / December. pp 96–109
2. Hussain Rabia (2015). “Well Engineering and Construction”, e-book
3. Asad Elmgerbi (SS 2019). Lecture, Advanced Well Construction, Torque and Drag.
4. Abdelaziz Gabr (2017). Guidelines for effective hole cleaning, IADC. <https://www.linkedin.com/pulse/guidelines-effective-hole-cleaning-abdelaziz-gabr/>
5. Hayatdavoudi, A. (2011, January 1). Shale Stickiness And Drill Bit Balling: Theory And Case Histories of Problems And Solutions In Louisiana And Gulf of Mexico. American Rock Mechanics Association.
6. De Stefano, G., & Young, S. (2009, January 1). The Prevention And Cure Of Bit Balling In Water Based Drilling Fluids. Offshore Mediterranean Conference.
7. Anton Lettner (SS 2019). Well Control Class.
8. Colin Bowes, Ray Procter (1997). *Drillers Stuck pipe Handbook*.
9. Sedco Forex (1997)
10. Payne, M. L., & Abbassian, F. (1996, January 1). Advanced Torque and Drag Considerations in Extended-Reach Wells. Society of Petroleum Engineers. doi:10.2118/35102-MS
11. Johancsik, C. A., Friesen, D. B., & Dawson, R. (1984, June 1). Torque and Drag in Directional Wells-Prediction and Measurement. Society of Petroleum Engineers. doi:10.2118/11380-PA
12. Reiber, F., Vos, B. E., & Eide, S. E. (1999, January 1). On-Line Torque & Drag: A Real-Time Drilling Performance Optimization Tool. Society of Petroleum Engineers. doi:10.2118/52836-MS
13. Tikhonov, V., Valiullin, K., Nurgaliev, A., Ring, L., Gandikota, R., Chaguine, P., & Cheatham, C. (2013, March 5). Dynamic Model for Stiff String Torque and Drag. Society of Petroleum Engineers. doi:10.2118/163566-MS
14. ©TDE Group, All rights reserved (2020), proNova Performance Measurements and Data Analytics. proNova Webportal Demo
15. Martinez, E., Ardoin, A., Cheatham, C., & Whitney, R. (2020, February 25). Applied Real-Time Data Analytics Improves Drillstring Life and Design. Society of Petroleum Engineers. doi:10.2118/199630-MS
16. Demirdal, B., & Cunha, J. C. S. (2007, January 1). Pressure Losses Of Non-Newtonian Fluids In Drilling Operations. Society of Petroleum Engineers. doi:10.2118/108711-MS
17. Ayeni, K., & Osisanya, S. O. (2004, January 1). Evaluation of Commonly Used Fluid Rheological Models Using Developed Drilling Hydraulic Simulator. Petroleum Society of Canada. doi:10.2118/2004-039

18. Zoellner, P., Thonhauser, G., Lueftenegger, M., & Spoerker, H. F. (2011, January 1). Automated Real-time Drilling Hydraulics Monitoring. Society of Petroleum Engineers. doi:10.2118/140298-MS
19. Reitsma, D. (2011, January 1). Development of an Automated System for the Rapid Detection of Drilling Anomalies using Standpipe and Discharge Pressure. Society of Petroleum Engineers. doi:10.2118/140255-MS
20. Noshi, C. I., & Schubert, J. J. (2018, October 5). The Role of Machine Learning in Drilling Operations; A Review. Society of Petroleum Engineers. doi:10.2118/191823-18ERM-MS
21. Hegde, C., Wallace, S., & Gray, K. (2015, October 13). Real Time Prediction and Classification of Torque and Drag During Drilling Using Statistical Learning Methods. Society of Petroleum Engineers. doi:10.2118/177313-MS
22. Ahmed, O. S., Aman, B. M., Zahrani, M. A., & Ajikobi, F. I. (2019, November 11). Stuck Pipe Early Warning System Utilizing Moving Window Machine Learning Approach. Society of Petroleum Engineers. doi:10.2118/197674-MS
23. Srikantha Mishra Akhil Datta-Gupta (2017). Applied Statistical Modeling and Data Analytics. ISBN: 9780128032794
24. Abbas, A. K., Flori, R., Almubarak, H., Dawood, J., Abbas, H., & Alsaedi, A. (2019, September 23). Intelligent Prediction of Stuck Pipe Remediation Using Machine Learning Algorithms. Society of Petroleum Engineers. doi:10.2118/196229-MS
25. Yu, Y., Chambon, S., Liu, Q., & Belaskie, J. P. (2018, March 6). Recorded Well Data Enriches the Testing of Automation Systems by Using a Deep Neural Network Approach. Society of Petroleum Engineers. doi:10.2118/189591-MS
26. Hou, X., Yang, J., Yin, Q., Liu, H., Chen, H., Zheng, J., ... Liu, X. (2020, May 4). Lost Circulation Prediction in South China Sea using Machine Learning and Big Data Technology. Offshore Technology Conference. doi:10.4043/30653-MS
27. Wang, Y., & Salehi, S. (2015, March 3). Drilling Hydraulics Optimization Using Neural Networks. Society of Petroleum Engineers. doi:10.2118/173420-MS

Acronyms

<i>TQA</i>	Average (surface) torque
<i>SPPA</i>	Average Standpipe Pressure
<i>WITSML</i>	Wellsite information transfer standard markup language
<i>WITS0</i>	Wellsite Information Transfer Standard Level 0
<i>HSE</i>	Health Safety Environment
<i>UI</i>	User Interface
<i>DSF</i>	Differential Sticking Force
<i>OD</i>	Outer Diameter
<i>BHA</i>	Bottom Hole Assembly
<i>RPM</i>	Rotations per Minute
<i>ROP</i>	Rate of Penetration
<i>LCM</i>	Loss Circulation Material
<i>BHP</i>	Bottom Hole Pressure
<i>WBM</i>	Water based Mud
<i>OBM</i>	Oil based Mud
<i>CH</i>	Cased Hole
<i>OH</i>	Open Hole
<i>WOB</i>	Weight on Bit
<i>DP</i>	Drill Pipe
<i>CSG</i>	Casing
<i>KOP</i>	Kickoff Point
<i>HWDP</i>	Heavy Weight Drill Pipe
<i>RIH</i>	Running in hole
<i>POOH</i>	Pulling out of hole
<i>ROB</i>	Rotating off bottom
<i>KPI</i>	Key Performance Indicator
<i>SPP</i>	Standpipe Pressure
<i>ADP</i>	Annular Discharge Pressure
<i>MSER</i>	Mean Squared Error
<i>SVM</i>	Support Vector Machines

<i>MLR</i>	Multilinear Regression
<i>ANN</i>	Artificial Neural Networks
<i>NARX</i>	Nonlinear Autoregressive with External (Exogenous) Input
<i>NAR</i>	Nonlinear Autoregressive
<i>IADC</i>	International Association of Drilling Contractors
<i>IWFC</i>	International Well Control Forum
<i>RSS</i>	Rotary Steerable System

Symbols

m	mass	[kg]
r	radius	[m]
F	Force	[N]
φ	angular	[°]
μ	friction factor	[-]

List of Figures

Figure 1: Example non-productive time (NPT) distribution (modified from Pritchard et al. 2012)	8
Figure 2: Differential sticking (Hussain Rabia, 2015)	9
Figure 3: Magnitude of differential sticking force (Hussain Rabia, 2015)	10
Figure 4: Sketch of "pack off" (a) and "bridging" (b) (Hussain Rabia, 2015)	11
Figure 5: Guidelines for effective hole cleaning (Abdelaziz Gabr, 2017)	11
Figure 6: Formation of a key seat (Sedco Forex, 1997)	16
Figure 7: Formation of a dogleg (Sedco Forex, 1997)	17
Figure 8: Free body diagram of a moving body on an inclined plane ($\mu=\mu_k$)	18
Figure 9: Drill string buckling behavior under increasing compressive load. (M. L. Payne, Fereidun Abbassian, 1997)	19
Figure 10: Torque on a rotating drill pipe at a low well inclination (a) and high well inclination (b) section ($\mu=\mu_k$)	20
Figure 11: Forces acting on drill string element during pickup. (C.A. Johancsik, D.B. Friesen, Rapier Dawson, 1984)	21
Figure 12: Example of a tension and compression plot for a planned drill string (soft-string model)	23
Figure 13: Simulated torque and drag broomstick plots, indicating simulations for RIH (blue), POOH (red), and ROB (green) for the different cased hole (CH) and open hole (OH) friction factors (number beside CH and OH) (©proNova by TDE)	24
Figure 14: Torque and drag real-time data vs. simulated curves (©proNova by TDE)	25
Figure 15: Dogleg severity for entire well - planned vs. actual (Eddie Martinez et al., 2020)	26
Figure 16: Example for pressure loss gradient analysis at open hole - drill collar annular section ($K=0.735$) (Demirdal, B., & Cunha, J. C. S 2007)	29
Figure 17: Drill string pressure loss plot for 8 3/4" hole (Ayeni, K., & Osisanya, S. O, 2004)	30
Figure 18: Pressure peak observed during pump start-up (Reitsma, D, 2011)	31
Figure 19: Calibration of SPP vs. ADP monitor (Reitsma, D, 2011)	31
Figure 20: System screen of fast kick test (left) and drill-pipe leak (right) (Reitsma, D, 2011)	32
Figure 21: Depth plotted against downhole torque in Tyler formation using Bootstrapped regression (Hegde, C., 2015)	34
Figure 22: Random forest visualization (Hegde, C., 2015)	35
Figure 23: Downhole torque versus depth using random forests with 80% of the data used for training (Hegde, C., 2015)	35
Figure 24: Change Point Detection algorithm. The black line is the input data stream, the green, and blue boxes are the right and left sliding window, respectively, and the red line is the calculated distribution divergence distance for data from both sliding windows evaluated at their adjacent point (Ahmed, O. S., 2019)	36
Figure 25: Hyperplane in SVM (Mishra and Datta-Gupa, 2017)	37
Figure 26: ANNs structure with one hidden layer (Abbas, A. K et al., 2019)	37
Figure 27: Overall architecture of the proposed DNN model (Yu, Y., Chambon, S., et al., 2018). N is the number of channels, CNN convolutional layers, LSTM long short-term memory layer and FC are fully connected layers	38
Figure 28: Simulated time sequence by the proposed DNN (Yu, Y., Chambon, S., et al., 2018)	38
Figure 29: Illustration of the safe drilling mud window (SDMDW) in Yingqiong Basin (Hou, X. et al., 2020)	39
Figure 30: Architecture of lost circulation prediction ANN (Hou, X. et al., 2020)	40
Figure 31: Accuracy (a) and loss (b) on training and testing set (Hou, X. et al., 2020)	41
Figure 32: Ranking of model input, one input channel (Wang, Y., & Salehi, S. 2015)	43

Figure 33: Ranking of model input (Wang, Y., & Salehi, S. 2015).....	43
Figure 34: Regression of the overall simulation results for three wells (Wang, Y., & Salehi, S. 2015).....	44
Figure 35: Flow chart of undertaken development steps for creating the hybrid model.....	45
Figure 36: Data acquisition and pre-processing procedure.....	46
Figure 37: Outcrop of raw surface sensor data, rig Maersk Inspire, well NO 15/9-F-15 A.....	48
Figure 38: Outcrop of pre-processed surface sensor data, rig Maersk Inspire, well NO 15/9-F-15 A.....	48
Figure 39: Predictive models creation workflow	49
Figure 40: NARX Neural Network architecture, prediction of actual time series.....	49
Figure 41: NARX Neural Network architecture, prediction of future time series	50
Figure 42: NAR Neural Network architecture, trend prediction, open loop	50
Figure 43: NAR Neural Network architecture, trend prediction, closed-loop	51
Figure 44: Workflow of safety window creation and triggering alerts.....	52
Figure 45: Principal of identifying outliers, in other words, abnormal behavior of the specific data channel	52
Figure 46: Normal distributed histogram of data samples (MSER of each timestamp), indicating mean and standard deviation	53
Figure 47: Outlook of the developed standalone application	55
Figure 48: Workflow of the developed Standalone Application	56
Figure 49: Visualization of the imported raw and filtered actual data in standalone application charts (well NO 15/9-F-15 A).....	57
Figure 50: Enter the start point (start time) and endpoint (end time) of training data (well NO 15/9-F-15 A)	57
Figure 51: NARX Neural Network architecture, prediction of actual TQA time series.....	58
Figure 52: NARX Neural Network architecture, prediction of future TQA time series.....	58
Figure 53: Enter start point (start time) and endpoint (end time) of training data (well NO 15/9-F-15 A).....	59
Figure 54: NARX Neural Network architecture, prediction of actual SPPA time series.....	59
Figure 55: NARX Neural Network architecture, prediction of future SPPA time series	60
Figure 56: Mean squared error (MSER) of actual torque prediction (TQA), Histogram.....	61
Figure 57: Mean squared error (MSER) of actual standpipe pressure prediction (SPPA), Histogram	61
Figure 58: Visualization of the actual results in the standalone application (well NO 15/9-F-15 A).	62
Figure 59: Visualization of the future results in the standalone application (well NO 15/9-F-15 A).	63
Figure 60: Standalone application view of the actual data training interval, imported, filtered, and trained networks, well NO 15/9-F-15 A.....	65
Figure 61: Manipulated input data, excessive torque	66
Figure 62: Performed Scenario to identify excessive torque behavior, manipulated well data (NO 15/9-F-15 A). a.) Standalone application view shows a warning message shown b.) Zoomed “Actual Torque Window” view indicates the actual outlier data in green from the predicted window in red c.) Zoomed “Actual Torque Window” view (II) provides a closer look into the outlier data range, whereas the actual TQA data in green is clearly exceeding the predicted window of uncertainty (upper border) in red.	67
Figure 63: Manipulated input data, decreased torque	67
Figure 64: Performed Scenario to identify decreased torque behavior, manipulated well data (NO 15/9-F-15 A). a.) Standalone application view shows a warning message shown b.) Zoomed “Actual Torque Window” view indicates the outlier actual data in green from the predicted window in red c.) Zoomed “Actual Torque Window” view (II) provides a closer	

look into the outlier data range, whereas the actual TQA data in green is clearly exceeding the predicted window of uncertainty (lower border) in red. 68

Figure 65: Manipulated input data, excessive standpipe pressure 68

Figure 66: Performed Scenario to identify excessive SPPA behavior, manipulated well data (NO 15/9-F-15 A). a.) Standalone application view shows a warning message shown b.) Zoomed “Actual SPPA Window” view indicates the outlier, actual data in green from the predicted window in red c.) Zoomed “Actual SPPA Window” view (II) provides a closer look into the outlier data range, whereas the actual SPPA data in green is clearly exceeding the predicted window of uncertainty (upper border) in red. 69

Figure 67: Manipulated input data, decreased standpipe pressure 70

Figure 68: Performed Scenario to identify decreased SPPA behavior, manipulated well data (NO 15/9-F-15 A). a.) Standalone application view shows a warning message shown b.) Zoomed “Actual SPPA Window” view indicates the actual outlier data in green from the predicted window in red c.) Zoomed “Actual SPPA Window” view (II) provides a closer look into the outlier data range, whereas the actual SPPA data in green is clearly exceeding the predicted window of uncertainty (lower border) in red. 70

Figure 69: WITSML (.xml) Well Data Outcrop before format conversion to CSV (.csv)..... 76

Figure 70: Python script, xml to csv converter 76

Figure 71: CSV Well Data Outcrop after format conversion 77

Figure 72: Import and filter data script, outcrop, heada parameters to be adjusted 77

Figure 73: Imported and filtered data table..... 78

Figure 74: Actual Torque Prediction Script, outcrop, input parameters 78

Figure 75: Actual Torque Prediction Script, outcrop, training parameters 79

Figure 76: Input data for Actual Torque Prediction, outcrop, table (left) and matrix (right) 79

Figure 77: Actual Standpipe Pressure Prediction Script, outcrop, input parameters 80

Figure 78: Actual Standpipe Pressure Prediction Script, outcrop, training parameters 80

Figure 79: Input data for Actual Standpipe Pressure Prediction, outcrop, table (left) and matrix (right) 81

Figure 80: Graphical User Interface for Developed Standalone Application 82

List of Tables

Table 1: Default friction factors based on historical well data (M.L. Payne &, F. Abbassian 1996)	19
Table 2: Confusion matrix used to evaluate the accuracy of classification algorithms in machine learning (Hegde, C., 2015)	36
Table 3: Metrics of six loss types (Hou, X. et al., 2020)	41
Table 4: Input and output parameters (Wang, Y., & Salehi, S. 2015)	42
Table 5: Applied filtering functions of the merged filtered data table	48
Table 6. Models of prediction description	51
Table 7: ANN for actual TQA prediction, data selection	58
Table 8: ANN for future TQA prediction, data selection	58
Table 9: ANNs for TQA and SPPA future trend prediction, data selection	58
Table 10: ANN for actual SPPA prediction, data selection	59
Table 11: ANN for future SPPA prediction, data selection	60
Table 12: Advantages and disadvantages of the standalone application	64
Table 13. Detailed Description of the GUI Panel	83